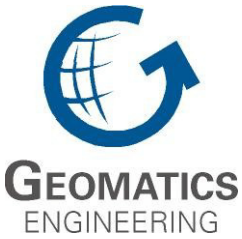

UCGE Reports
Number 20375

Department of Geomatics Engineering

An integrated modeling system to simulate the impact of land-use changes on hydrological processes in the Elbow River watershed in Southern Alberta

(URL: http://www.geomatics.ucalgary.ca/graduatetheses)

by

Gayan Wijesekara

January 24, 2013

UNIVERSITY OF CALGARY

An integrated modeling system to simulate the impact of land-use changes on hydrological processes in the Elbow River watershed in Southern Alberta

by

Gayan Wijesekara

A THESIS
SUBMITTED TO THE FACULTY OF GRADUATE STUDIES
IN PARTIAL FULFILMENT OF THE REQUIREMENTS FOR THE
DEGREE OF DOCTOR OF PHILOSOPHY

DEPARTMENT OF GEOMATICS ENGINEERING

CALGARY, ALBERTA
JANUARY, 2013

Abstract

The Elbow River watershed (ERW), in southern Alberta, Canada, covers an area of 1,238 km^2 and is subjected to considerable pressure for land development due to the rapid population growth in the City of Calgary. In this study, a comprehensive modeling system was developed to investigate the impact of land-use change on hydrological processes considering the complex surface-groundwater interactions existing in the watershed. Specifically, a spatially explicit land-use change model was coupled with MIKE-SHE and MIKE-11, a distributed physical based catchment and channel flow model. The modeling system was designed such that it has the following unique features: simulate dominant land-use changes in a spatially distributed way using a spatially explicit land-use change model, integrate spatially distributed land-use based parameters through the coupling of the land-use change model and the hydrological model, use comprehensive mechanisms to simulate the surface water and groundwater processes and their interactions, and incorporate a flexible design so that new land-use change plans can be incorporated easily for scenario analysis. Following a rigorous sensitivity analysis along with the calibration and validation of the integrated models, four land-use change scenarios were simulated for the period 2016-2031: business as usual (BAU), new development concentrated within the Rocky View County (RV-LUC) and in the Hamlet of Bragg Creek (BC-LUC) respectively, and development based on projected population growth within the ERW (P-LUC). The simulation results reveal that the rapid urbanization and deforestation create an increase in overland flow, and a decrease in evapotranspiration, baseflow, and infiltration mainly in the east sub-catchment of the watershed. Furthermore, BC-LUC is the most preferable scenario, while the BAU scenario with the same amount of new built-up area is found less preferable in terms of

the impact on overland flow and baseflow. The scenario P-LUC is found the least preferable out of all scenarios mainly due to the aggressive new development associated to the high population growth. The land-use/hydrological modeling system described in this study is resourceful and could be used to reduce the negative impact of land-use changes on the hydrological processes in the Elbow River watershed. This study is the first of this nature carried out in the Elbow River watershed, and is unique mainly due to its comprehensive framework that facilitates spatial explicit land-use change modeling, physical based and distributed hydrologic modeling, and the connection between these via distributed land-use based parameters. Furthermore, the design of this modeling system is flexible enough to extend this study to consider more aspects of the environment, e.g., incorporate climate change data to evaluate the impact of land-use and climate changes on hydrological processes.

Acknowledgements

First of all I express my gratitude to Dr. Arjuna Madanayake and Dr. Chan Wirasinghe for all the help given to me in finding this wonderful opportunity at the University of Calgary, a well reputed university within Canada, and study in the best GIS program in the department of Geomatics Engineering with the guidance of the best supervisor.

It was quite a blessing to find Dr. Danielle Marceau as my supervisor to guide me through many hurdles in my Ph.D. program. Her wisdom and experience helped me in overcoming my weaknesses, achieving success in scientific research, and also in achieving significant improvement in scientific writing. Also, I'm very thankful to other members of my advisory committee, Dr. Caterina Valeo and Dr. Anil Gupta for their invaluable advices, assistance, and for providing me with many research materials.

I'm very thankful to Sarah Hamza, Rob Dunn, Ralph Wright, Dr. Stephen Sheppard,
David J. Spiess, and Tony Brierley for all the valuable data, feedback, and assistance given to me and in finding the information as required.

I'm very grateful to all the collaborative partners for my study, DHI Water and Environment Canada, and Alberta Environment for providing me the necessary data and the modeling technology needed. I especially would like to thank Ying Qiao and Patrick Delaney for their wonderful support given to me throughout.

I’m delighted to have the best support from my colleagues at the Geocomputing laboratory and I’m very grateful to them for that. Special thanks to Dr. Christina Semeniuk, Dr. Niandry Moreno, Jean-Gabriel Hasbani, Dr. Fang Wang, Majeed Pooyandeh, Babak Farjad, Hamid Kiavarz, and David Birkigt. I would not have accomplished this without their support.

I’m deeply grateful and thankful to my loving family, my wife Kumudu, and my sons Rithira, and Kevan for the inspiration and the support to me throughout, especially for enduring all the sad moments and enjoying the happy moments together during this period. I’m also blessed by my family and extended families in Sri Lanka and this blessing certainly reached me to accomplish my Ph.D. program. Love you all.

Dedication

To Kumudu, Rithira, Kevan, and my parents in Sri Lanka

Table of Contents

List of Tables

List of Figures

List of Abbreviations

Symbol	Description
AESRD	Alberta Environment and Sustainable Resource Development
BAU	Business as usual
BC-LUC	Bragg Creek based land-use change
BF	Baseflow
CA	Cellular Automata
CC	Correlation Coefficient
DHI	Danish Hydraulic institute
ERWHM	Elbow River Watershed Hydrology Model
ET	Evapotranspiration
GEOIDE	GEOmatics for Informed DEcisions
Inf	Infiltration
K_{sim}	Kappa simulation
$K_{transition}$	Kappa Ttransition
$K_{transLoc}$	Kappa location of transition
LAI	Leaf Area Index
Ln	Natural logarithmic
MAE	Mean absolute error
NDVI	Normalized Difference Vegetation Index
NSE	Nash and Sutcliffe coefficient of efficiency
OL	Overland flow
P-LUC	Population based growth land-use change
RD	Root Depth
RI	Resemblance index
RV-LUC	Rocky View based land-use change
SZ	Saturated Zone
UZ	Unsaturated Zone
WB	Water balance
WPP	Western Prairie Provinces

Chapter 1: Introduction

Our world is a mixture of interacting complex systems functioning at a variety of spatial and temporal scales such as society, economy, and climate. Natural resource management and the design of policies for sustainable development raise the problem of dealing with some of these systems in which natural and human factors are thoroughly intertwined. Therefore, these systems must be understood and managed as coherent dynamic entities to ensure their integrity (Engelen *et al.* 1995, 2003). The modeling of these systems in the past has been simplified and limited to studying few individual systems in isolation without considering the influence of components of indirect or minor impact due to the overall complexity and computational intensity. For this reason, certain environmental models such as climate models have demonstrated limited reliability to produce accurate predictions. They are known to be over-simplified using few adjusting parameters to reproduce the many diverse attributes that constitute the complex behavior of the entire system (Thorpe 2005). Land and water are two intricate systems in our world. To avoid the pitfalls mentioned above, they must be understood and managed as coherent dynamic entities that interact with each other.

Water is an essential component in our environment that humans often take for granted, and forecasting its availability for the next generation has become an essential task in planning and resource management for rapidly growing cities. Forecasting the spatial distribution of water availability requires hydrologic modeling of groundwater and surface water. In growing cities and surrounding areas, one of the primary factors that cause changes in water resources is the constant evolution in land use. This transformation of earth's land surface has many consequences on biophysical systems at all scales ranging from local urban heat islands and alterations in stream flow patterns to altered patterns of global atmospheric circulation and long-

term extinction of species. Understanding the consequences of land-use change on hydrological processes, such as changes in water demand and supply from altered hydrological processes of infiltration and groundwater recharge and runoff, and integrating this understanding into the emerging focus on land-change science is a major need (DeFries and Eshleman 2004).

Canada has an extensive reserve of freshwater and therefore is taken for granted (Coote and Gregorich 2000). However, in some places in Canada the water is scarce, such as in the Western Prairie Provinces (WPP), an area 1/5 of the size of Europe. Lying in the rain shadow of the Rocky Mountains, WPP are the driest area of southern Canada (Schindler and Donahue 2006, Coote and Gregorich 2000). Amongst the major rivers in the WPP, there has been a moderate decline in the total annual stream flows over the 20th century (Gan 2000, Rood *et al.* 2005, Chen *et al.* 2006, Rood *et al.* 2008, Shepherd *et al.* 2010). In contrast to annual flows, the summer flows in major rivers of the WPP have declined significantly during the 20th century. Worst affected is the South Saskatchewan River with a reduction of summer flows by 84% since early 20th century. The Oldman, Bow, which Elbow is part of, and Red Deer Rivers contribute to the South Saskatchewan River and have been subjected to increased withdrawals to variable land-use activities such as irrigation, municipal and industrial uses. All of these tributaries flow through semiarid and sub-humid ecozones, where average annual potential evapotranspiration is higher (800-900 mm) than the average annual precipitation (400 – 600 mm) (Schindler and Donahue 2005, 2006, Coote and Gregorich 2000). It is predicted that in the near future, climate warming, through its effect on glaciers, snow packs and evaporation, will combine with cyclic droughts and rapidly increasing human activity to cause a crisis in water availability in this area

(Schindler and Donahue 2006). The Elbow River watershed is one of the catchments in the WPP that is critically affected.

As a result of the recent industrial development in Alberta within WPP, southern Alberta has been subjected to a rapid increase in population, particularly in Calgary, which results in considerable pressure for land development in the Elbow River watershed. The watershed is also under pressure due to forecasted developments in Bragg Creek, Redwood Meadows, and Rocky View County (Fig. 1.1). During the period 1985-2010, the civic census reveals a 71% population increase in Calgary (The City of Calgary 2010, Schindler and Donahue 2006). Forecasted population growth of the Calgary Economic region from 2011 to 2021 is estimated at 26% (Statistics Canada 2012, The City of Calgary 2012). The new development to the west of the City of Calgary combined with the developments occurring in the areas of Bragg Creek, Redwood Meadows, and the Rocky View County has the potential of evolving into several major and minor business corridors along the main highways (Municipal District of Rocky View 2012) (Fig. 1.1). Therefore, to ensure water resource sustainability in the watershed, it is crucial to investigate the changes in land-use (historical and future) and their impact over the land phase of the hydrological cycle.

The Elbow River watershed drains an area of 1,238 km^2 through the Elbow River and its tributaries (Fig. 1.1). Sixty-five percent of the watershed is located in the Kananaskis Improvement District while the remaining area is divided among the Rocky View County (20%), the Tsuu T'ina nation (10%), and Calgary (5%), a fast growing city of over one million inhabitants. The land-use composition within the watershed consists of urban area (5.9%), agriculture (16.7%), rangeland/parkland (6.2%), evergreen (34%) and deciduous forest (10%);

forest clear-cuts areas can be observed in about 1.8% of the watershed (the remaining of the area being rock, road, and water).

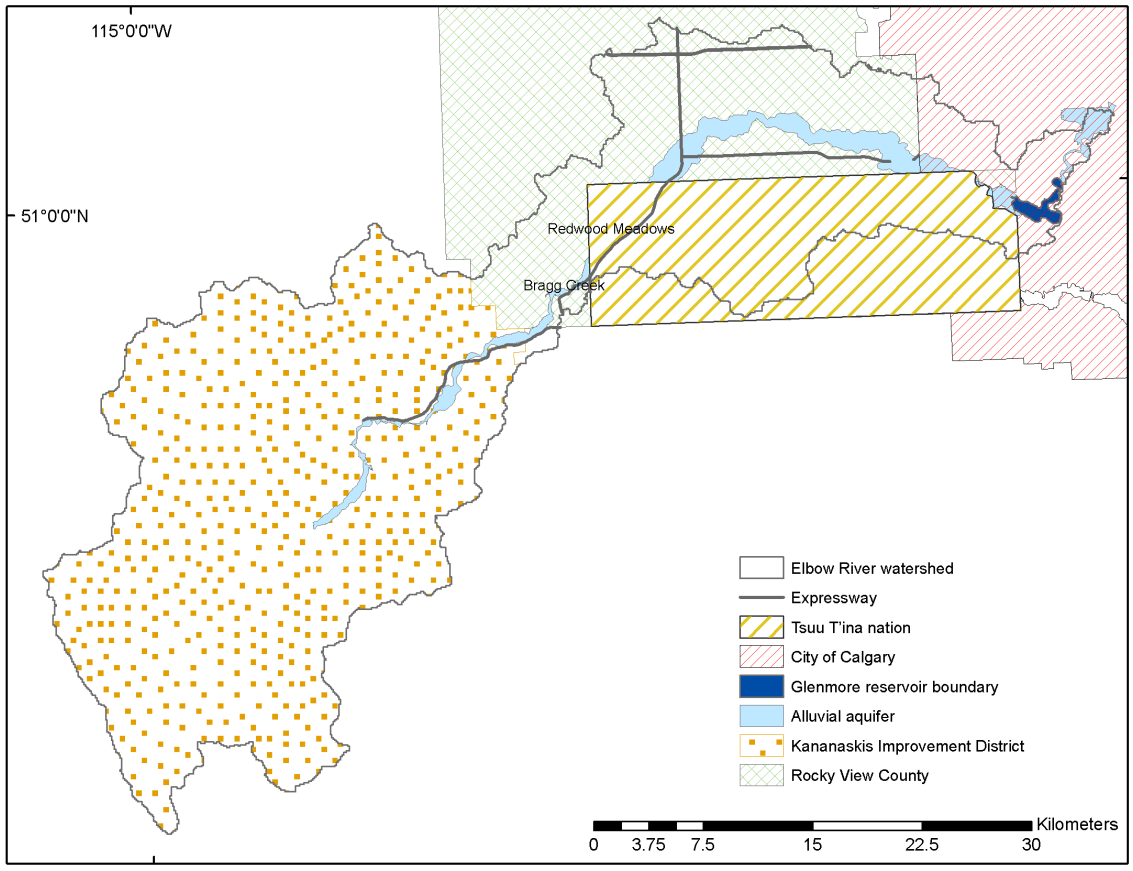

Figure 1.1: Map of the Elbow River watershed

1.1 The Elbow River watershed

The Elbow River flows for approximately 120 km; it drops from 2000 m elevation at Elbow Lake to 1000 m where it enters the Bow River in downtown Calgary. Compared to other major rivers in the region, it is a short and steep river system where any impacts at the upstream due to land-use activities are readily transmitted downstream (ERWP 2012, Bow River Basin Council 2010). Furthermore, the watershed is characterized by a complex hydrological regime (Wijesekara *et al.* 2012, ERWP 2012) in which considerable surface – groundwater interaction

exists between the river and the alluvial aquifer throughout the watershed (Manwell and Ryan 2006), with little flow generation in the lower part of the watershed (Meyboom 1961) (Fig. 1.1).

The alluvial aquifer is a shallow unconfined aquifer representing 5% of the entire area of the watershed. It was formed by alluvial deposition and is generally very permeable and highly hydraulically connected to the river, resulting in relatively fast groundwater flow through the shallow aquifer. A study carried out by Meyboom (1961) revealed that 73% of the actual groundwater discharge to the river flow during a normal river flow recession is contributed by the bank storage flow while the remaining is attributed to contacts springs (19%), and bedrock leakage (8%). The high percent of bank storage flow through the baseflow to the river during low discharge of the river helps the river to sustain the water flow throughout the year. In addition to be an important source of water for irrigation, the Elbow River supplies approximately 40% of Calgary's drinking water through the Glenmore reservoir (Valeo *et al.* 2007). The water production for municipal use has almost reached its maximum capacity. As a result, sustaining the future demands of the city of Calgary will be a challenging task.

1.2 Evaluating the impact of land-use changes on hydrological processes: past studies

In previous studies conducted to evaluate the impact of land-use changes on hydrological processes, scientists have attempted to use both conceptual/semi-distributed or lumped (Gustard and Wesselink 1993, Harbor 1994, Fohrer *et al.* 2005, Thanapakpawin *et al.* 2006, Lin *et al.* 2007, Du *et al.* 2012), and physical/distributed (Niehoff *et al.* 2002, Oogathoo 2006, Bithell and Brasington 2009, Elfert and Bormann 2009, Im *et al.* 2009, Chu *et al.* 2010) modeling approaches. Gustard and Wesselink (1993) applied a lumped conceptual model to Balquhidder

catchments in UK based on land-use change and found that with increasing afforestation, the mean flow decreases, the flow duration curve shifts down (i.e., stream flow at any instant is reduced), the annual minimum series decreases, and the storage needed to maintain a given yield increases. In that study, mainly three dominant land uses (upland pasture, coniferous, forest and heather) were used to simulate the flows by using aggregated values of daily rainfall and evaporation corresponding to the catchments. The authors concluded that the accuracy of input data is vital for a successful sensitivity analysis and calibration of the applied hydrological model. Harbor (1994) introduced a practical method for estimating the impact of land use on surface runoff, groundwater recharge and wetland hydrology, based on a simple spreadsheet analysis that can be used by planners. The author found that the method used in simulating the surface runoff (SCS curve number method) was too simple, and that the surface runoff portion generated by melted snow was ignored. Furthermore, the author concluded that this method could not be used to simulate the flow/levels of stream or rivers as significant groundwater contribution takes place as baseflow and are not represented.

Fohrer *et al.* (2005) evaluated the impact of different average agriculture field sizes (from 0.5 to 20 ha) produced by the economic model ProLand on hydrological processes using the IOSWAT model in the German Aar watershed. They emphasize the importance of using a comprehensive groundwater representation compared to a simple linear storage approach in areas characterized by a complex hydrological regime with an underlying aquifer system. Thanapakpawin *et al.* (2006) applied a distributed hydrology soil vegetation model (DHSVM) to the Mae Chaem River basin, in Thailand, to simulate forest-to-crop expansion and crop-to-forest reversal scenarios based on land-cover transitions observed from 1989 to 2000. The calibration and validation

carried out revealed that the preferential flows were not reasonably captured by the simple linear-reservoir routing mechanism used to represent the sub-surface flows.

Bithell and Brasington (2009) coupled three models (applied to a small catchment in Nepal middle hills) representing society, ecology, and hydrology to investigate how demographic changes influence deforestation, which in turn affects the forest ecology, along with the stream hydrology and water availability. Their results revealed that as the number of households increased from 3 to 337 in 200 years of simulation, the predicted storm response becomes progressively flashier. The expansion of agriculture and the loss of forest contributed to a 4% increase in total evaporative losses, a 22% decrease in annual discharge and an 18% increase in the internal storage of water and loss to deep ground water. In the hydrological model setup, vegetation transpiration, and deep groundwater flow were not incorporated. Furthermore, the distribution of rainfall data and soil properties was considered uniform throughout the catchment. The authors emphasize that their approach is more exploratory/explanatory than the descriptive approach that attempts to make a simulation of a particular real-world system. Du *et al.* (2012) developed an integrated modeling system by coupling a dynamic land-use change model with HEC-HMS hydrologic model. HEC-HMS is mostly considered as a lumped, single event, empirical-conceptual based model; the runoff method used in the model is considered as a quasi-distributed method (USACE 2000). Future land-use changes were generated using integrated Markov Chain and Cellular Automata model. Simulated spatial data of urbanization up to 2018 were overlaid on a reference map of 1988 to simulate the runoff generation up to 2018. The authors found that when urban areas were changed from 3% (1988) to 31% (2018), the daily peak discharge of eight selected floods increased from 2.3% to 13.9%. They concluded that

integrating a dynamic and distributed land-use change model (e.g., a cellular automaton) combined with a distributed hydrological model is a good approach to evaluate the hydrologic impacts of urbanization. They noted that this type of modeling system would be essential for watershed management, water resources planning, and flood management for sustainable development.

Lin *et al.* (2007) linked a spatially-explicit land-use change model (CLUE-s) and a distributed/lumped hydrological model developed by Haith and Shoemaker (1987) to investigate the impact of land-use changes on the hydrology in the Wu-Tu watershed in Northern Taiwan. They conclude that combining a spatially-explicit land-use simulation model with a hydrological model is an effective tool for investigating the impact of land-use change on hydrological processes, and promote the development of a landscape eco-hydrological decision-support system for watershed land-use planning, management and policy. In a subsequent study conducted in the same watershed, Chu *et al.* (2010) also used CLUE-s, but this time combined with a physical-based distributed hydrological model (DHVSM). They conclude that the hydrological processes in a watershed are highly sensitive to the spatial distribution of hydrologic parameters and that therefore it is important to use distributed hydrological models when investigating the impacts of land-use composition and patterns on the hydrology of a watershed. Niehoff *et al.* (2002) generated land-use change scenarios using a spatially distributed land-use change modeling kit (LUCK). This was accomplished by increasing the current land-use composition by a percentage and then investigating its impacts on hydrological processes using a process-oriented distributed hydrological model (WaSiM-ETH). These authors found

that the combination of spatially distributed land-use scenarios and process-oriented hydrological models has great potential.

Following a similar approach, Elfert and Bormann (2009) applied the WaSiM-ETH hydrological model to a meso-scale lowland catchment in northern Germany. They evaluated the impact of historical land-use changes and possible future land-use changes based on IPCC (Intergovernmental Panel on Climate Change) scenarios. They found that WaSiM-ETH is hardly sensitive to the slight changes observed in the last decade of the 20th century, but has produced considerable impacts on the water flows due to forecasted agricultural scenarios. These authors noted that well-validated physical-based hydrological models are suitable tools to quantify the impact of land-use changes on the hydrological processes. Furthermore, it is not sufficient to focus on the changes of one land use, i.e. agricultural land-use; it is important to consider the transition of land uses, (e.g., from agriculture to urban), to estimate the impact of land-use change on the hydrological behavior of the watershed.

Im *et al.* (2009) applied the physical-based distributed MIKE-SHE model to investigate the watershed response to land-use changes in the Gyeongancheon watershed in Korea. Using proportional changes in five land-use classes derived from multi-temporal Landsat TM images, they observed an increase of total runoff (5.5%) and overland flow (24.8%), predominantly due to an increase (10%) of urbanization. The authors only considered the historical land-use changes and the transition from forest to urban. They conclude that assessing the hydrologic effects due to land-use changes is a vital requirement for water resources development and management. Furthermore, the use of MIKE-SHE as a physically based distributed hydrological model can

precisely identify the effects of land-use and land-cover changes on the hydrologic processes in a watershed. Within the Canadian context, Oogathoo (2006) applied MIKE-SHE to the Canagagigue Creek watershed located in the Grand River Basin, in Ontario, Canada to evaluate the impact of management scenarios on the hydrological processes of the watershed by applying land-use increase/decrease percentages (e.g., increase urbanization from 0.2% to 2%). A comprehensive surface runoff (2-D diffusive wave approximation of the Saint Venant equations) and groundwater flow (3-D finite difference method) methods were employed. The author emphasized the potential of MIKE-SHE for investigating hydrologic problems of diverse complexity and for simulating alternative management practices, particularly in Canadian contexts.

These previous studies illustrate that in order to correctly assess the impact of future land-use changes on hydrological processes, it is essential to forecast reasonably well the possible land-use changes at the individual cell level considering all dominant land uses in the area. Spatially-explicit land-use change models can capture significant changes in the landscape patterns (White and Engelen 2000). Similarly, physical watershed characteristics that might be affected by land-use changes should also be investigated using a spatially-distributed, physically-based hydrological model. In addition, processes of the entire hydrological cycle should be taken into consideration during this investigation to obtain a more accurate and comprehensive understanding. Furthermore, a hydrological model that operates at a spatially-distributed level using physical properties that are both land-use based (e.g., surface roughness) and non-land-use based (e.g., soil characteristics) will produce more detailed and potentially more accurate results compared to a model that operates at lumped level (Refsgaard 1996, Yang *et al.* 2000).

Therefore, coupling these two models (a spatially-explicit land-use change model and a physically-based distributed hydrological model) is the focus of the current study.

1.3 Objective of this research

The objective of this research is to develop an integrated modeling system to evaluate the impact of past and future potential land-use changes on the hydrological processes in the Elbow River watershed. This integrated modeling system will have the following unique features:

1. Simulate dominant land-use changes in a spatially distributed way using a spatially explicit land-use change model.
2. Integrate spatially distributed land-use based parameters through the coupling of the land-use change model and the hydrological model.
3. Use comprehensive mechanisms to simulate the surface water and groundwater processes and their interactions.
4. Incorporate a flexible design so that new land-use change plans can be explored easily for scenario analysis.

In achieving this objective the following steps will be carried out:

1) Select the most appropriate model codes (computer programs to setup the models applied in the watershed).
2) Configure the land-use change and the hydrological models.

3) Implement a rigorous sensitivity analysis, calibration and validation procedure for both the land-use change and the hydrological models; the later involves multiple time periods, weather conditions, and land-use allocations.
4) Using the calibrated models, simulate the impact of land-use changes on hydrological processes for the historical period of 1992-2010 and for the period of 2016-2031 based on four land-use change scenarios and compare their preferability.

This modeling system is designed to be used as an interactive spatial decision support system for scenario analysis of land-use planning and decision making in water resource management. This study was undertaken in collaboration with Alberta Environment and Sustainable Resource Development (AESRD) and DHI Water and Environment Canada.

1.4 Organization of the thesis

The remaining of this thesis is organized as follow.

In Chapter 2, entitled Methods, the selection of the models for this study is discussed and justified, followed by a description of the design and implementation of the proposed modeling system. This section presents a description of the particular land-use change model used in the study, including its setup, calibration and validation and the simulation procedure. Section 2.2.2 includes the model configuration, data and parameters selected for the hydrological model, followed by a presentation of the rigorous calibration and validation that was carried out (section 2.2.3). Section 2.2.4 describes how the evaluation of the impact of land-use changes on the hydrological processes was executed.

In Chapter 3, entitled Results and Interpretation, the results of the calibration and validation of the hydrological model are first presented (section 3.1). This is followed by a description of the impact of land-use change on the hydrological processes for the historical period of 1992 to 2010 (section 3.2), along with a description of the future impacts for the period 2016 – 2031 (section 3.3). Chapter 4 presents the conclusions of the study and recommendations for future research.

Chapter 2: Methods

In this chapter, the rationale for selecting the cellular automata, MIKE-SHE and MIKE-11 models for the study is presented. This is followed by the configuration of the modeling system resulting from the coupling of the land-use change model and the hydrological model. Details regarding the model setup, parameterization, design, implementation, calibration and validation of the models followed by the approach used to evaluate the impact of land-use change scenarios on the hydrological processes are finally presented.

2.1 Selection of the models

To achieve the objectives of this study, three dynamic model were linked: (1) a cellular automata (CA) model applied to simulate land-use changes, (2) a hydrological model, MIKE-SHE, set up with physical based, distributed surface and groundwater components to simulate the hydrologic cycle, and (3) the MIKE-11 river model, a distributed detailed channel model to simulate the channel component as part of the surface water.

2.1.1 Cellular Automata (CA)

A CA is a dynamic simulation model that represents geographic space as a matrix of regularly arranged cells with each cell having its own state, such as land use. The model incorporates transition rules that dictate the next state of the current cell considering the values of the cells within its local or extended neighborhood and some additional constraints that can be incorporated in the model. The state of each cell evolves through discrete time steps with transition rules applied to all cells iteratively (White and Engelen 2000).

CA models have been used to simulate a wide range of dynamic geographical phenomena including natural hazards (Malamud *et al.* 2000), landslide simulations (Calidonna *et al.* 2001), forest planning (Mathey *et al.* 2008), epidemic propagation (Quan-Xing and Zhen 2005, Sirakoulis *et al.* 2000) and fire spreading (Hu *et al.* 2005, Hargrove *et al.* 2000). Wu and David (2002) and Syphard *et al.* (2005) used CA in eco-system modeling and found that it captures the non-linear emergent behavior as typically found in complex systems like watersheds (where various processes in natural systems like land-cover changes, hydrological processes, along with human activities interact with each other).

CA models are particularly suitable for land-use change modeling for several reasons. They are explicitly spatial and can be constrained in various ways to reflect local tendencies (Li and Yeh 2000, Jenerette and Wu 2001). It is also possible to specify for each simulated time step the quantity of land that should change from one land use to another (Jantz and Goetz 2005). Information from a-spatial models, like a population growth model, can be integrated into the CA model to spatially allocate the land-use changes (White *et al.* 1997). Over the recent past, CA modeling has been found remarkably effective in the simulation of land-use/land-cover changes (White and Engelen 2000, Ward *et al.* 2000, Li *et al.* 2003, Borredo *et al.* 2003, Puliafito 2006, Ménard and Marceau 2007, Stevens *et al.* 2007, Almeida *et al.* 2008, Shen *et al.* 2009, Santé *et al.* 2010, Wang 2012, Marceau *et al.* 2012). This shows that CA is capable in simulating complex spatial patterns and structures of the landscape. Unlike conventional land-use modeling techniques, they are inherently spatial, compatible with most of the spatial datasets, able to represent dynamic spatial processes, highly adaptable and simple while at the same time exhibiting rich behavior (White and Engelen 2000).

Distributed land-use change models other than CA have been used in previous studies to simulate the impact of land-use changes on hydrological processes. Two commonly used models are CLUE-s (Lin *et al.* 2007, Chu *et al.* 2010) and LUCK (Niehoff *et al.* 2002). CLUE-s is a spatial allocation model that employs a stepwise logistic regression and a non-spatial demand module to calculate the area that changes before the model spatially converts this area into land-use changes (Verburg *et al.* 2002). In the LUCK model, spatially averaged, large-scale trends of land-use development have to be provided externally. Land-use changes are simulated by specific modules built-in (e.g., urban module to simulate urbanization). Furthermore, these modules run based on a hierarchy (i.e., urban module is ranked highest followed by agriculture).

Comparatively, the land-use change model used for this study extracts the demand for each land-use change based on historical land-use changes. The model can operate on user-defined land-use transitions without a limit to the number of transitions. Once the demand for each land-use change is determined within the model, it simulates the cell-based changes for each land-use transition simultaneously. Furthermore, the model design is generic enough to learn the historical change patterns for each land-use transition. Therefore, the model can simulate a particular land-use change based on a user-defined land-use transition without any modification to the model code.

The land-use change CA model (called land-use CA) selected for this study has been calibrated, tested and successfully applied in the Elbow River watershed in a previous study (Hasbani 2008, Hasbani *et al.* 2011). This cell-based CA model allows a user to dynamically select the

parameters and parameter values from an analysis of historical data to create conditional transition rules that are further automatically transformed into mathematical rules. This procedure provides a direct relationship and understanding of the factors, both internal and external, that drive land-use changes in the study area. More details regarding the implementation of the land-use CA model are described in Section 2.2.1.

2.1.2 MIKE-SHE and MIKE-11

Hydrological simulation models provide the information required to make decisions related to the development and management of water and land resources especially in a watershed. Though many hydrological models have been designed and developed in the past that could be used for a watershed, some of them operate as lumped conceptual models e.g., the Stanford watershed model and the Sacramento watershed model, i.e., they refer to the spatially averaged condition of the entire basin (Sittner *et al.* 1969, Holtan *et al.* 1975). Furthermore, the values of the model parameters are conceptual which cannot easily be derived from measuring properties of the basin. Thus, they have no direct physical meaning (Singh *et al.* 1999; Sahoo *et al.* 2006). In comparison, physically distributed hydrologic models use parameters directly related to the physical characteristics of the watershed (e.g., topography, soil types, vegetation types, and geology) and the spatial variability in both physical characteristics and meteorological conditions. MIKE-SHE/MIKE-11 models represent a major development in this direction.

The MIKE-SHE flow model along with the MIKE-11 river model is a comprehensive, deterministic, distributed, and physically-based modeling system capable of simulating all major processes in the land phase of the hydrologic cycle compared to other hydrological models

(Sahoo *et al.* 2006). Successful applications of MIKE-SHE are found in the fields of irrigation planning and management (Jayatilaka *et al.* 1998, Singh *et al.* 1999), flood forecasting (Jasper *et al.* 2002), characterization of soil hydraulic properties (Romano and Palladino 2002, Christiaens and Feyen 2001), assessment of ground-water contamination (Refsgaard *et al.* 1999), and surface- and ground-water hydrology (Refsgaard 1997, Feyen *et al.* 2000, Andersen *et al.* 2001, Va´zquez 2003, Johnson *et al.* 2003). MIKE-SHE simulates the major components of the land-based phases of the hydrologic cycle, including snowmelt, evapotranspiration (ET), overland flow, unsaturated flow, and groundwater flow. For each of these processes, MIKE-SHE offers several configuration approaches that range from simple, lumped, and conceptual, to advanced, distributed, and physically based. MIKE-SHE has been selectively used by AESRD for water-related studies in the province of Alberta, Canada. MIKE-11 is a model for simulating flows, water quality, and sediment transport in channels, rivers, irrigation systems, and estuaries. It implements one-dimensional simulation of river flows and water levels using the fully dynamic Saint Venant equations. This model provides flow hydrographs at any desired location in the watershed. It includes a comprehensive, user-friendly graphical interface and strong 1D, 2D, and 3D visualization capabilities.

A comprehensive evaluation of several well-known hydrologic models (MIKE-SHE, GSFLOW, HydroGeoSphere, MODHMS, ParFlow) conducted in Ontario, Canada, confirmed MIKE-SHE as being the most comprehensive and flexible modeling environment in hydrological impact studies (AquaResource Inc 2011). Amongst these models, MIKE-SHE was found having several advantages including a flexible and robust representation of surface water hydrology and hydraulics, a well modularized structure, a flexible grid space, and a user friendly interface.

Camp Dresser and McKee (2001) evaluated numerous integrated surface water and groundwater modeling tools and found MIKE-SHE to be highly efficient. These authors compiled seventy-five models for a preliminary screening process after which they selected nine of them for further evaluation, which included: MIKE SHE, HMS, FHMFIPR, SWATMOD, MODFLOW, DYNFLOW, MODBRANCH, SWMM, and HSPF. They submitted these models through an evaluation that included criteria like: regulatory acceptance, cost, ease of use, inter model connectivity, GIS integration, services and support, model limitations, limit on model size, expandability, platform-flexibility of operating system, experience required, percent of market share, and documentation and testing. Based on a selected ranking mechanism with respect to the thirteen criteria, MIKE-SHE has earned the highest ranking.

The current study therefore uses Cellular Automata, MIKE-SHE and MIKE-11 models. Through appropriate parameterization, sensitivity analysis, calibration and validation, relevant model setups were developed for the watershed. The coupling of these models allows us to accommodate the physical and distributed nature of the land-use changes, and to successfully simulate the complex surface-groundwater interaction that exists in the watershed. The following section presents the coupled/integrated modeling system, along with the design and implementation of each model used.

2.2 Design and implementation of the proposed modeling system

Figure 2.1 displays the flow of operations conducted in coupling the three models. First, the data required for the three models (historical land-use maps, driving factors, climate data, topography,

vegetation properties, land-use based parameters, geological data, channel network, channel cross sections, and boundary conditions), were verified and corrected for their inconsistencies, e.g., temporal inconsistencies of historical land-use maps. The land-use CA model was calibrated using a semi-interactive method and validated until satisfactory results were obtained. A conceptual hydrological model was developed combining MIKE-SHE and MIKE-11 models, which is called the “Elbow River Watershed Hydrology Model” (ERWHM). It was subjected to rigorous and manual calibration and validation. The coupling between the land-use CA and ERWHM was implemented through land-use based parameters. These models were finally run to investigate the impact of past and future land-use changes on the hydrological processes of the watershed.

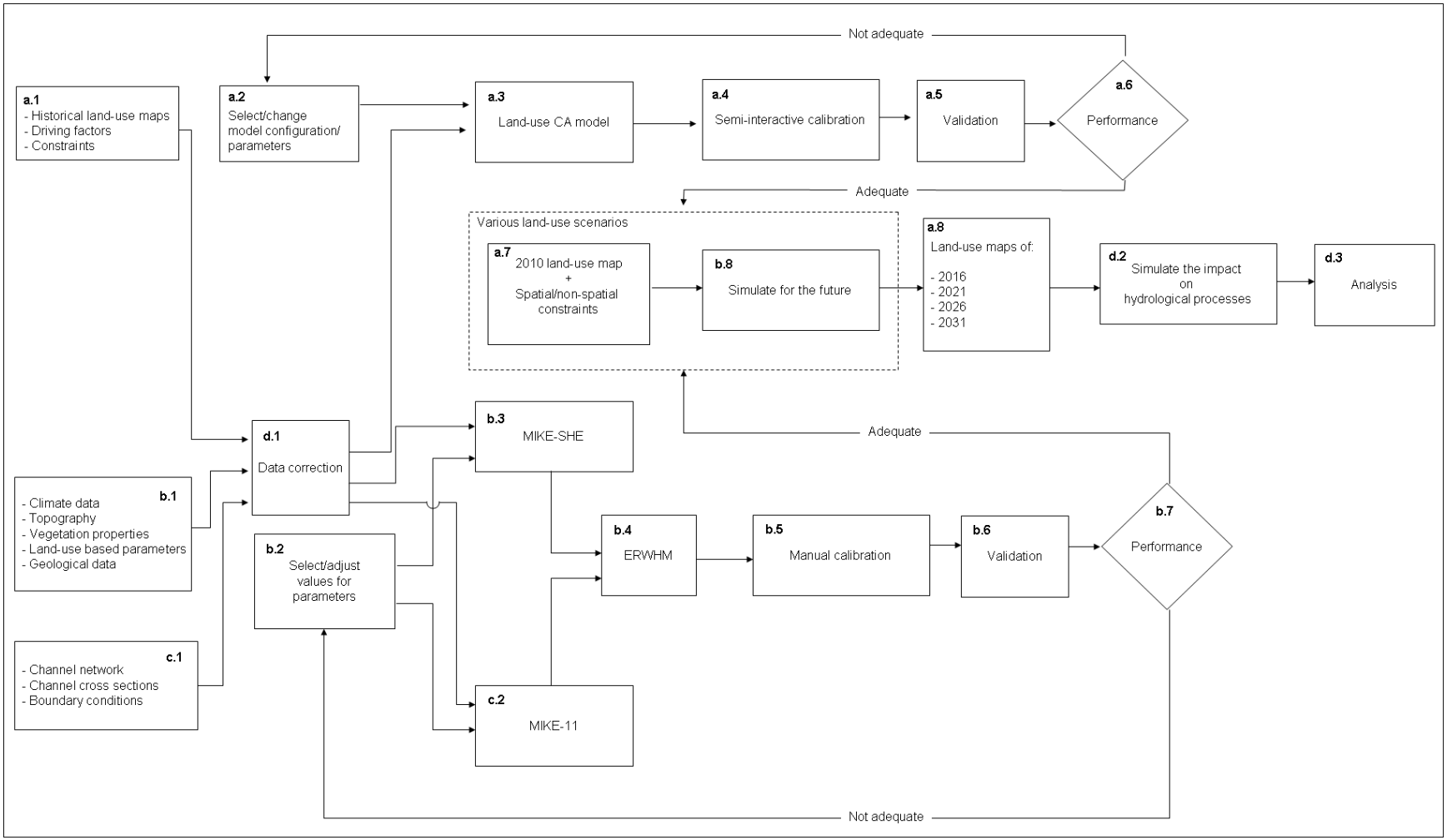

Figure 2.1: Flow diagram displaying the steps involved in developing the proposed modeling system. Steps with codes a.x, b.x, c.x, and d.x are relevant to land-use CA, MIKE-SHE, MIKE-11, and the coupled modeling system respectively

The following sections explain the flow of operations displayed on Figure 2.1. Section 2.2.1 describes the steps: a.1 to a.6 while Sections 2.2.2, 2.2.3 and 2.2.4 describe the steps (b.1, b.3, b.4, c.1, c.2), (b.2, b.5, b.6, b.7), and (a.7, b.8, a.8, d.2, d.3) respectively. The step d.1 (data correction) corresponding to the land-use CA model is described under the section 2.2.1, while the ones corresponding to MIKE-SHE and MIKE-11 are described in the section 2.2.2.

2.2.1 Land-use CA model: parameterization, calibration and validation

The implementation of the CA model includes five main steps: 1) the creation of the historical land-use maps needed to calibrate the CA, 2) the definition of the neighborhood configuration, cell size, and driving factors, 3) the transition rule extraction and the model calibration, 4) a sensitivity analysis to cell size, neighborhood configuration, selection of external driving factors and parameter values, and 5) the simulation procedure.

2.2.1.1 Generating the historical land-use maps to calibrate the CA

For the calibration of the CA model, a set of historical land-use maps were generated by a remote sensing specialist using Landsat Thematic Mapper imagery acquired during the summers of 1985, 1992, 1996, 2001, 2006 and 2010. These maps are at 30 m resolution and cover the whole watershed. This historical sequence of data allows the identification/detection of trends in land-use changes over a period of 25 years and a variety of factors influencing land-use changes.

In the historical land-use classification, the following land-use classes were identified:

1-Water: water bodies including rivers, creeks, lakes and ponds

2-Road: principal and secondary roads

3-Rock: bare rocks located in the Rockies, as well as on low elevation ground

4- Forest: including conifer and deciduous stands, woods and shrubs

5-Agri-Land: crop-on and harvested agricultural lands

6- Grassland: mostly located above the tree line, sometimes mixed with small shrubs

7- Parkland: vegetated lands mixed with trees, shrubs, and weeds

8- Construction/Open Area: construction sites

9- Recreation Area: golf courses and parks

10- Clear-cut: forested zones where most trees have been cut and removed

11- Urban Area: built up and urbanized areas

13- Forest Reserves: reserves within forest areas

14- Developed Land: cleared land, prepared for construction

15- Undeveloped Land: cleared land, but with low vegetation.

In the above classification, forest is represented as one class. A division into evergreen and deciduous types was essential to define time-varying vegetation properties more accurately. For example, the leaf area index (LAI) value of evergreen forests stays more or less the same across the year whereas the LAI value of deciduous forests is lower during the fall and the winter seasons than during spring and summer. The class forest was therefore divided into ‘Evergreen’ and ‘Deciduous’. The other vegetation types were grouped into two classes: agriculture and rangeland/parkland.

To perform the discrimination of evergreen forests against deciduous forests, two temporal Landsat TM images collected from the Geographic Information Centre at the University of

Calgary library were used. One image was acquired in May 2000 and the other in September 2000. The algorithm ‘Tasseled Cap’ was applied to produce an index measuring the ‘greenness’ of the image. Using a selected lower and upper threshold of the greenness index, the evergreen forest areas were discriminated from the deciduous. This method was applied on the two TM images of May and September 2000 to create the 'evergreen' and 'deciduous' classes within the land-use map of 2001 assuming that the land use has not changed significantly from 2000 to 2001 in the study area. Additional satellite images (TM) of 1993 and 1997 (for the month of May) were downloaded from USGS to differentiate between ‘evergreen’ and ‘deciduous’ on the land-use maps of 1992 and 1996. A program was written to read the 1992, 1996, and 2001 land-use maps and apply this above classification on all historical land-use maps to re-classify the forest class into evergreen and deciduous. Furthermore, a different index (NDVI - Normalized Difference Vegetation Index) was used to verify the classification.

The final land-use maps include the following classes:

1 – Water, 2 – Road, 3 – Rock, 4 – Evergreen, 5 – Deciduous, 6 – Agriculture, 7 - Rangeland/Parkland, 8 - Built-up, and 9 - Clear-cut.

The generated land-use maps were compared with high resolution third party imagery from Google© maps. At the spatial locations where the land-use classification could not be verified correctly, field visits were done by the remote sensing specialist and gathered data were used to correct the classification. The obtained overall classification accuracy of the land-use maps is 79% for the year 1985, 77% for 1992, 80% for 1996, 82% for 2001 and 82% for 2006 and 2010. In addition, experts were consulted to verify some of the land-use distribution. For example,

officials at the administration office of the Tsuu T'ina nation were met to verify the boundary of their territory and to confirm the very limited land-use changes in that area. Meetings were conducted with industry and government representatives (a list of participants during one of the meetings organized is presented in Appendix G.1) to obtain feedback on the historical land-use changes and gathered spatial data to cross-verify the classification. The additional data obtained for this purpose include agricultural maps (raster maps of crop data for the years 2009 and 2010 obtained from Agri-Environment Services Branch (AESB), Agriculture and Agri-Food Canada), the Alberta vegetation inventory, a map showing different categories of vegetation existing in southern Alberta (AEP 1991) .

Finally, an in-house computer program was applied to detect and correct minor spatial-temporal inconsistencies in the historical maps due to classification and georeference errors. The following rules were applied within each land-use map and the found errors were corrected.

a) The cells or patches of rock and agriculture that have changed to forest in a land-use map of a later year were changed back to rock or agriculture. Also, cells of forest reserves which belong to some other classes in a land-use map of a later year were changed back to forest reserves.
b) Individual cells that were of one particular land-use while being surrounded by cells that were in other land uses were changed to the majority of land use within their Moore neighborhood (that comprises eight adjacent cells).
c) For cells that were built-up consecutively on two or three land-use maps, the corresponding cells in the next land-use map if different were changed back to built-up.

d) If the cells within the land-use map at time instance t=0 were of built-up and the corresponding cells of the land-use maps of time instances t=1 and t=2 were of the same land-use class but not built-up, then the corresponding cells at t=0 was changed from built-up to the state of the cells of the land-use maps corresponding to t=1 and t=2. This was applied to all historical maps.

e) For the cells that were built-up in the land-use maps at time instance t=0 and t=2, then the corresponding cells in the land-use map at time instance t=1 were changed to built-up if they have a different attribute. This was applied to all historical maps.

f) If cells were not evergreen or deciduous in a map, and the corresponding cells were evergreen or deciduous in the other land-use maps, these cells were changed to the appropriate forest class (evergreen or deciduous).

g) Vector datasets of water bodies (ponds, river network) were used to correct the classification in the land-use maps. The cells that were located outside the identified water regions were changed to the majority class within its Moore neighborhood.

These steps ensured the quality of the land-use maps required for the calibration of the CA model. The historical maps generated using the above procedure, are presented in Appendix A. The model domain selected for the land-use CA model is the east part of the Elbow River watershed from the vertical dashed line as displayed on the Figure 2.2. The west part of the watershed from the vertical dashed line is mainly mountainous where rock and forest classes exist. The forested areas are forest reserves; therefore this portion of the watershed is considered mostly unchanged compared to the rest of the watershed during the historical period considered in this study (1985-2010). Removing this unchanged portion from the land-use maps made the

calibration and simulation process of the land-use CA model significantly more efficient. After simulating the land-use changes in the east part of the watershed (Fig 2.2), the west part was mosaicked to produce the simulated land-use change maps for the entire watershed.

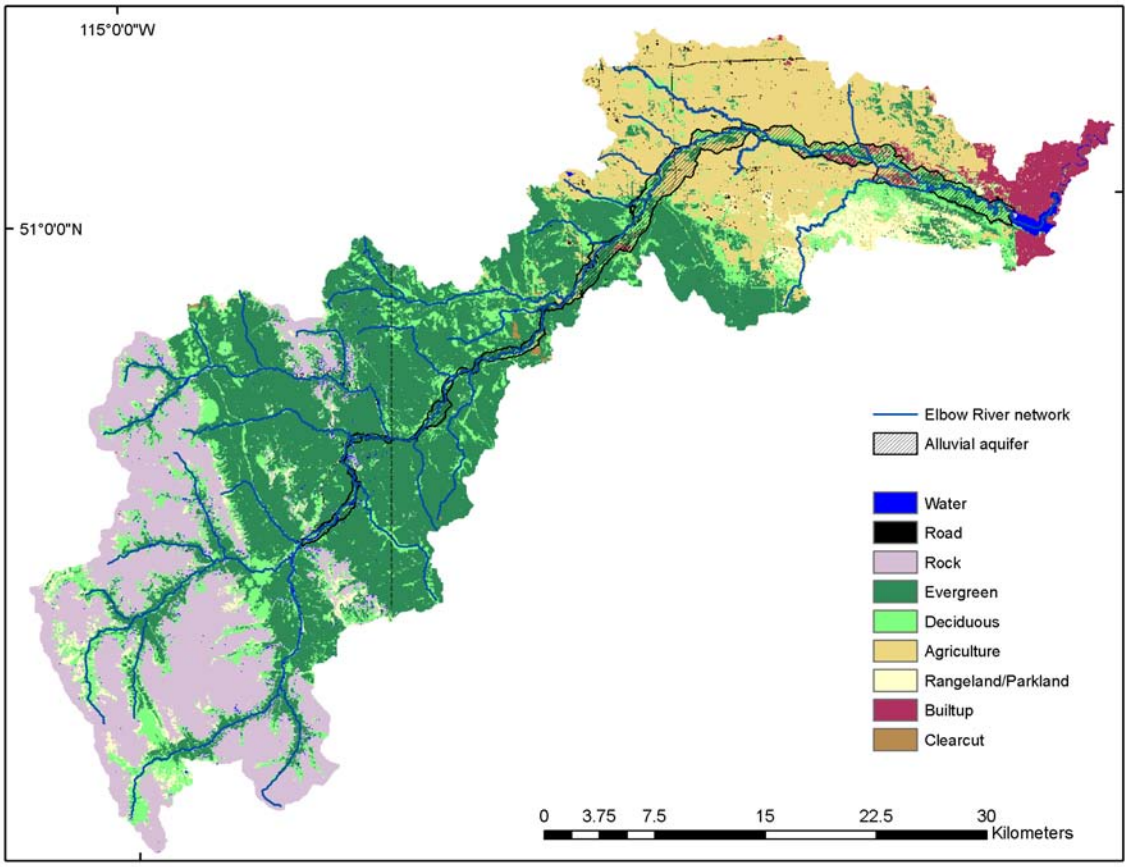

Figure 2.2: Land-use map of 1985 displaying the model domain of the land-use CA model. The east portion of the watershed from the vertical dash line is the model domain selected for the land-use CA model

2.2.1.2 Cell size, neighborhood configuration, and driving factors selection

The land-use CA model used in this study operates on a regular cell-based structure. Several studies have shown that the cell size and the neighborhood configuration have an impact on the outcomes of cell-based CA models and should not be arbitrarily chosen (Benenson 2007, Chen and Mynett 2003, Kocabas and Dragicevic 2006, Ménard and Marceau 2005, Moreno *et al.*

2009, Pan *et al.* 2010, Samat 2006). To guide the selection of the cell size, an examination of the historical land-use maps was performed; it revealed that most land-use changes were occurring over four or more contiguous pixels. To reduce computational time while maintaining the desired level of spatial details for the study, the land-use maps were resampled at 60 m and 100 m (these scales are more appropriate to create land-use based parameters for MIKE-SHE) using the nearest neighbor algorithm available in ArcGIS 9.1 (ESRI 2006). A sensitivity of the CA model to these two cell sizes was further conducted.

The neighborhood configuration of the CA model approximates a circle around a center cell and comprises several concentric neighborhood rings (Fig. 2.3). The influence of the neighboring cells on the central cell is constant within each ring, but differs between the rings. This configuration reduces spatial distortions, when compared to an extended Moore neighborhood as every cell located at a given distance from the center cell is considered in the neighborhood (Li and Yeh 2002). The modeler can choose the desired number and size of concentric neighborhood rings around a cell. While testing all neighborhood configurations was beyond the scope of this study, a sensitivity analysis was conducted using several neighborhood configurations defined around each central cell. The number of circular rings within the neighborhood configuration was changed between 2 and 3 and different distances to each ring were systematically tested.

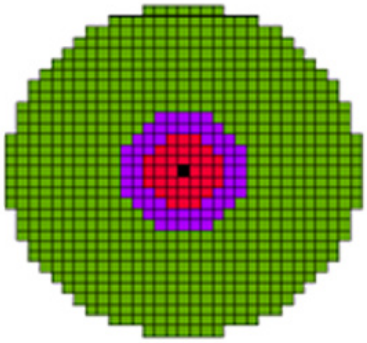

Figure 2.3: Neighborhood configuration of the land-use CA model

Land-use changes are complex spatial processes resulting from the interactions of socio-economic (e.g., population growth), biophysical (e.g., slope and soil quality), and geographic (e.g., proximity and accessibility to services) factors operating at different spatial and temporal scales (Liu and Phinn 2003, Verburg *et al.* 2004). In this study, in addition to the influence of the cells located within local and extended neighborhoods as previously described, four external driving factors were considered as parameters in the transition rules, namely the distance to Calgary city center, the distance to a main road, the distance to a main river, and the ground slope. Such factors are commonly recognized in the literature as influencing land-use changes (Fang *et al.* 2005, Li and Yeh 2002, Pijanowski *et al.* 2002, Wu 2002). Spatial maps with each cell defining the level of influence for these driving factors were prepared using existing tools (Euclidian distance, Slope) available in ArcGIS 9.1 (ESRI 2006). The resulting distance files were stored as raster images of the same resolution and extent as the land-use maps. A sensitivity analysis was carried out to evaluate which external driving factors will adequately capture the dynamics of the study area and generate the best land-use simulation outcomes. All four external factors and the possible combinations of three factors were tested in the sensitivity analysis.

2.2.1.3 Transition rule extraction and model calibration

A detailed description of the model calibration can be found in Hasbani *et al.* (2011). A summary of the procedure is presented here. The transition rules are dynamically extracted during the calibration of the model. The number of cells of a particular state in the neighborhood of each central cell is computed using the set of historical maps. For each type of land-use change that is under consideration, all cells that have changed state in the historical maps are identified. Using this information, for each land-use transition, frequency histograms are generated displaying the percentage of cells that have changed state when considering values of a particular driving factor and the number of cells of a particular state in the neighborhood.

Figure 2.4 provides an example of a frequency histogram. Line A of the Figure 2.4a shows the total number of Evergreen cells in the watershed against the distance to a main road while line B shows the Evergreen cells that have changed to Built-up as observed in the historical data (reveals the relative contribution of the transition from Evergreen to Built-up). A detailed analysis of the cells that have changed from Evergreen to Built-up areas when considering their distance to a main road (Figure 2.4b) reveals that 8% of these cells are located between 150 and 180 m of a main road while 98% of the cells are within 1250 m of a main road. At 1250 m, there is an inflexion point on the cumulative occurrence curve, expressing that this distance is critical for interpreting the influence of a main road on this land-use change. The farther a cell was located from a main road, the less often it changed from Evergreen to Built-up area.

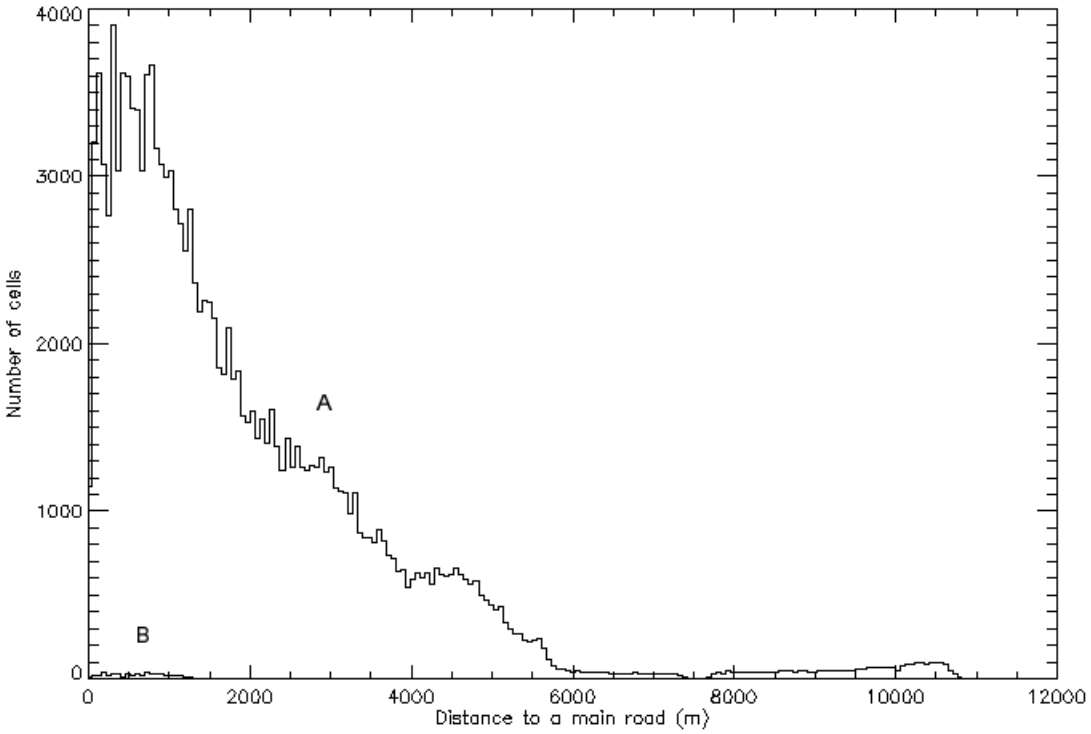
4000
3000
2000
1000
0
Number of cells
A
B
0
2000
4000
6000
8000
10000
12000
Distance to a main road (m)

a)

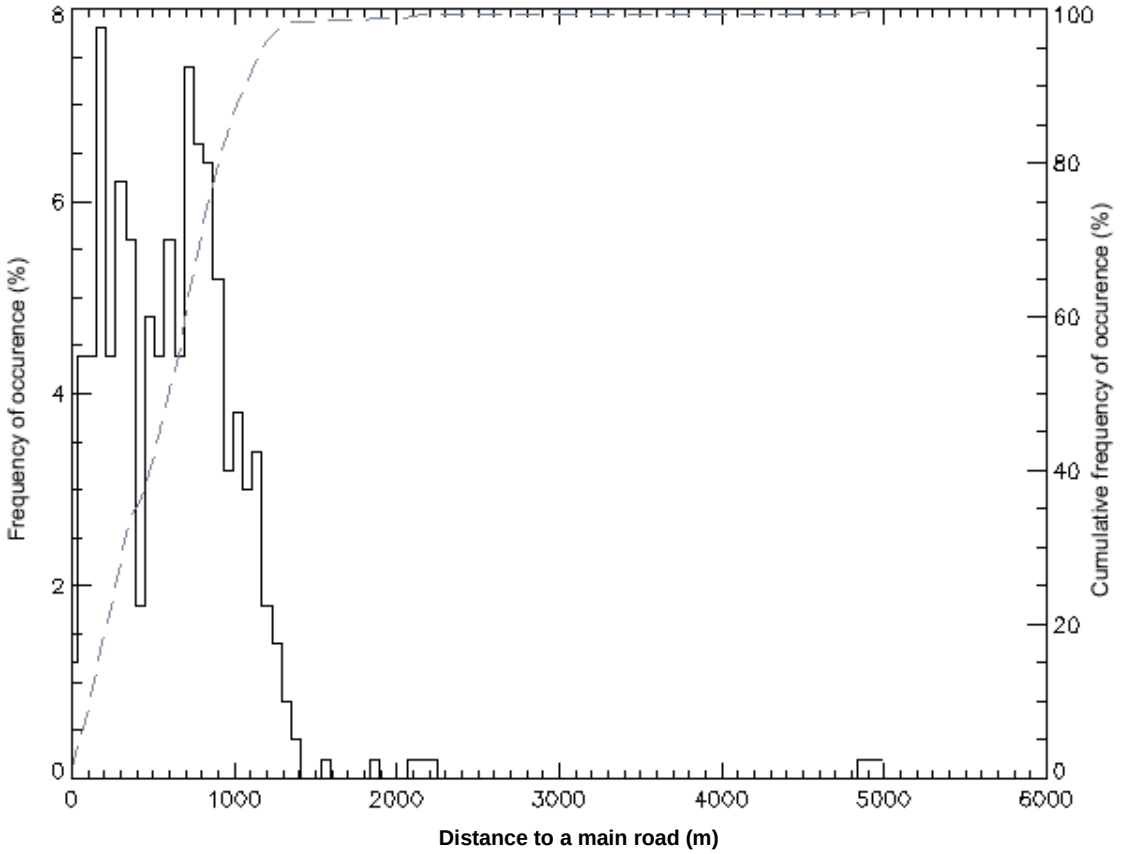

b)

Figure 2.4: a) Frequency histogram comparing the total number of Evergreen cells located at a certain distance from a main road (A) with the number of Evergreen cells that have changed from Evergreen to Built-up areas when considering their distance to a main road (B); b) Frequency histogram displaying the percentage of cells that have changed from Evergreen to Built-up areas when considering their distance to a main road; the dashed curve represents the cumulative occurrence of the cells located at a certain distance from a main road (Hasbani *et al.* 2011)

Figure 2.5 shows the graphical user interface where these histograms are displayed and interpreted by the modeler who can identify the ranges of values of each driving factor and neighborhood composition to be included in conditional transition rules.

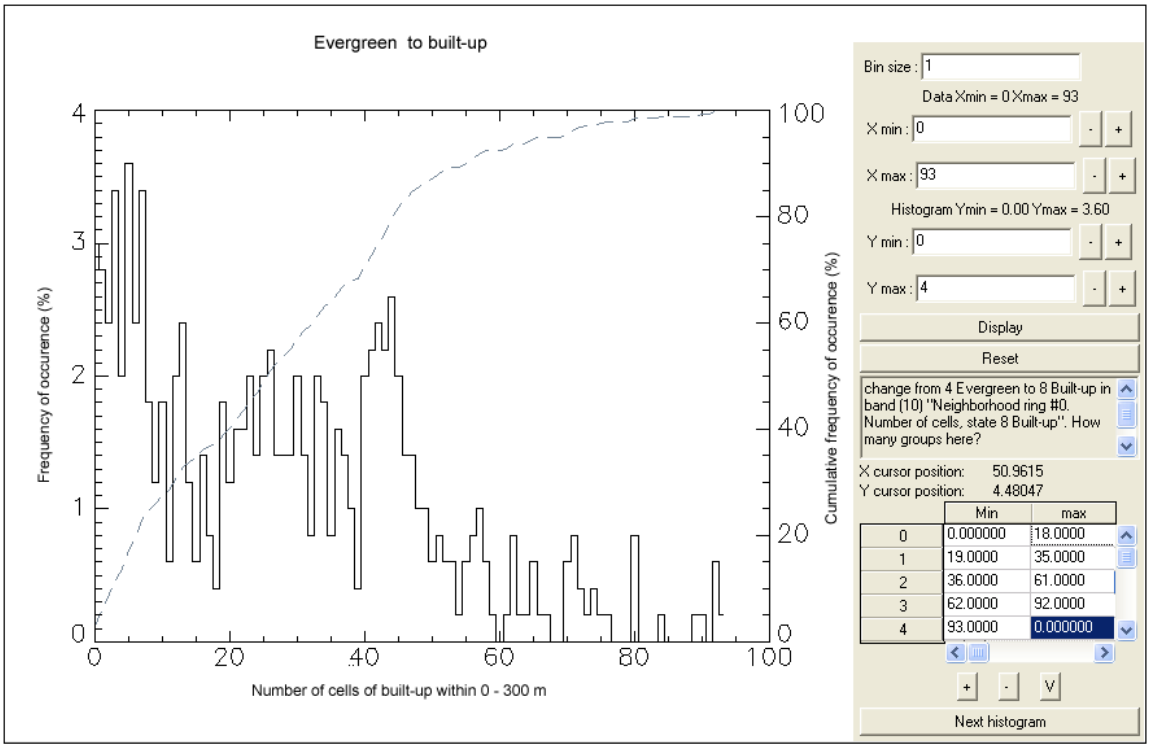

Figure 2.5: On the left: Frequency histogram displaying the percentage of cells that have changed from Evergreen to Built-up when considering the number of Built-up cells within 300 m of these cells; on the right: graphical interface designed for the selection of the range of values to be considered in the conditional transition rules (Hasbani *et al.* (2011)

By clicking on the histogram, the modeler can identify and set the ranges of values (minimum and maximum) for each neighborhood configuration, driving factor and cell state within that neighborhood. These values are stored in a table (Table 2.1) and are used to construct the conditional transition rules within the land-use CA model. An example of such a rule defined from Table 2.1 is:

If distance to a main road is between 0 and 427 m

and number of evergreen cells within the first neighborhood ring is between 0 and 17

and number of built-up cells within the second neighborhood ring is between 0 and 14

and number of agriculture cells within the third neighborhood ring is between 0 and 168

then the central Evergreen cell has a high probability to change from Evergreen to Built-up area (becomes one of the transitional rule considered for a cell transition).

Table 2.1: Ranges of values identified from the frequency histogram to be used for determining the conditional transition rules

Cell state	Distance to a main road (m)	Number of Evergreen cells located within the first neighborhood ring [0 to 300) m	Number of Built-up cells located within the second neighborhood ring [300 to 540) m	Number of Agriculture cells located within the third neighborhood ring [540 to 1020) m	…..
Evergreen	0 to 427	0 to 17	0 to 14	0 to 168	
	428 to 1408	18 to 50	15 to 59	169 to 258	
		51 to 74	60 to 92	259 to 377	

These conditional rules are then automatically converted into mathematical rules. The mean and standard deviation of the defined ranges of values on the frequency histograms are computed to become the coefficients of the parameters of the mathematical transition rules. Using the coefficients of each transition rule, a resemblance index (RI) is calculated using Equation 2, which quantitatively describes the similarity between the neighborhood content of a cell at the time of the simulation and the neighborhood contents that have been used to generate the values of the parameters of the transition rule.

$$RI = \sum_{i=1}^{m} \frac{| n_i - \overline{x}_i |}{\sigma_i} \qquad \text{Equation 2}$$

where m is the number of layers (corresponding to the number of driving factors plus the number of land-use classes multiplied by the number of neighborhood rings), n_i is the value in layer i, $\overline{x}_i$ is the mean value for layer i in the transition rule and σ_i is the standard deviation for

layer *i* in the transition rule. Eight land-use state transitions as listed in Table 2.2 were considered during the extraction of the transition rules from the historical data (Hasbani *et al.* 2011).

Table 2.2: Land-use transitions considered during the simulations

From	**To**
Evergreen	Agriculture
Deciduous	Agriculture
Evergreen	Built-up
Deciduous	Built-up
Agriculture	Built-up
Rangeland/Parkland	Built-up
Rangeland/Parkland	Agriculture
Agriculture	Rangeland/Parkland

2.2.1.4 Sensitivity analysis to cell size, neighborhood configuration, selection of external driving factors and their values from frequency histograms

A sensitivity analysis of the land-use CA model was conducted in order to find the best configuration parameters (cell size, neighborhood configuration, selection of external driving factors and their values from frequency histograms). To conduct this sensitivity analysis, the land-use CA model was calibrated using the historical land-use maps of 1985, 1992, 1996, and 2001. The land-use map of 2006 was simulated by the calibrated land-use CA model using the initial land-use map of 2001. The simulated land-use map of 2006 was then compared with the reference map of the same year. The Kappa simulation index (K_{sim}), designed to compare

categorical maps generated by simulation models as proposed by Van Vliet *et al.* (2010) was used to compare the simulated map with the reference map. These coefficients express the percentage of agreement between two categorical maps including both quantity ($K_{transition}$) and location information ($K_{transLoc}$) (Hagen 2003, Visser and de Nijs 2006, Pan *et al.* 2010,). This index overcomes the drawback of the standard kappa statistics which tend to over-estimate the agreement between a simulated map and a reference map as they do not distinguish between the cells that change and do not change from the initial land-use map. Kappa simulation index, on the other hand take into account the cells that do not change when evaluating the agreement between a simulated and a reference map. As a result, the calculated kappa index simulation is very sensitive to changes in the spatial patterns of the simulated map when compared with the reference map. Therefore, this method was used for the sensitivity analysis to investigate the impact of different parameterization of the land-use change model on the simulation of the 2006 land-use map. The values of K_{sim} range from -1 (no agreement) to 1 (perfect agreement).

During the sensitivity analysis, the cell size was changed between 60 m and 100 m (Appendix F.1), and 20 different neighborhood configurations listed in Appendix F.2 were selected with different number of rings and different distances to those from the center cell. Furthermore, different methods of selecting the parameter values from the frequency histograms listed in Appendix F.3 were tested. Five different combinations out of four external driving factors were also tested (Appendix F.4).

Additional details regarding the sensitivity analysis and its interpretation can be found in Hasbani *et al.* (2011). The results of the sensitivity analysis are summarized in Appendices F.1,

F.2, F.3, and F.4. They revealed that the best simulation outcomes were obtained with a cell size of 60 m, a neighborhood configuration defined by three rings of respectively 5, 9 and 17 cells, or 300, 540 and 1020 m, a selection of the parameter values from the frequency histograms concentrated around the modes, and the use of all four external driving factors. This overall configuration was therefore selected for further simulations (Appendix F).

2.2.1.5 Simulation procedure

Using the mathematical transition rules that were created during the calibration, the simulation of land-use maps corresponding to future time instances was implemented. The procedure is as follow. For each time step, the neighborhood composition of every cell is read and the level of correspondence with the parameters of the transition rules is computed. The cells having the highest level of correspondence based on user-specified constraints and influence of each transition rule are subjected to state changes. Decision on which cell should be associated to each type of land-use change is made by recursively sorting the type of land-use changes and selecting the cell having the smallest RI value. Once the required number of cells associated to each type of land-use change is met or when no more cells can be assigned, the model writes the new land-use map and updates the statistics that correspond to the percentage of cells associated to each rule and each type of change. If the numbers of cells associated to each rule and each type of land-use change is different than the numbers found from the historical data and previous time steps, a correction is applied at the next time step (Hasbani *et al.* 2011).

To assess the quality of the simulation results, the CA model was calibrated using the historical land-use maps of 1985, 1992, 1996, and 2001 and the most appropriate cell size, neighborhood

configuration, driving factors, and parameter values from the frequency histograms as revealed by the sensitivity analysis. Based on the dynamically derived transition rules during the calibration, and using the land-use map of 2001 as the initial map, the land-use maps of 2006 and 2010 were simulated. In all simulations, two local constraints were applied to forbid new built-up development within the Tsuu T'ina Nation reserve and to restrict any changes in the forest reserves within the Kananaskis Improvement District. Using these constraints, the quality of the calibration of the CA model was evaluated by comparing the simulated land-use maps of 2006 and 2010 with the reference land-use maps. The comparison was done using a neighborhood of five cells to capture the land-use patterns while dismissing the exact spatial location within the neighborhood (Hasbani 2008). A percentage of correspondence is calculated by dividing the correct number of cells in all land-use categories by the total number of cells within the neighborhood and by taking an average of the calculated percentages for the entire map. A correspondence of 96% and 91% was obtained for the years 2006 and 2010, respectively. Based on these results, the CA model was considered sufficiently well calibrated for the purpose of this study (Wijesekara *et al.* 2012).

2.2.2 The Elbow River Watershed Hydrology Model (ERWHM): the model setup

To obtain a complete representation of the Elbow River network, MIKE-SHE was dynamically linked to the one-dimensional hydrodynamic surface water model MIKE-11 to create the Elbow River Watershed Hydrology Model (ERWHM). The configuration of the ERWHM includes comprehensive surface water and groundwater components (Fig. 2.6).

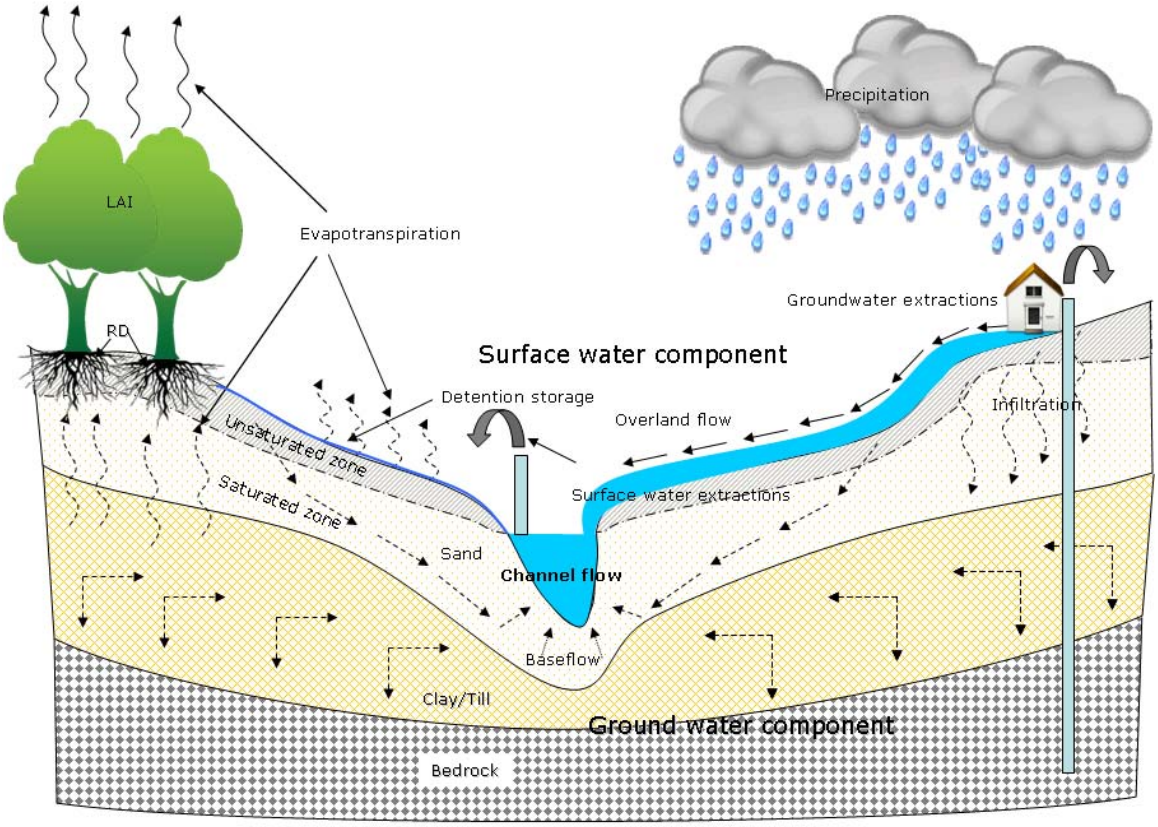

Figure 2.6: Diagram representing the hydrologic processes that are modeled by the ERWHM and some of the data required in configuring the surface and groundwater components

The first task in configuring the ERWHM was to determine its model domain. The configuration of the MIKE-11 channel module within ERWHM requires a boundary condition assigned at the downstream end of the watershed. Beyond the downstream end of the Glenmore reservoir, the existing measured data (e.g., river flow) are based on the operational rules of the reservoir gates. The boundary condition of the ERWHM could not be dependent on these data since the operational rules of the reservoir gates were not available for the configuration of ERWHM. Therefore, the downstream end of the boundary of the selected model domain was extended only up to the end of the Glenmore reservoir (Fig. 2.7). Taking the model domain boundary any further downstream of the Elbow River could introduce uncertainty in the model simulations.

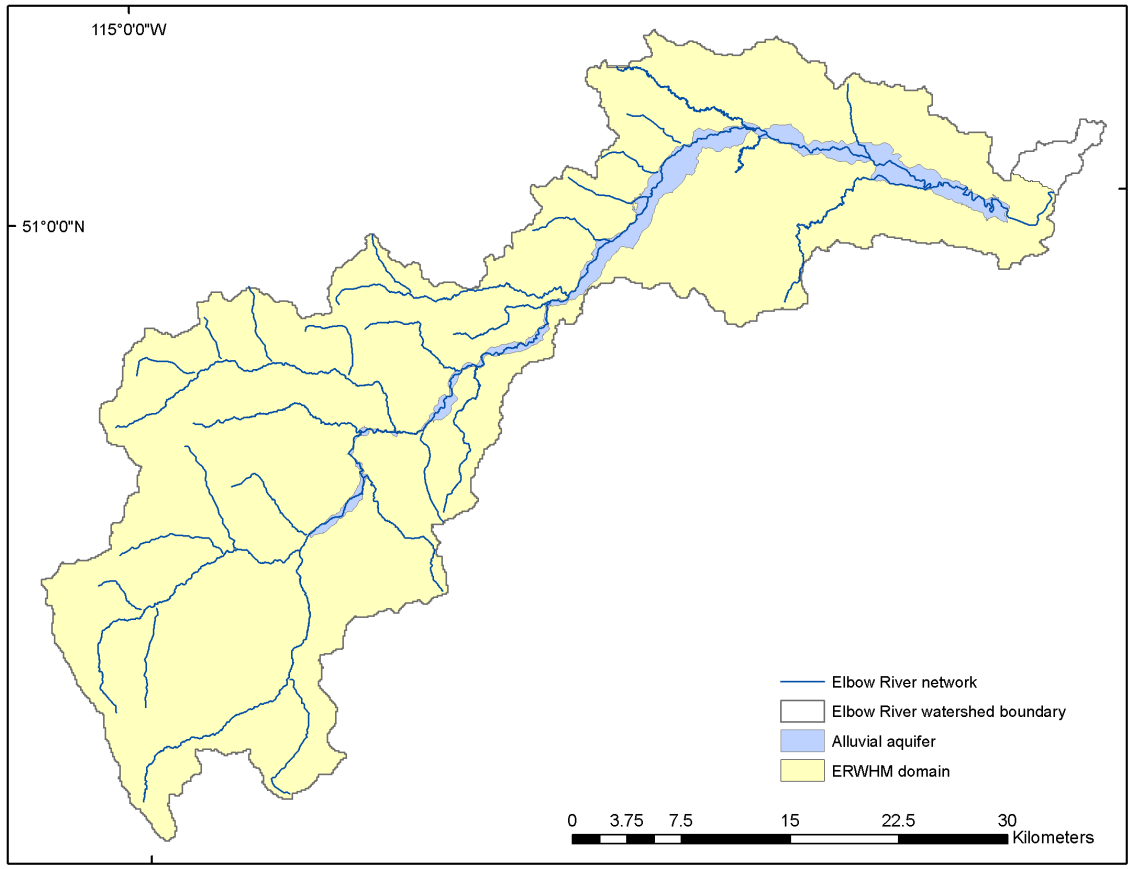

Figure 2.7: ERWHM model domain

The following section provides a description of each category of relevant data and parameters used for developing the ERWHM, including climate data, topography, vegetation parameters, land-use based hydrologic parameters, channel flow data, and the initial groundwater table.

2.2.2.1 Data and parameters

I. Topography

An 80 m resolution DEM from GeoBase (GeoBase 2008), re-sampled at 200 m (to fit the model operating scale – explained under section 2.2.3), was used (Fig. I.1). This DEM was revised by adding the bathymetry data of the Glenmore Reservoir (DHI Water and Environment 2010).

II. Climate data

Daily precipitation, temperature, and potential evapotranspiration available for 1961-2008 were acquired from the Agroclimatic Atlas of Alberta that includes climate data from over 1200 stations in Alberta and about 1400 stations bordering Alberta and British Columbia, Saskatchewan, Yukon, Northwest Territories, Nunavut and the United States. These climate data have been interpolated for each township of Alberta by the Government of Alberta (2008). In setting up MIKE-SHE, raw station-based precipitation data were used by developing Thiessen polygon 'areas of influence' for each station. The temperature and potential evapotranspiration data remained township based (Wijesekara and Marceau 2012) (Fig. 2.8). Furthermore, the orographic effect on precipitation and temperature was represented by temperature lapse rate of -0.75°C/100 m and precipitation lapse rate of 10%/100 m (DHI Water and Environment 2010). In configuring MIKE-SHE with the temperature data, minimum and maximum temperatures for each day for each township was set at 2.00 AM and 2.00 PM, respectively. Within each model time step and when used within components like snowmelt, MIKE-SHE interpolates the temperature value.

III. LAI (leaf area index) and RD (Root depth)

The leaf area index (LAI) and root depth (RD) define the vegetation properties of the model domain. These components govern the precipitation interception on leafs and the evaporation and water transpiration through roots. Each land use on the historical land-use maps has these properties that vary through time. LAI values vary from 0 to 7. During the full leaf period, Evergreen and Deciduous have a value of 5 while agriculture has a value between 2 and 4 during the summer period (Table 2.3). For seasonal vegetation, this value drops to 0.2 during the winter months. Root depth values are average depths of actual root zone of the vegetation. Forest areas are usually defined with a higher root depth which is considered a constant. Root depth values for agricultural areas begin at 0, peak when the crops are fully grown, and drop down to 0 when the crops are harvested. In order to setup ERWHM, the LAI values were calculated for each land-use class for each month of the year for the period Sept. 2000 – Sept, 2001 based on remotely sensed LAI maps and on scientific literature (with comparison to standard LAI values based on types of vegetation) (Myneni *et al.* 2003, LPDAAC, 2009, Scurlock *et al.* 2001, Zeng 2001). Values for RD relevant to agricultural areas were derived by averaging the RD values of the four most commonly harvested crops (wheat, barley, canola, and tame hay) in southern Alberta. The temporal changes of the root depth for the agricultural areas and the root depth values for the rest of the vegetation classes were obtained from the literature (Allen *et al.* 1998, Task Committee on hydrology handbook 1996, Heritage community foundation 2002, Kim *et al.* 2005).

IV. Manning number M (Inversion of standard Manning's n)

Manning's M defines the surface roughness of the land surface and governs the surface runoff. These values are derived from the literature while their spatial distribution is based on each land-use map (Wijesekara *et al.* 2012). The values of Manning's M assigned to each land-use were: Water: 25.04, Road: 76.9, Rock: 40.0, Evergreen: 10.0, Deciduous: 10.0, Agriculture: 28.57, Rangeland/parkland: 33.33, Built-up: 90.9, Clear-cut: 90.9. Maps of manning's M generated for each historical land-use map are found in Appendix B.

V. Detention storage

Detention storage represents the threshold storage depth at land surface in each cell that must be filled before overland flow is generated. This parameter was used when the DEM could not adequately represent the details of topographic depressions due to the coarse scale of the model grid. Detention storage was defined for each land-use class as follows: Water: 0mm; Road: 0mm; Rock: 10mm; Evergreen: 20mm; Deciduous: 20mm; Agriculture: 20mm; Rangeland/Parkland: 20mm; Built-up: 0mm; Clear-cut: 0mm. These values were derived through sensitivity analysis and calibration. Generated maps of detention storage corresponding to each historical land-use map are provided in Appendix D.

VI. Paved runoff coefficient

Paved runoff coefficient assigned under land-use determines the fraction of water from the overland flow that is directly transferred to the near by ponds/lakes/river links. Based on each land-use, the built-up areas was assigned a value of 1 (100% of overland flow is drained without

any infiltration). Distributed paved runoff coefficient maps generated based on this are found in Appendix E.

VII. Overland-groundwater leakage coefficient

The overland-groundwater leakage coefficient reduces the infiltration rate at the ground surface to the value specified with this parameter. Assigning this parameter reduces both the infiltration rate and the seepage outflow rate across the ground surface. For each land-use change, a distributed parameter value of 1e-013 m/s is assigned to built-up areas and the Glenmore reservoir. Distributed overland-groundwater leakage coefficient maps generated based on this are found in Appendix E.

VIII. Snowmelt parameters

Snowmelt can dramatically affect the spring runoff timing and volume. In MIKE-SHE, it is determined by data and parameters such as air temperature, melting threshold temperature, degree day coefficient (determines the rate of melting), minimum snow storage (determines the minimum snow storage needed to cover an entire cell), and maximum wet snow fraction (determines the maximum amount of wet snow from snow melting that can be held by snow, additional wet snow will form runoff). A temporal changing value for the degree day coefficient parameter was derived using the information obtained from Kuusisto (1980) and was adjusted during calibration (Fig. 2.9). A value of 0.5 °C for the melting threshold temperature in the mountainous area (elevation higher than 1700 m) and a uniform value of 0 for the remaining area were used in ERWHM. These values were found during the calibration. Additional parameter

adjustments done during calibration included setting the minimum snow storage value to 100 mm and the maximum wet snow fraction to 0.1 (DHI Water and Environment 2010).

IX. Unsaturated zone flow/ ET

An 11-class soil classification map was included to represent the unsaturated zone. Appropriate soil parameters for each class were created and values were assigned to soil water content (at saturation, field capacity, and wilting point) and saturated hydraulic conductivity. MIKE-SHE uses these parameters to determine the infiltration in the saturated zone. The 11-class soil classification and relevant properties were obtained and calculated initially from the Agricultural Region of Alberta Soil Inventory Database and the Canadian Soil Information Service Data sources. These properties were subsequently revised and re-calculated using the average physical properties of different horizons in the unsaturated zone (Table 2.4). Furthermore, the soil maps were overlaid with the land-use maps and the built-up areas were combined with the soil maps. This was done to define the paved areas and assign them a low saturated hydraulic conductivity value so that most water runs off instead of infiltrating into the soil. The newly added areas (paved) in the soil map were assigned the soil code 11 and appropriate soil properties (Wijesekara and Marceau 2012) (Appendix C).

A uniform value of 0.1 m was applied for the entire basin to define the evapotranspiration (ET) surface depth. This parameter corresponds to the thickness of the capillary zone that determines the ET from the unsaturated zone (Wijesekara and Marceau 2012).

X. Channel flow

The representation of the channel flow is managed by MIKE-11 and is dynamically linked to MIKE-SHE. A total of 35 river branches were added to the current river network consisting of main and several minor tributary branches in the upper watershed to help direct the overland flow into the main tributaries and rivers. A total of 353 cross sections were added, which include field surveyed and LiDAR generated cross sections. Surveyed cross sections of the Elbow River and its branches were revised to correct inconsistencies with the topography. 76 surface water extractions (28 seasonal and 48 all season) were included to the existing river network. All upstream unconnected river branches begin at the headwaters of the river network and were set as no-flow boundaries (water is introduced to the streams via overland and baseflow). The downstream boundary of the model was selected as the water level in Glenmore Reservoir. Appropriate value for the riverbed resistance in Manning's M (30.0) and riverbed leakage coefficient, the parameter that regulates the exchange of water between the groundwater and channel flow components of the model (1e-006 s^{-1}) were found through sensitivity analysis (DHI Water and Environment 2010, Wijesekara *et al.* 2012, Wijesekara and Marceau 2012).

XI. Initial groundwater table

The initial groundwater levels played a key role in the calibration of the model. The initial groundwater potential for each geological layer was derived by running MIKE-SHE (from 1961 to 1981) in steady-state mode using a constant, spatially variable recharge, and using a constant water level boundary condition along the river network (DHI Water and Environment 2010).

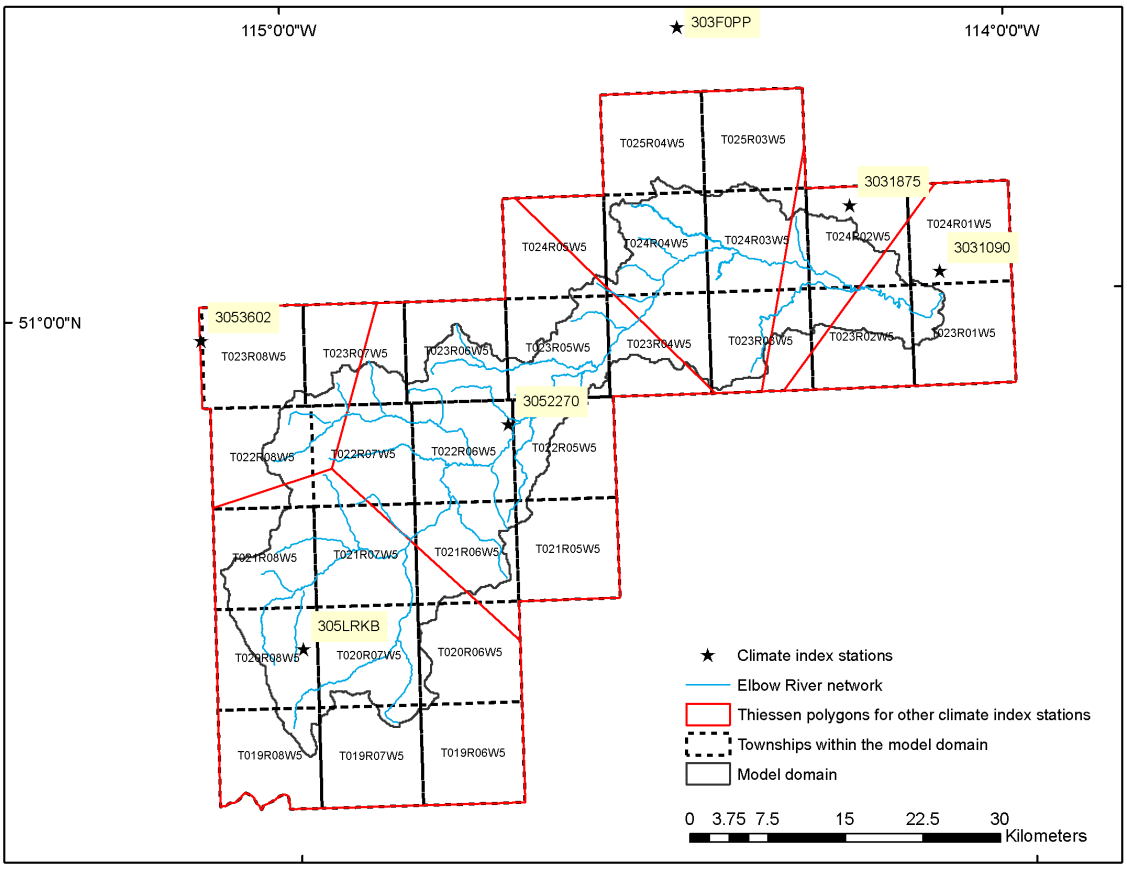

Figure 2.8: Thiessen polygons generated from the climate index stations and township boundaries within the Elbow River watershed

Table 2.3: Derived LAI and RD values for each land-use class. This table shows the constant or temporal changing values for LAI and RD for each land use. Temporal changing LAI and RD values are illustrated in graphical format. For example: Deciduous forest areas have a constant RD value of 2000 mm, where the LAI values change from 1 (in January) to 5 (in June) and back to 1 (in December)

Land-use	**LAI**	**RD (mm)**
Water	0	0
Road	0.2	10
Rock	0.2	10
Evergreen	5	2000

Deciduous	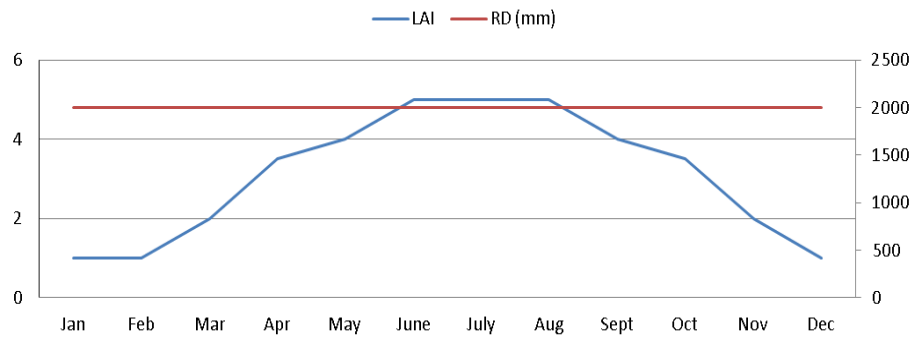	
Agriculture	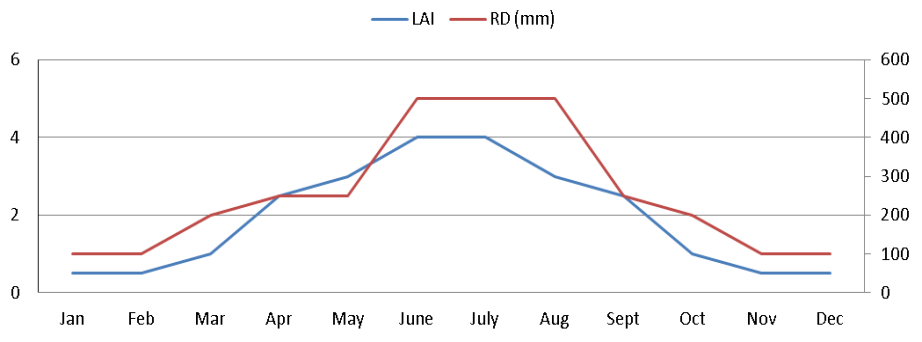	
Rangeland/parkland	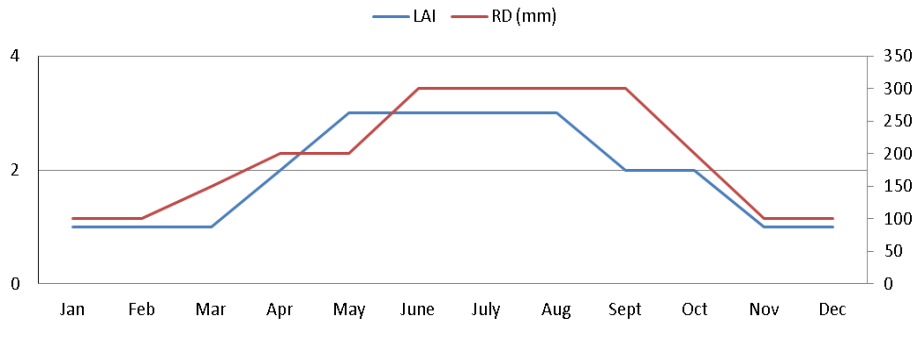	
Built-up	0.5	100
Clear-cut	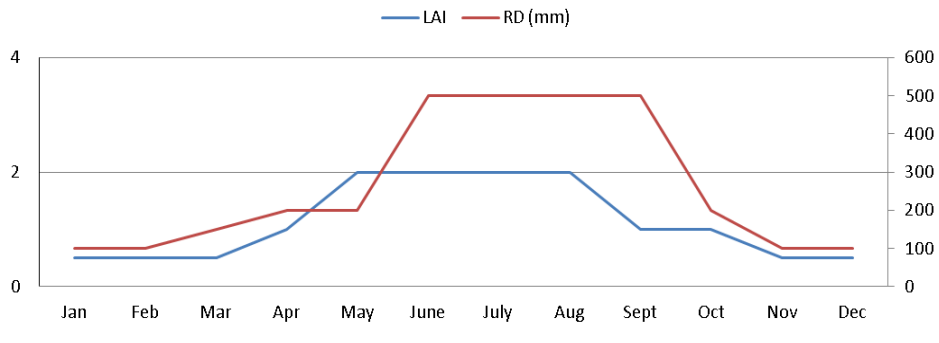	

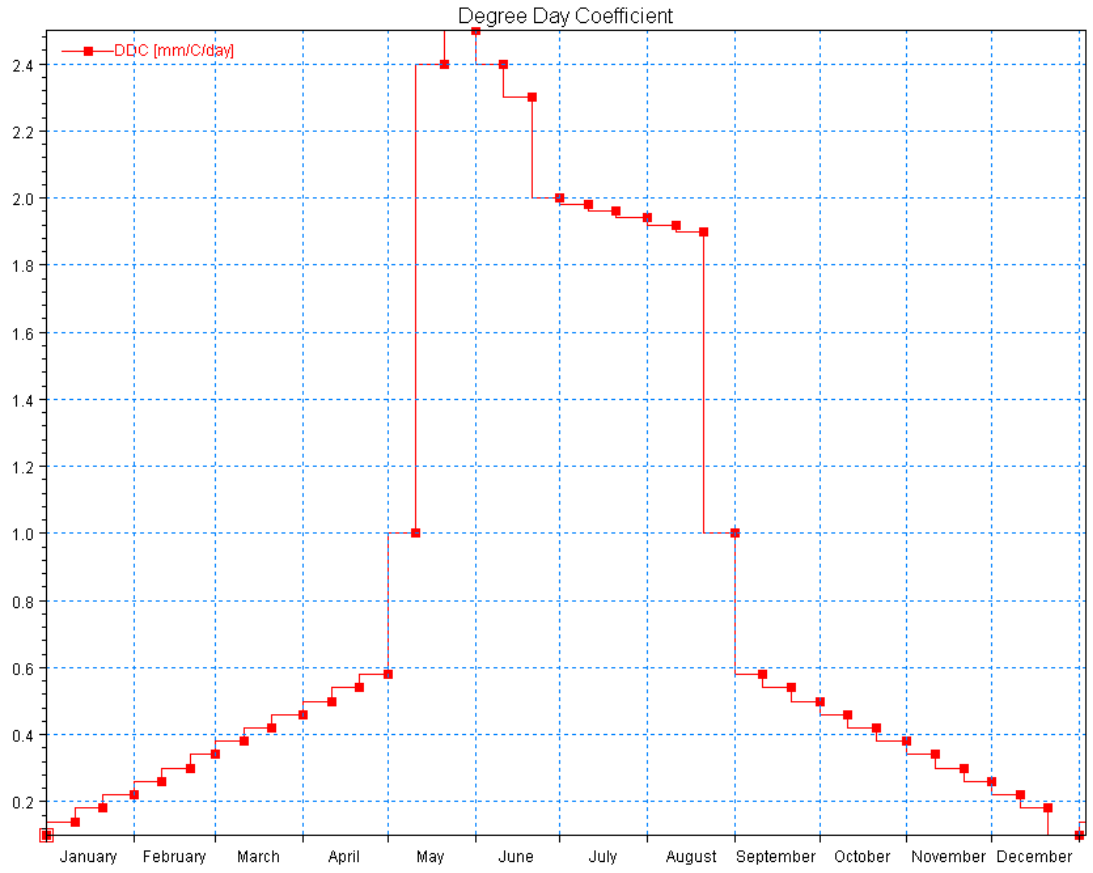

Figure 2.9: Annual distribution of degree day coefficient values (mm/C/day)

Table 2.4: Soil properties for each soil code used within the UZ zone in MIKE-SHE

Soil Type (Grid code)	Saturated Hydraulic Conductivity K_{sat} (m/s)	Water Content at Saturation, θ_s	Water Content at Field Capacity θ_{fc}	Water Content at Wilting Point θ_{wp}
1	3.4e-005	0.49	0.27	0.20
2	1.5e-005	0.53	0.36	0.27
3	1.7e-005	0.54	0.36	0.30
4	2.9e-005	0.48	0.28	0.21
5	5.3e-005	0.48	0.21	0.16

6	4.4e-005	0.61	0.14	0.19
7	2.7e-005	0.46	0.30	0.19
8	6.3e-005	0.53	0.21	0.15
9	4.1e-005	0.48	0.26	0.17
10	2.7e-005	0.47	0.30	0.19
11	2.7e-12	0.49	0.31	0.23

Using the above mentioned data, relevant modules/components within MIKE-SHE and MIKE-11 were configured in developing the ERWHM. The following sections include the details about the comprehensive surface water, ground water components, and snowmelt, ET, and unsaturated zone modules used in developing the ERWHM.

2.2.2.2 Surface water component

The surface water component in ERWHM includes the overland flow and channel flow processes that are represented by comprehensive methods. Each grid element representing the watershed contains a unique set of physical properties that governs the changes of the overland flow. The ERWHM uses a finite difference method for simulating overland flow. This method solves a two-dimensional diffusive wave approximation of the Saint Venant equations to calculate the surface flow in the x- and y-directions and the water depths for each grid cell of the model domain using the following equations:

$$uh = K_x(-\frac{\partial z}{\partial x})^{1/2} h^{5/3} \qquad \text{Equation 3}$$

$$vh = K_y(-\frac{\partial z}{\partial y})^{1/2} h^{5/3} \qquad \text{Equation 4}$$

where:

h is the flow depth above ground surface (m)

uh and *vh* represent discharge per unit length along the cell boundary in the x- and y-directions, respectively [m^2s^{-1}],

K_x and K_y are Manning M or Strickler coefficient in the x- and y- directions, respectively.

Using Equations 3 and 4, the flow across any boundary between grid cells is given by:

$$Q = \frac{K\Delta x}{\Delta x^{1/2}}(Z_U - Z_D)^{1/2} h_u^{5/3} \qquad \text{Equation 5}$$

where:

K is the appropriate Strickler coefficient,

h_u is the depth of water that can freely flow into the next cell, and

Z_u and Z_D are the maximum and minimum water levels, respectively (mm).

The associated data and parameters for simulating the overland flow in the ERWHM are topography, surface roughness, detention storage, and unsaturated zone flow/ ET (section 2.2.2.1).

Channel flow is modeled by MIKE-11, which uses fully dynamic, diffusive, or kinematic approximations of the Saint Venant equations. In this study, a fully dynamic solution of Saint Venant equations was used to simulate surface water along the river channels in order to

accurately calculate the exchange flow between the channels and the overland flow. The governing equations used in this method are the vertically integrated equations of conservation of volume and momentum (Equations 6 and 7).

$$\frac{\partial Q}{\partial x} + \frac{\partial A}{\partial t} = q \qquad \text{Equation 6}$$

$$\frac{\partial Q}{\partial t} + \frac{\partial (\alpha \frac{Q^2}{A})}{\partial x} + gA\frac{\partial h}{\partial x} + \frac{gQ|Q|}{C^2 AR} = 0 \qquad \text{Equation 7}$$

where,

Q is the discharge,

A is the flow area,

q is the lateral inflow,

h is the stage above datum,

C is the Chezy resistance coefficient,

R is the hydraulic or resistance radius, and

α is the momentum distribution coefficient.

The numerical solution of these equations is based on the implicit finite difference scheme developed by Abott and Ionescu (1967). In this scheme, the equations are transformed into a set of implicit finite difference equations and are applied in a computational grid consisting of alternating points of the discharge, Q and water level h, and are computed at each time step. The relevant data and parameters associated in setting up the MIKE-11 channel flow module, i.e.,

digitized river network with tributaries, cross sections, surface water extractions, boundary conditions, and river bed resistance are described in the section 2.2.2.1. MIKE-SHE and MIKE-11 were integrated using links created with each river reach/branch in MIKE-11 with the surface water components of MIKE-SHE.

2.2.2.3 Groundwater component

A groundwater model based on a 3D finite difference method was adopted to represent the saturated zone of the Elbow River watershed. This approach uses sub-surface layer information including hydro-geologic stratification and hydro-geologic properties for each layer. The 3D finite difference algorithm calculates flow by describing the spatial and temporal variations of the dependent variable (hydraulic head) mathematically using a 3-dimensional Darcy equation (Equation 8) solved numerically by an iterative implicit finite difference technique. The saturated zone component of flow interacts with the other components in MIKE SHE primarily by using flow terms from the other components implicitly or explicitly as source or sink terms.

$$\frac{\partial}{\partial x}\left(K_h \frac{\partial h}{\partial x}\right)+\frac{\partial}{\partial y}\left(K_h \frac{\partial h}{\partial y}\right)+\frac{\partial}{\partial z}\left(K_v \frac{\partial h}{\partial z}\right)-Q=S\frac{\partial h}{\partial t} \qquad \text{Equation 8}$$

where:

$h(x, y, z)$ is the hydraulic head,

K_v, K_h are the hydraulic conductivities in vertical and horizontal directions,

S is the specific storage coefficient, and

Q is the volumetric source/sink term.

Three geological layers (sand, clay/till, bedrock) were used to represent the saturated zone (Fig. 2.6). Twenty-four new geological parameters were created for these layers i.e., vertical and horizontal hydraulic conductivity, specific yield, and specific storage for six geological units used to define the three layers: alluvial aquifer, sand and gravel, clay/till, bedrock, top layer of the mountains, and clay/river. Initial values were assigned from past studies and field measurements and were further used to calibrate the groundwater model. The final values of each geological parameter after calibration are listed in Table 2.5. To consider the water extraction from the bedrock aquifers within the 3D groundwater module, a total of 145 licensed groundwater pumping wells were included; it was assumed that 50% of the water extracted from these wells will return to the groundwater following its use. The details of the initial groundwater table used as the initial condition in running simulations of the comprehensive groundwater component are provided in the section 2.2.2.1.

Table 2.5: Values of geological parameters in saturated zone after calibration

Geological unit	Soil code (SZ)	Horizontal conductivity (m/s)	Vertical conductivity (m/s)	Specific yield (-)	Specific storage (m^{-1})
Alluvial aquifer	1	0.0004	4e-005	0.2	0.001
Sand&Gravel	2	1e-005	2e-006	0.2	0.001
Clay/Till	3	1e-008	1e-009	0.05	0.0005
Bedrock	4	5e-008	5e-009	0.05	0.0005
TopLayer_Mt	5	0.0005	0.0002	0.1	0.001
Clay/River	6	1e-006	1e-007	0.2	0.001

2.2.2.4 Snowmelt, ET, and unsaturated zone modules

The method selected in the snowmelt module in the ERWHM is the modified degree day method, whereby the rate of melting increases as the air temperature increases. Snow melting for each cell by air temperature (M_T) is determined by multiplying the degree day coefficient (C_T) by the difference of the current air temperature (T_{air}) and the temperature threshold at the corresponding cell (T_0) (Equation 9). Air temperature, which varies considerably throughout the watershed over time, is the most important input parameter in determining the ability of the model to predict snow accumulation and melt. Compared to models based on the energy balance method, this method requires less data and is less computationally intensive. Energy balance methods are considered more appropriate for dense forests and mountain areas; however they significantly contribute to increasing the total computational time. The well-parameterized degree-day method can usually be calibrated for all climatic conditions; it was therefore implemented in this study.

$$M_T = C_T.(T_{air} - T_0) \qquad \text{Equation 9}$$

Between surface water and groundwater, the flow within the unsaturated zone was assumed vertical and was modeled using the two-layer water balance method in the current setup of ERWHM. This method uses a simple mass-balance approach to represent the unsaturated zone, and accounts for interception storage changes, surface ponding, and water content in the root zone, infiltration, evapotranspiration, and groundwater recharge. The ET module in MIKE-SHE uses meteorological, vegetation-based parameters such as LAI and RD and soil moisture to simulate ET. It simulates evaporation from interception storage in the canopy, evaporation from

the soil surface, transpiration of water by plant roots based on soil moisture in the unsaturated zone, and transpiration from groundwater if the rooting depth exceeds the thickness of the unsaturated zone. This method assumes that if sufficient water is available in the root zone, it is available for evaporation. The calculation of ET proceeds using a top down approach. This method calculates ET from the canopy (E_{can}), ponded water (E_{pon}), unsaturated zone (E_{uz}), and saturated zone (E_{sz}) consecutively. The total ET is calculated as the total of all (Equation 10).

$ET_a = E_{can} + E_{pon} + E_{uz} + E_{sz}$ Equation 10

If the average water content calculated exceeds the maximum water content of the unsaturated zone, the groundwater recharge is produced. The infiltration is determined based on the following equation.

Inf = min (pw, sat. cond. x t, ($\theta_{sat} - \theta_{actual}$) x D_{layer}) Equation 11

where :

Inf = Infiltration

pw = ponded water

sat. cond. = saturated conductivity

t = duration of a time step

θ_{sat} = water content at saturation

θ_{actual} = actual water content, and

D_{layer} = layer depth.

The two-layer water balance method considers that the unsaturated zone consists of one or two layers (Fig. 2.10). The upper layer is considered from the ground surface to the ET extinction depth. The ET extinction depth is defined as the maximum depth where water can be removed from the saturated zone by the roots through ET, and is the root depth + the thickness of the capillary fringe. If the water table is at the ground surface, then the thickness of the upper layer becomes zero. If the water table is below the ET extinction depth, then a second layer is added that extends from the bottom of the first layer to the water table. If the water table is above the ET extinction depth, the thickness of the lower layer is zero.

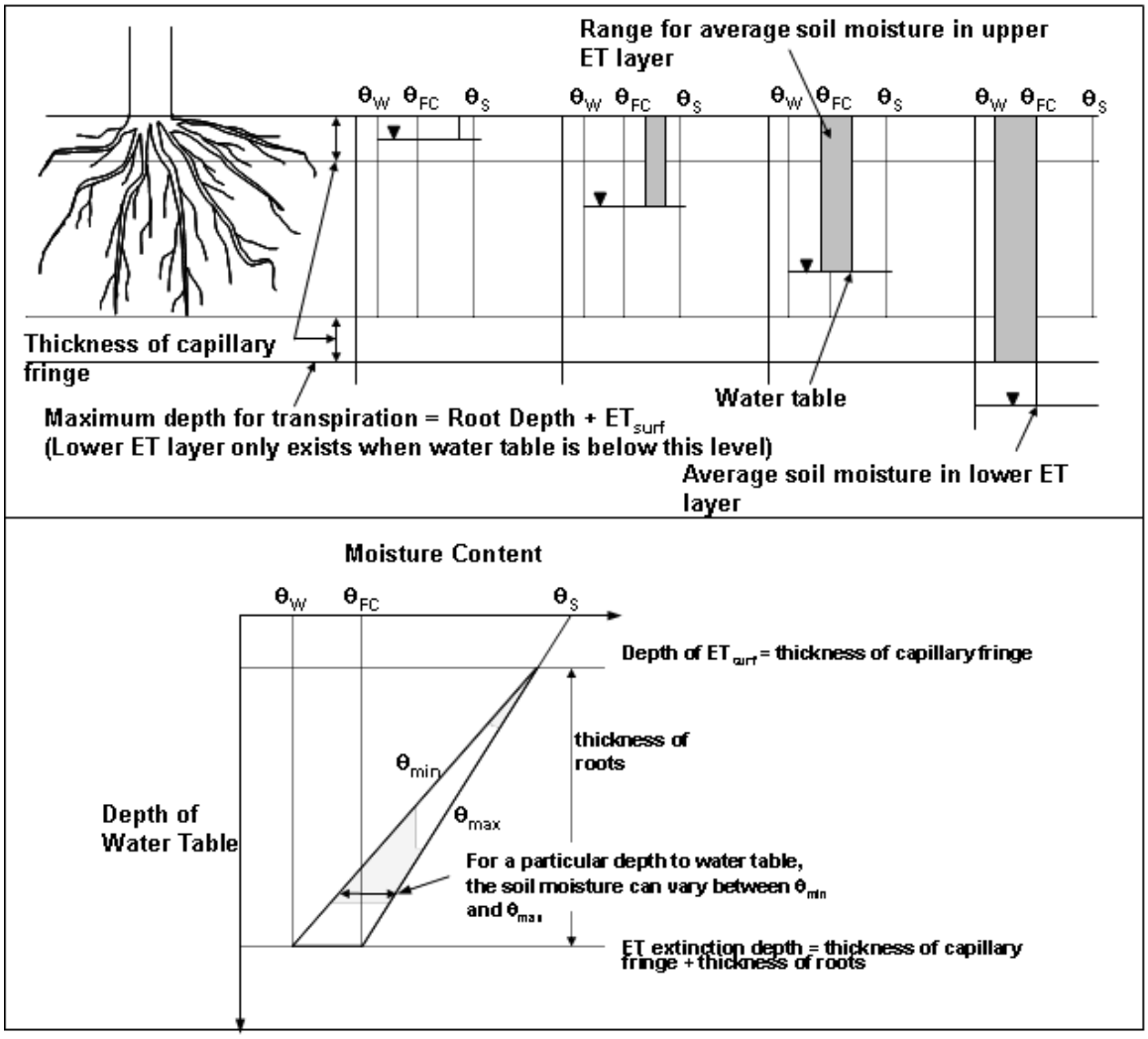

Figure 2.10: How soil moisture condition varies with the depth of water table in the two-layer water balance method (adapted from DHI (2009))

If the water table is at the ground surface, then the average moisture content of the unsaturated zone equals the saturated moisture content, θ_s. When the water table is below the ground surface and above the ET extinction depth, then the average water content in the upper UZ layer varies between $\theta_{\min}$, a minimum water content, and $\theta_{\max}$, a maximum water content calculated according to Fig. 2.10. $\theta_{\max}$ is the water content that would be present if no ET occurred. $\theta_{\min}$ is the minimum water content in the upper layer when ET is active. Both $\theta_{\min}$ and $\theta_{\max}$ decrease linearly with the depth of the water table from the ground surface, i.e., the average water content of the entire UZ soil column decreases as the water table drops. When the water table is at the ET extinction depth, the average water content of the upper UZ soil layer is between the field capacity, θ_{FC} and wilting point, θ_W. When the water table is below the ET extinction depth, then a lower UZ layer is added. The moisture content of the lower UZ layer is generally equal to θ_{FC} since ET is not active in the lower UZ layer.

The interaction between SZ zone and UZ zone occurs when the water table is above or at the ET extinction depth. If the actual water content calculated for the UZ zone θ_{act} is below $\theta_{\min}$, the UZ zone is supplied with water from the SZ zone until θ_{act} is equal to $\theta_{\min}$. When θ_{act} is above $\theta_{\max}$, water is transferred to the UZ zone and the groundwater is recharged until θ_{act} becomes $\theta_{\max}$. When the water table is below the ET extinction depth, there is no interaction between the SZ zone and the UZ zone.

2.2.3 Calibration and validation of ERWHM

The flowchart of actions taken to carry out a complete calibration and validation of the ERWHM is illustrated in Figure 2.11. With the configured surface water and groundwater components in ERWHM, a sensitivity analysis was first carried out for selected parameters, e.g., detention storage. Based on the sensitivity of ERWHM to these parameters, the most suitable parameterization was applied to the ERWHM. If the quality of the calibration was not found adequate, the parameters were further adjusted. The quality of calibration was assessed by comparing the observed and simulated data. This calibration procedure was carried out recursively until the best performance of the model was achieved. Once the quality of the calibration was improved, the ERWHM model was subjected through a rigorous validation based on a variety of conditions, details of which are elaborated below.

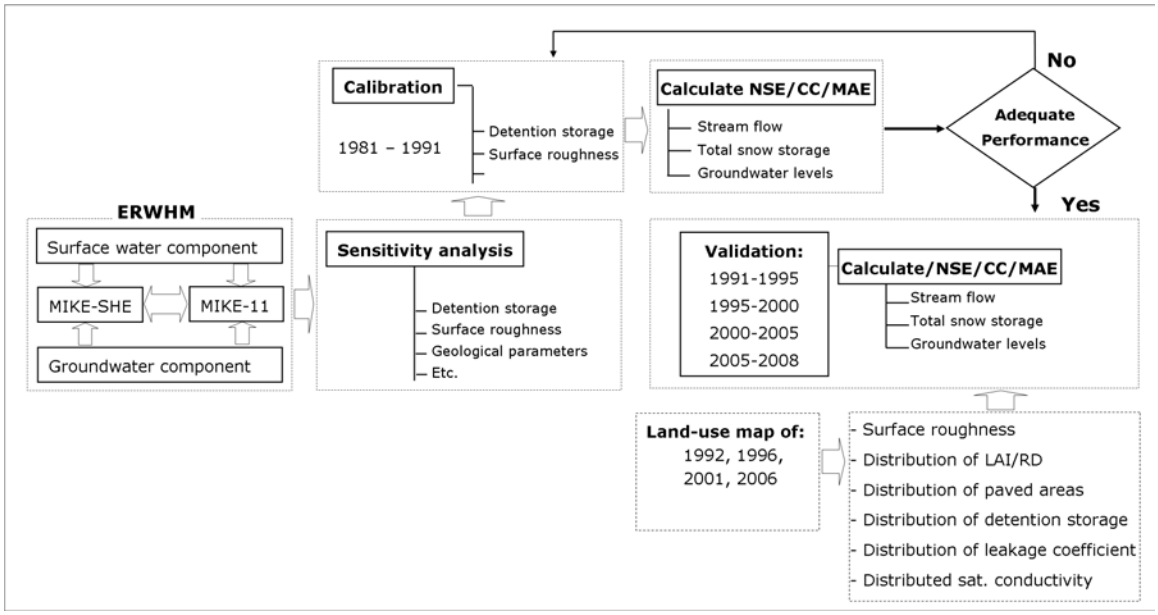

Figure 2.11: Diagram representing the calibration and validation procedure for the ERWHM

The sensitivity of the ERWHM to various model parameters (detention storage, snowmelt parameters, riverbed leakage coefficient, riverbed resistance, and geological parameters

associated with the geological layers) was analyzed first. A sensitivity analysis based on surface water parameters (detention storage, snowmelt parameters, riverbed leakage coefficient, and riverbed resistance) was conducted by manually changing the values of each parameter at a time and running the simulation of the ERWHM from 1981-1991. With each run, the goodness of fit of the model was evaluated by comparing observed and simulated total snow storage and stream flow data (details of this are found later in this chapter). This was repeated by changing the values of the parameters in combination (changing values of more than one parameter at a time). This approach was implemented intuitively (the combinations were selected based on the understanding on how parameter values impact the simulation results) since the number of combinations of parameter values can be large.

Secondly, an exhaustive sensitivity analysis was carried out for all 24 geological parameters of the 3D groundwater module; groundwater level measurements at groundwater wells (20 wells) and stream flow data were used to evaluate the sensitivity of the model. The sensitivity analysis was done at different stages: (i) changing the value of a single parameter for each geological unit at a time, (ii) changing two or more (maximum 4) parameters for each geological unit at a time, (iii) changing the value of a single parameter in more than one geological unit at a time, and (iv) changing multiple parameters in multiple geological units at a time, in a sequence. The remaining geological parameters at each stage were kept constant. Since testing every combination was practically unattainable, about 150 different combinations were selected intuitively.

The sensitivity analysis carried out based on surface water parameters revealed that snow melt parameters affected the total snow storage, while the other surface water parameters affected the stream flow. This further showed that the performance of ERWHM based on stream flow was mostly sensitive to detention storage, while total snow storage is sensitive to degree day coefficient, wet snow fraction, melting threshold, and minimum snow storage. The sensitivity analysis carried out based on geological parameters revealed that mainly the vertical and horizontal hydraulic conductivity parameters of the 3D groundwater model had an impact on the stream flow generation (as a result of changing baseflow and infiltration) and the temporal changing pattern of the generated groundwater table (with the change of infiltration). Based on this sensitivity analysis, initial values were assigned to each hydrological component and the values for the horizontal and vertical hydraulic conductivity were refined further during the calibration. When adjusting the values for the horizontal and vertical hydraulic conductivity, the fact that the horizontal conductivity is typically 5 to 10 times higher than the vertical hydraulic conductivity was considered.

A rigorous calibration and validation procedure was applied to the whole ERWHM based on different methods as recommended by Refsgaard (1997) i.e., split-sample, multi-criteria, and multi-point. The split-sample method emphasizes the use of different time periods for the calibration and the validation and a different land-use map as input for each validation. The multi-criteria method emphasizes the use of different criteria to evaluate the goodness of fit of the model based on different categories of observed data (i.e., use of stream flow and groundwater level to evaluate the overall goodness of fit). The multi-point method emphasizes the use of observed data from different spatial locations for the evaluation of the goodness of fit

for the calibration and the validation (i.e., use observed data at points A and B for calibration, and observed data at points C and D for validation).

Two grid sizes (100 m and 200 m) were considered as the model operating scale of the ERWHM based on the following factors:

- The scale at which localized land-use changes are better captured,
- The scale of the available data,
- The computational time required by the MIKE-SHE/MIKE-11 model setup,
- The extent of the study area, and
- Some technical limitations (the grid size of the input data must be an integer multiplum or fraction of the model grid size) of the MIKE-SHE model configuration in selecting the model grid size.

The grid size of 100 m has the advantage of capturing land-use changes and topography at a finer scale. Topographic data at finer scale are considered to be important in simulating water movements in MIKE-SHE mainly due to the fact that the topographic variations are lost at coarser scale (Refsgaard 1997). However, at that grid size, the method for simulating the groundwater component must be simplified to reduce the computational time required to complete hydrological simulations. Using a simple groundwater component, the linear reservoir method, the performance of the ERWHM was tested at 100 m grid size. The linear reservoir method is considered as a simple, conceptual, and aggregated method to simulate the saturated zone flow. Additional details on the linear reservoir method are available in Appendix J. The

performance tests using this model setup revealed that the complex surface-groundwater interactions existing in the Elbow River watershed were not accurately simulated. The 200 m grid size was found as being the best compromise between completing the simulation with ERWHM within a reasonable time period and capturing the effect of localized land-use changes when simulating the hydrological processes. Previous hydrological studies have shown that the loss of topographic details affects the model performance when the grid is coarser than 500 m (Refsgaard 1997), i.e., when the model grid size is coarser than 500 m, the topographic details such as the river valleys tend to disappear or be under-represented. This causes the model to perform poorly. Therefore, the selected grid size was considered an acceptable compromise.

The calibration of the ERWHM was done based on the time period 1981 – 1991. Its quality was measured using goodness-of-fit coefficients calculated on the total snow storage, stream flow, and groundwater levels. Observations from several stations were used to implement a rigorous calibration with the available data: measurements of snow storage at one snow station (Little Elbow, which is the only station where snow storage measurements were available), measurements of stream flow at four hydrometric stations (05BJ004, 05BJ006, 05BJ009, and 05BJ010), and measurements of groundwater level at 20 groundwater wells (Fig. 2.12).

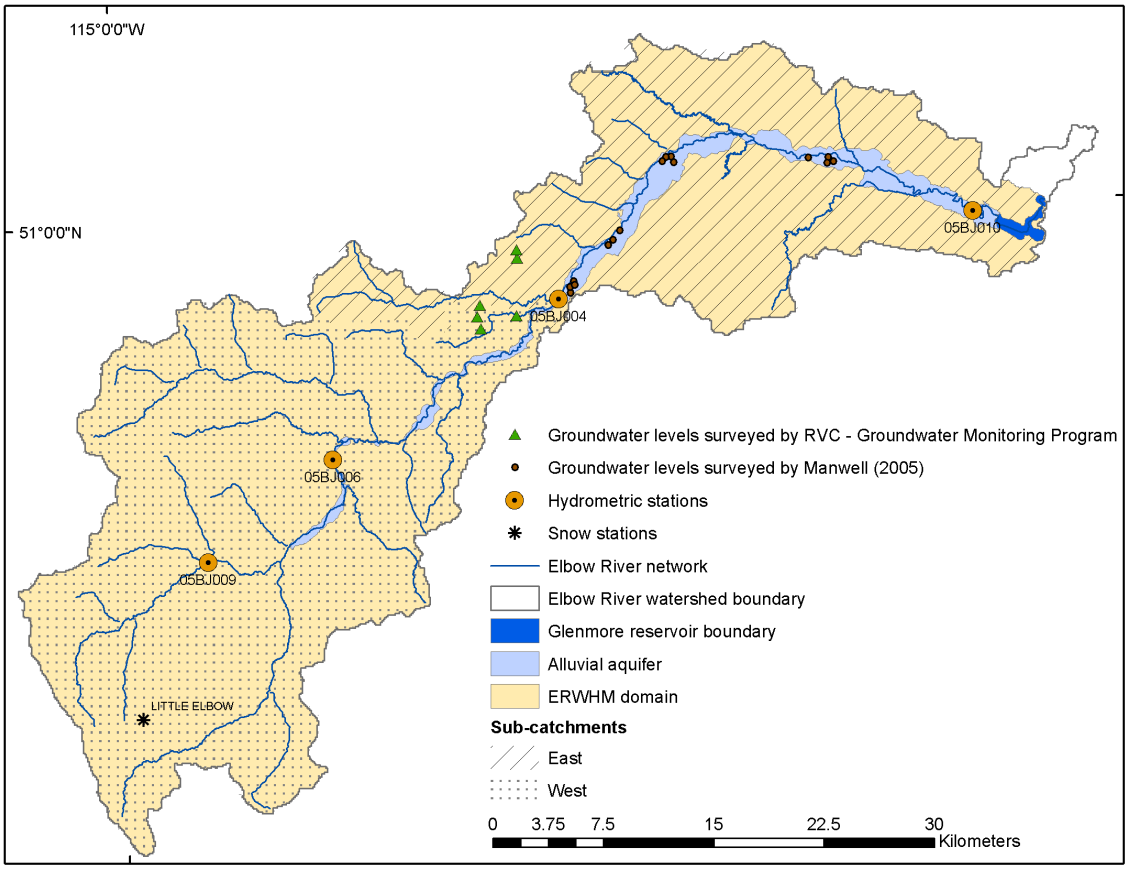

Figure 2.12: ERWHM model domain, location of the hydrometric stations, snow stations, and groundwater level stations in the east and west sub-catchments used for the calibration and validation of ERWHM

The validation was carried out based on four different time periods (1991-1995, 1995-2000, 2000-2005, and 2005-2008) using different land-use maps relevant to each validation period, i.e., 1992 land-use map for 1991-1995, 1996 land-use map for 1995-2000, 2001 land-use map for 2000-2005, and 2006 land-use map for 2005-2008. The goodness of fit of the ERWHM was evaluated in various ways. The correlation coefficient (Equation 12) was calculated by comparing observed and simulated total snow storage data. For the stream flow comparison, the Nash and Sutcliffe coefficient of efficiency (NSE) (Equation 12), the natural logarithmic (Ln) NSE (Equation 14), the coefficient of determination (Equation 15), and the relative NSE (Equation 16) for both daily and monthly data were calculated. The correlation coefficient (CC)

and mean absolute error (MAE) were calculated between observed and groundwater levels. The initial distributed groundwater potential value within the 3D groundwater module for each sub-surface layer within each simulation carried for the calibration and validation was derived from the previous corresponding simulation.

$$\text{NSE} = 1 - \frac{\sum_t (Obs_{i,t} - Calc_{i,t})^2}{\sum_t (Obs_{i,t} - \overline{Obs_i})^2} \qquad \text{Equation 12}$$

$$\text{Correlation Co.}(R_i) = \frac{\sum_t (Calc_{i,t} - \overline{Calc_i}).(Obs_{i,t} - \overline{Obs_i})}{\sqrt{\sum_t (Calc_{i,t} - \overline{Calc_i})^2 . \sum_t (Obs_{i,t} - \overline{Obs_i})^2}} \qquad \text{Equation 13}$$

$$\text{Ln NSE} = 1 - \frac{\sum_t (\ln Obs_{i,t} - \ln Calc_{i,t})^2}{\sum_t (\ln Obs_{i,t} - \overline{\ln Obs_i})^2} \qquad \text{Equation 14}$$

$$\text{Coefficient of determination} = (R^2{}_i) = \left(\frac{\sum_t (Calc_{i,t} - \overline{Calc_i}).(Obs_{i,t} - \overline{Obs_i})}{\sqrt{\sum_t (Calc_{i,t} - \overline{Calc_i})^2 . \sum_t (Obs_{i,t} - \overline{Obs_i})^2}} \right)^2 \qquad \text{Equation 15}$$

$$\text{NSE}_{rel} = 1 - \frac{\sum_t \left(\frac{Obs_{i,t} - Calc_{i,t}}{Obs_{i,t}}\right)^2}{\sum_t \left(\frac{Obs_{i,t} - \overline{Obs_i}}{\overline{Obs_i}}\right)^2} \qquad \text{Equation 16}$$

$Calc_{i,t}$ is the simulated flow at time *t*, at location *i*

$Obs_{i,t}$ is the observed flow at time *t*, at location *i*

$\overline{Calc_i}$ - is the mean simulated flow, at location *I,* and

$\overline{Obs_i}$ - is the mean observed flow, at location *i.*

2.2.4 Evaluating the impact of land-use changes on hydrological processes using ERWHM

Evaluating the impact of land-use changes on hydrological processes involves the following steps (Fig. 2.13):

- Providing the initial land-use map and relevant spatial/non-spatial constraints to simulate land-use changes,
- Extracting relevant land-use based parameters and deriving their spatial distribution from each forecasted land-use map,
- Configuring the ERWHM based on changed land-use based parameters using the new model setup of ERWHM to run simulations, and
- Extracting information related to each hydrological component which are then compared and analyzed considering the different land-use changes.

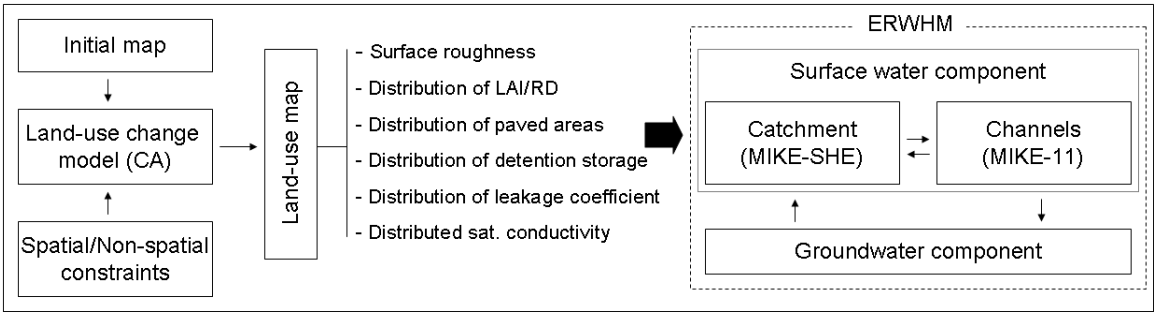

Figure 2.13: The architecture of land-use/hydrology modeling framework to evaluate the impact of land-use changes on hydrological processes

Evaluating the impact of historical land-use changes on hydrological processes involves the same procedure as described above, except that historical land-use maps were used to extract relevant land-use based parameters.

For evaluating the impact of future land-use changes on hydrological processes, a total of four scenarios of land-use changes were simulated with the CA (Table 2.6). They include: the business as usual scenario (BAU), a scenario with a new centralized development plan (RV-LUC) based on a potential growth point identified by Municipal District of Rocky View (2012), a scenario with a new centralized development in the area of Bragg Creek (BC-LUC), and a scenario where land-use is changed based on the forecasted population trends according to the City of Calgary (2011) (P-LUC). These scenarios differ from those used in a previous study conducted by Hasbani (2008) who applied the CA model to implement the scenarios: business as usual, population growth, and the creation of a new virtual town in the Elbow river watershed. For all scenarios, the simulations were carried out for the years 2016, 2021, 2026, and 2031 using the initial land-use map of 2010. Using future forest harvest sequence data obtained from AESRD, clear-cut areas relevant to each future year (2016, 2021, 2026, and 2031) were overlaid on each simulated land-use map in order to take into account the possible changes in the forested portions of the watershed.

Table 2.6: Land-use change scenarios and corresponding spatial/non-spatial constraints

Scenario	Description	Applied constraint
BAU	Business as usual, following trends detected from the	N/A

	historical land-use maps	
RV-LUC	New centralized development within the Rocky View county	Local spatial constraint to promote new urban development
BC-LUC	New centralized development in the area of Bragg Creek	Local spatial constraint to promote new urban development
P-LUC	Development based on projected population growth	Global constraint set based on population growth for each future year

The simulated land-use maps were used to extract land-use based parameters needed for the ERWHM. Assigning corresponding values to each land-use class, spatially distributed maps of surface roughness (Manning's M) were created for each land-use map. Areas of urban development were overlaid onto the soil maps to define paved areas; these areas within the soil distribution maps were assigned a low saturated hydraulic conductivity value of 2.7e-012 m/s. The spatial distribution of vegetation properties (LAI and RD) was changed according to the distribution of the corresponding land-use class in each land-use map. Furthermore, for each land use, a distributed value for detention storage, paved runoff coefficient, and overland-groundwater leakage coefficient was created as indicated in the section 2.2.2.1.

To evaluate the impact of historical and future land-use changes on the hydrological processes, hydrological simulations were carried out with ERWHM for a period of 5 years based on each land-use change. Corresponding to each land-use change (for the years 1992, 1996, 2001, 2006, 2010, 2016, 2021, 2026, and 2031) the land-use based parameters were extracted at the spatial

resolution of 50 m[1] from the land-use maps. Based on historical and future land-use changes, a total of 21 simulation runs were carried out with the ERWHM (Table 2.7). The non-land-use based data (i.e., river channel, topography, geological layers, etc.) and other parameters (i.e., snow melt parameters, ET surface depth, etc.) were kept unchanged. The climate data (daily precipitation, reference ET, daily temperature) used for these simulations were the same as the data used within the validation period (2000–2005). The initial value of snow storage was set at 0 mm as each simulation was started on the 1st of September (start of fall season). The initial conditions for sub-surface potential heads were derived from the previous simulation (1995-2005).

Table 2.7: Details of the hydrologic simulations carried out with the ERWHM based on each land-use change

ERWHM simulation period	Land-use map	Scenario(s)	Total number of simulation runs
2000-2005	1992	historical	1
	1996	historical	1
	2001	historical	1
	2006	historical	1
	2010	historical	1
	2016	BAU, RV-LUC, BC-LUC, P-LUC	4
	2021	BAU, RV-LUC, BC-LUC,	4

[1] MIKE-SHE requires the spatial resolution of each dataset to be an integral multiple of the domain resolution (200 m). Therefore, the land-use maps at 60 m resolution were re-sampled to 50 m, the land-use based parameters were extracted and were then used to configure the MIKE-SHE setup.

		P-LUC	
	2026	BAU, RV-LUC, BC-LUC, P-LUC	4
	2031	BAU, RV-LUC, BC-LUC, P-LUC	4
Total number of simulations			21

The simulations were carried out with the output frequency of channel flow set at 24 h and at 72 h for overland flow, snow melt, ET, and unsaturated zone flow. Since daily observed channel flow data were available for comparison with the simulated data, 24 h output frequency was selected for the channel flow. After each simulation, the total water balance error, total overland flow (OL), total ET, total infiltration (Inf), and baseflow (BF) within the 5 year simulation period were derived and tabulated for the east and west sub-catchments of the watershed as illustrated on Figure 2.12.

The model simulation time step (temporal resolution) is dynamically controlled by the model simulation engine. A user can set the maximum allowed time step control parameter values for each module separately. These values also depend on the output frequency specified for the corresponding component. For example, if the maximum allowed time step for SZ component is 24h, the output frequency of the SZ component can only be a multiple value of 24h. Furthermore, in setting the maximum allowed time step values, these values must be set according to the guidelines within MIKE-SHE (e.g., the OL storing time step must be an integer multiple of the maximum UZ time step value). In the current study, the time step control values

were determined based on the model stability and performance. After carrying out various simulations to test the performance and the model stability, the time step control parameter values assigned for the OL, UZ, SZ components, and MIKE-11 were 2h, 8h, 8h, and 3 min, respectively. The initial time step for all components within MIKE-SHE was set to 1h.

Relative preferability of a land-use change scenario in this study is evaluated based on how much water is retained within the watershed when a particular land-use change pattern has been persistent for a long period. When a scenario of land-use change generates low overland flow and high infiltration, baseflow, and evapotranspiration, it is considered as more preferable. In comparison, when a scenario creates high overland flow, and low infiltration, baseflow, and evapotranspiration, it is considered as less preferable.

To compare the preferability of each future land-use change scenario, their impact on hydrological processes was extrapolated (using a simple linear regression analysis) up to 2066 assuming that the corresponding land-use changes persist during that period; 50 years was found long enough to clearly distinguish the impact between the scenarios. To do this, the initial magnitude and the rate of change of each hydrological impact were combined using Equation 17. For each hydrological process, it was assumed that the average rate of change calculated for the period 2016-2031 will be the same for the period 2016-2066 along with the same land-use change trend corresponding to each scenario.

$$\mathrm{Im}_{50} = Val_{2016} + (Val_{2016} \times \frac{rate}{1500} \times 50) \qquad \text{Equation 17}$$

Im_{50} is the impact after 50 years of land-use change for the corresponding hydrological process,

Val_{2016} is the initial impact of land-use changes on hydrological processes in storage depth (mm) corresponding to hydrological simulations run for 5 years using the land-use map of 2016, and $rate$ is the average percentage rate of increase or decrease of the impact of the land-use changes on the hydrological process over the years; this was calculated using the results of the impact of land-use changes of 2016, 2021, 2026, and 2031 on hydrological processes.

Chapter 3: Results and Interpretation

In this chapter, the results of the calibration and validation of the ERWHM are first presented, followed by the results and interpretation of the simulations carried out for evaluating the impact of historical and future land-use changes on the hydrological processes. The future land-use changes are based on land-use change scenarios: BAU, RV-LUC, BC-LUC and P-LUC. Finally the relative preferability of these land-use change scenarios was interpreted and compared.

3.1 Results of the calibration and validation of the ERWHM

The results of the calibration and validation of the ERWHM against total snow storage are presented in Table 3.1. An average correlation coefficient of 0.80 was achieved for the validation of ERWHM against total snow storage while it is 0.86 for the calibration (Table 3.1). This indicates a good performance of the ERWHM in calculating the snow storage in colder climate conditions (when precipitation is mainly by snow) for the watershed.

Table 3.1: Results of the calibration/validation of ERWHM using correlation coefficient values based on total snow storage

	Calibration/Validation period	Correlation coefficient
		Little Elbow
Calibration	Sept. 1981 to Sept. 1991	0.86
Validation	Sept. 1991 to Sept. 1995	0.77
	Sept. 1995 to Sept. 2000	0.70
	Sept. 2000 to Sept. 2005	0.84
	Sept. 2005 to Sept. 2008	0.86

In evaluating the performance of hydrologic models, stream flow comparison takes a significant place. Therefore, different indices must be analyzed to determine the performance of the hydrologic model used. The indices used in this study to compare simulated and observed hydrographs are: the coefficient of determination, NSE, Ln NSE, and the relative NSE.

The coefficient of determination estimates the combined dispersion against the single dispersion of the observed and predicted flow data. NSE presents an improvement over the coefficient of determination in evaluating the model performance in that it is sensitive to differences in the observed and simulated means and variances. The main disadvantage of NSE is that larger discharge values in a hydrograph are overestimated whereas lower values are neglected. Therefore, NSE is not sensitive to the model over or under-prediction, especially during low flow periods. In calculating Ln NSE, the peak discharge values are flattened and the low flows are kept at the same level of magnitude; as a result the influence of the low flow values is increased. The relative NSE index is calculated based on the differences between the observed and simulated flow values as relative deviations, which reduces significantly the influence of the absolute differences (as in the case of the other indices) during high flow (Krause *et al.* 2005, Legates and McCabe 1999).

Tables 3.2, 3.3, 3.4, and 3.5 show the results of the calibration/validation of ERWHM expressed with NSE, Ln NSE, relative NSE, and the coefficient of determination using daily and monthly values of stream flow data, respectively. An average NSE value of 0.63 was achieved for both the calibration and validation using daily observed and simulated stream flow data while it is 0.74 using monthly observed and simulated data (Table 3.2). According to hydrological model

guidelines (Moriasi *et al.* 2007), this indicates a good model performance in generating stream flow through surface water processes and groundwater processes.

Table 3.2: Results of the calibration/validation of ERWHM using daily and monthly values of NSE based on stream flow and the WB error (%). 004, 006, 009, and 010 correspond to the hydrometric stations 05BJ004, 05BJ006, 05BJ009, and 05BJ010 respectively

	Calibration/Validation period	WB error (%)	NSE - daily				NSE - monthly			
			004	006	009	010	004	006	009	010
Calibration	Sept. 1981 to Dec. 1991	0.04	0.72	0.63	0.53	0.63	0.83	0.75	0.63	0.75
Validation	Sept. 1991 to Dec. 1995	0.06	0.75	0.63	0.25	0.75	0.90	0.69	0.23	0.86
	Sept. 1995 to Dec. 2000	0.08	0.77	N/A	N/A	0.64	0.87	N/A	N/A	0.79
	Sept. 2000 to Dec. 2005	0.05	0.72	N/A	N/A	0.64	0.83	N/A	N/A	0.82
	Sept. 2005 to Dec. 2008	0.04	0.53	N/A	N/A	0.60	0.69	N/A	N/A	0.77

Table 3.3: Results of the calibration/validation of ERWHM using daily and monthly values of Ln NSE based on stream flow, and the WB error (%). 004, 006, 009, and 010 correspond to the hydrometric stations 05BJ004, 05BJ006, 05BJ009, and 05BJ010 respectively

	Calibration/Validation period	WB error (%)	Ln NSE - daily				Ln NSE - monthly			
			004	006	009	010	004	006	009	010
Calibration	Sept. 1981 to Dec. 1991	0.04	0.73	0.80	0.62	0.53	0.78	0.86	0.70	0.77
Validation	Sept. 1991 to Dec. 1995	0.06	0.81	0.75	-0.31	0.85	0.88	0.78	-0.62	0.92
	Sept. 1995 to Dec. 2000	0.08	0.68	N/A	N/A	0.21	0.76	N/A	N/A	0.48
	Sept. 2000 to Dec. 2005	0.05	0.73	N/A	N/A	0.66	0.80	N/A	N/A	0.72
	Sept. 2005 to Dec. 2008	0.04	0.71	N/A	N/A	0.49	0.80	N/A	N/A	0.75

Table 3.4: Results of the calibration/validation of ERWHM using daily and monthly values of relative NSE based on stream flow, and the WB error (%) 004, 006, 009, and 010 correspond to the hydrometric stations 05BJ004, 05BJ006, 05BJ009, and 05BJ010 respectively

	Calibration/Validation period	WB error (%)	rel NSE - daily				rel NSE - monthly			
			004	006	009	010	004	006	009	010
Calibration	Sept. 1981 to Dec. 1991	0.04	0.82	0.89	0.84	0.85	0.82	0.90	0.83	0.88
Validation	Sept. 1991 to Dec. 1995	0.06	0.89	0.90	0.67	0.91	0.92	0.90	0.44	0.92
	Sept. 1995 to Dec. 2000	0.08	0.84	N/A	N/A	0.38	0.86	N/A	N/A	0.43
	Sept. 2000 to Dec. 2005	0.05	0.89	N/A	N/A	0.83	0.89	N/A	N/A	0.78
	Sept. 2005 to Dec. 2008	0.04	0.84	N/A	N/A	0.84	0.89	N/A	N/A	0.82

Table 3.5: Results of the calibration/validation of ERWHM using daily and monthly values of coefficient of determination based on stream flow, and the WB error (%) 004, 006, 009, and 010 correspond to the hydrometric stations 05BJ004, 05BJ006, 05BJ009, and 05BJ010 respectively

	Calibration/Validation period	WB error (%)	CD - daily				CD - monthly			
			004	006	009	010	004	006	009	010
Calibration	Sept. 1981 to Dec. 1991	0.04	0.72	0.66	0.58	0.64	0.85	0.79	0.71	0.76
Validation	Sept. 1991 to Dec. 1995	0.06	0.76	0.74	0.48	0.77	0.92	0.88	0.71	0.94
	Sept. 1995 to Dec. 2000	0.08	0.81	N/A	N/A	0.69	0.90	N/A	N/A	0.85
	Sept. 2000 to Dec. 2005	0.05	0.76	N/A	N/A	0.72	0.86	N/A	N/A	0.85
	Sept. 2005 to Dec. 2008	0.04	0.79	N/A	N/A	0.74	0.88	N/A	N/A	0.85

The average Ln NSE values of 0.67 and 0.56 were respectively obtained for the calibration and validation periods based on daily data. The corresponding values based on monthly data are 0.78 for the calibration and 0.63 for the validation. In terms of relative NSE, average values of 0.85 and 0.80 were obtained based on daily data during the calibration and validation respectively, while they are 0.86 and 0.79 based on monthly data. The calculated coefficient of determination indicates average values of 0.65 and 0.73 based on daily data during the calibration and validation respectively, while the average values based on monthly data are 0.78 for the calibration and 0.86 for the validation. These results reveal a good performance of the ERWHM.

In contrast, the daily and monthly NSE and Ln NSE values calculated for the station 05BJ009 for the period 1991-1995 are relatively low (Tables 3.2 and 3.3). But the relative NSE and coefficient of determination values corresponding to the station 05BJ009 during the period 1991-1995 reach a relatively high value (Tables 3.4 and 3.5). Furthermore, Ln NSE and relative NSE

values calculated for the station 06BJ010 for the period 1995-2000 also appear relatively low (Tables 3.3 and 3.4) indicating that the performance of the ERWHM is poor when the low flows are considered for this particular instance. However, NSE and the coefficient of determination show a good performance of the model (Tables 3.2 and 3.5). The values of Ln NSE and relative NSE indices corresponding to the results of calibration/validation other than the above two instances show a good performance as far as the low stream flows (which are mainly contributed by the baseflow) are considered. In overall, these indices indicate that an adequate performance of the ERWHM was achieved when peak discharges, mean discharges, and low flow values are considered.

No similar studies have been conducted for the Elbow River watershed before; previous studies were based on lumped conceptual models and lack the level of details of this research. However, the study carried out by Oogathoo (2006) in the Canagagigue Creek watershed in Ontario contains a similar calibration and validation of MIKE-SHE; it reveals an average performance of 0.59 and 0.40 for NSE during the calibration and validation, respectively, indicating a lower performance of their model configuration compared to ERWHM.

Considering the characteristics of the Elbow River watershed , the achieved performance with MIKE SHE/MIKE 11 in this study is considered a success. To further improve this performance, the following factors need to be addressed:

I. In the current study, the land-use changes that occurred within the calibration and validation periods were neglected; one constant land-use map was used throughout each

corresponding calibration and validation period assuming that any significant land-use changes within these periods would occur.

II. The observed flow values obtained for comparison with the simulated stream flow values were daily mean values of stream flow corresponding to each hydrometric station. The stream flow values on the other hand were instantaneous (generated at a certain time of the day) and were compared with daily mean observed stream flow. (Ideally, observed stream flow should be instantaneous values to be compared with the instantaneous values of simulated stream flow).

III. Unsaturated zone flow and evapotranspiration were simulated by simple techniques due to the lack of data and the need of high computational time for the simulations (if implemented, MIKE-SHE simulations would take an unreasonable amount of time to complete).

The WB error (%) in each simulation period represents the total water balance error (mm) as a percentage of the total precipitation (mm) (WB error/Total precipitation * 100) during the corresponding simulation period. This error is considered minimal when it is less than 1% (Oogathoo 2006).

During the calibration and validation of the ERWHM, both the correlation coefficient (CC) and the mean absolute error (MAE) were considered as indicators in evaluating the model performance based on groundwater levels. However, it was noted that in calculating these indicators, too few observed points were available relative to the generated simulated values in each station. For example, a maximum of nine observed values were available for a station

where almost hourly simulated values were generated during a simulation period of five years (Wijesekara and Marceau 2012). Therefore, it was found that these indicators cannot produce a valid comparison between the simulated and observed groundwater levels due to inadequate observed data. Furthermore, the data of the observed groundwater levels presented quality issues. For example, in some of the stations, the observed groundwater water levels were found higher than the observed ground surface elevations (Wijesekara and Marceau 2012). Typically, the calibration of a hydrological model against groundwater levels is required to find the appropriate values for the geological parameters and to obtain a good performance in simulating the groundwater levels. Since the impact of land-use changes on groundwater levels are not being explicitly investigated in this study, the calibration of the ERWHM against groundwater levels was not considered a mandatory requirement. However, to determine the best fitting values for the geological parameters, the contribution of baseflow in the total stream flow was recognized as a better indicator compared to groundwater levels. The obtained results of the attempted calibration and validation of the ERWHM against groundwater levels using 20 groundwater measurement wells are summarized in Appendix L.

Figure 3.1 shows three selected graphs (amongst 19 different graphs, which can be found in Appendix K) illustrating the comparison between the observed and simulated stream flow at stations 05BJ004 and 05BJ010, and total snow storage at the Little Elbow station. These graphs (displayed more widely in Appendix K) show a very good visual correlation between the observed and simulated stream flow and total snow storage at the corresponding stations. Overall, these results indicate a good performance of ERWHM, which was considered adequate to assess the impact of land-use changes on hydrological processes.

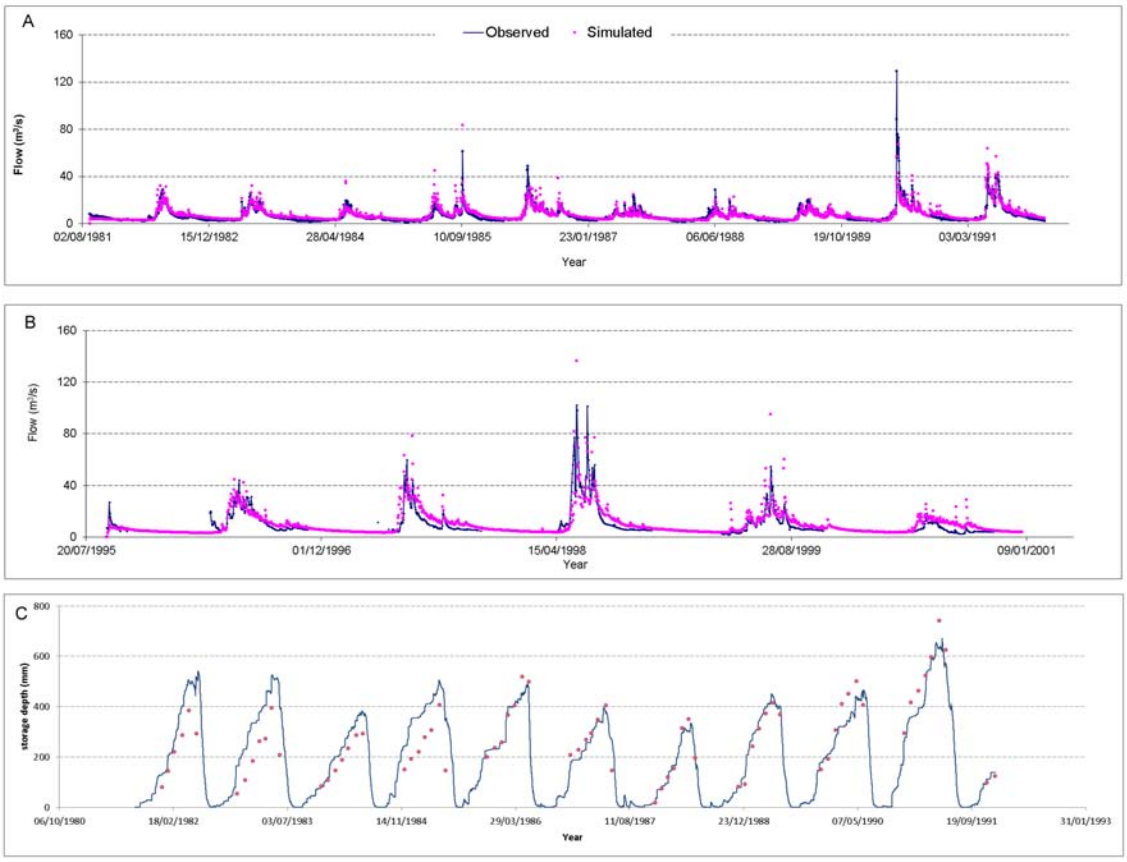

Figure 3.1: Observed and simulated stream flow at station 05BJ004 during the period 1981-1991 (A), 05BJ010 during the period 1995-2000 (B), and total snow storage data at station Little Elbow during the period 1981-1991 (C)

3.2 Impact of land-use changes on hydrological processes for the period 1992-2010

Since different land-use changes dominate in the east and west sub-catchments of the watershed, they are described separately in this section. The east sub-catchment is dominated by built-up areas and agriculture. Due to the considerable growth of built-up areas (117%) over the period 1992-2010, the evergreen and deciduous forest areas have been reduced by about 8% and 11%, respectively along with agricultural areas (9%) (Fig.3.2a). Areas of rangeland/parkland have increased by 3%. The west sub-catchment is dominated by evergreen and deciduous forests. From 1992 to 2010, evergreen forest was reduced by 8%, while the reduction is 28% for the

deciduous forests (Fig. 3.2b). Clear-cuts are minimal in 1992, but start increasing in the year 2000 to reach a peak value in 2010 (2.7% of the west sub-catchment). This results in an increase in rangeland/parkland.

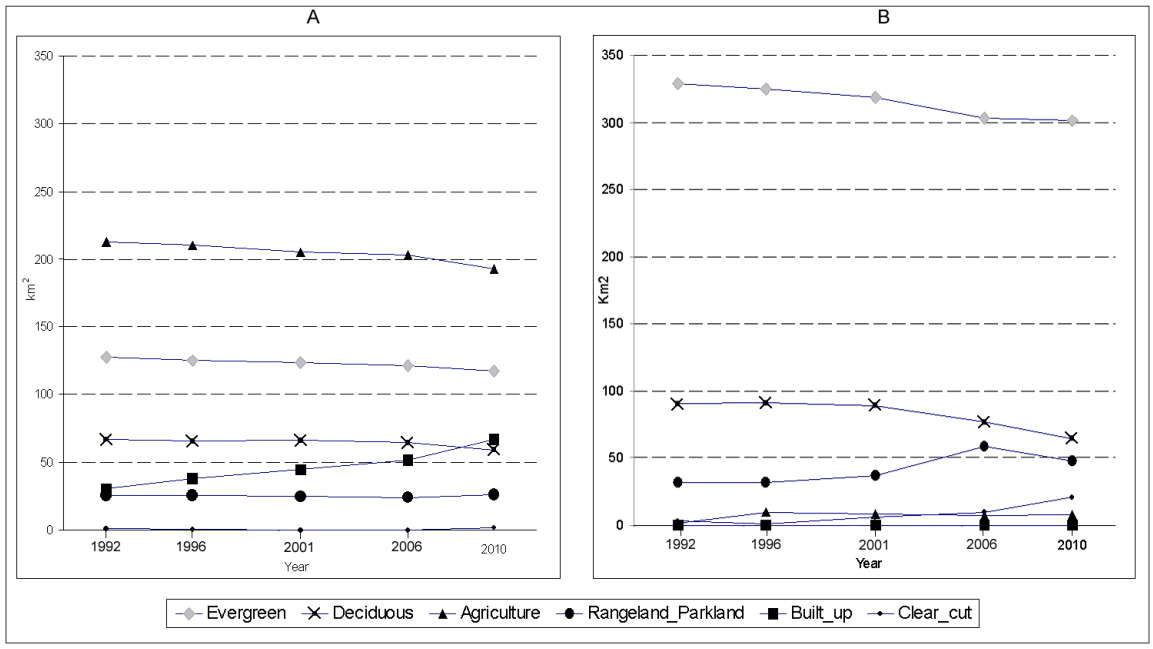

Figure 3.2: Land-use change for the period 1992-2010 in the east sub-catchment (A) and the west sub-catchment (B)

Figure 3.3 shows the variation of each hydrological process in storage depth (mm) within the east and west sub-catchments over the period of 1992-2010 as a result of the above land-use changes. Within the east sub-catchment, the dominant variations are an increase of 121% in OL, and a decrease of 1.7% in BF, 3.5% in ET, and 15% in Infiltration (Fig. 3.3a). These variations are explained by the increased urbanization over the years and the reduction of forested areas.

The west sub-catchment is dominated by forest and rangeland/parkland areas that have high and low vegetation respectively. These two classes produces relatively less overland flow providing more opportunity for water to infiltrate (Manning's M is 33.33 indicating high surface resistance)

compared to built-up areas (Manning's M is 90.9 indicating very low surface resistance). Furthermore, the detention storage is about 20 mm for both forest and rangeland/parkland areas providing a higher detention of water for infiltration and evapotranspiration compared to built-up where the detention storage is almost 0 mm. As a result, these vegetated areas generate low OL with higher Inf, ET, and BF. In the east sub-catchment on the other hand, forest areas and agriculture are mostly replaced by built-up areas. These areas generate more OL with less Inf, ET and BF. Therefore, compared to the variations of hydrological processes in the east sub-catchment, the changes in the west sub-catchment are minimal (Fig. 3.3b).

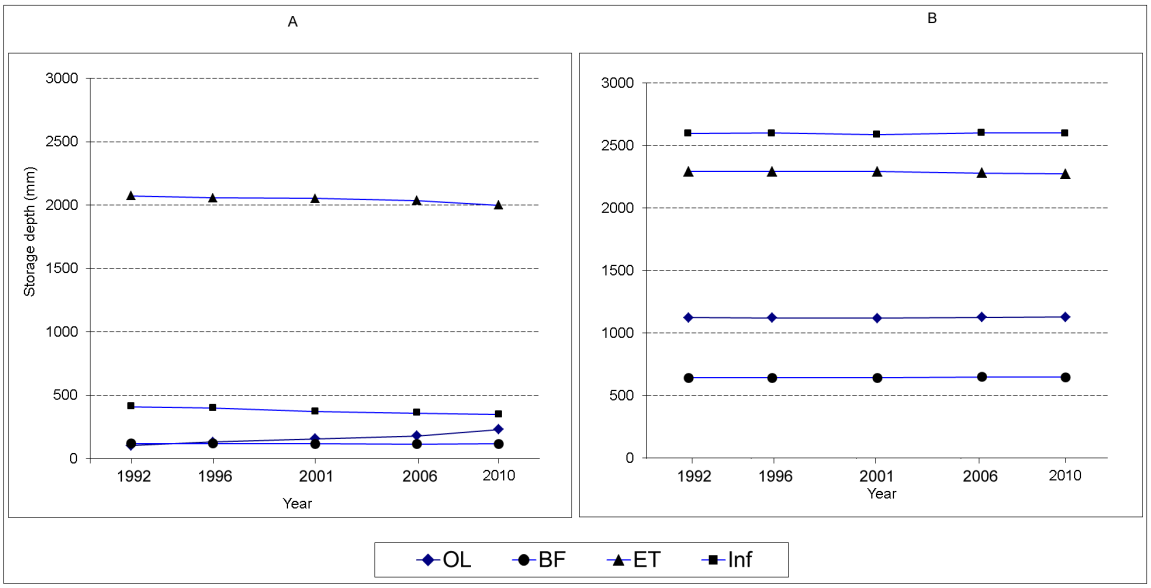

Figure 3.3: Variation of OL, BF, ET, and Inf for the east sub-catchment (A) and the west sub-catchment (B) for the period 1992-2010

3.3 Impact of land-use change scenarios on the hydrological processes for the period 2016 – 2031

Since the dominant land-use changes occur within the east sub-catchment of the Elbow River watershed, the following results are presented for that sub-catchment only. The trends in the simulated land-use changes appeared to be the same for the scenarios BAU, RV-LUC and BC-LUC, and are presented in a unique graph in Fig. 3.4a. The growth of built-up areas reaches 25%

with a corresponding reduction of agriculture (1%), evergreen (2.6%) and deciduous (19%) areas. For the scenario P-LUC (Fig. 3.4b), there is a substantial growth of built-up between 2016 and 2031 (46%), while the areas of agriculture, evergreen and deciduous decrease by 5%, 4%, and 19%, respectively. The higher change rate for built-up reflects the projected population growth represented in that scenario.

Despite the same rate of land-use change for the scenarios BAU, RV-LUC, BC-LUC, they have generated different spatial patterns due to the different spatial constraints applied during the simulations (Fig. 3.5). In the BAU scenario, new areas of built-up are sparsely distributed to the west of Calgary compared to the scenarios RV-LUC and BC-LUC, where concentrated built-up areas appear within the Rocky View County and in the area of Bragg Creek respectively. The scenario P-LUC generates more built-up areas appearing further west of the city of Calgary and in the north part of the watershed than the other scenarios. The spatial distribution of built-up areas in this scenario (P-LUC) is the same as for the scenario BAU. The simulated land-use changes in the east sub-catchment for the years 2016, 2021, 2026, and 2031 for all land-use change scenarios are illustrated in Appendix H.

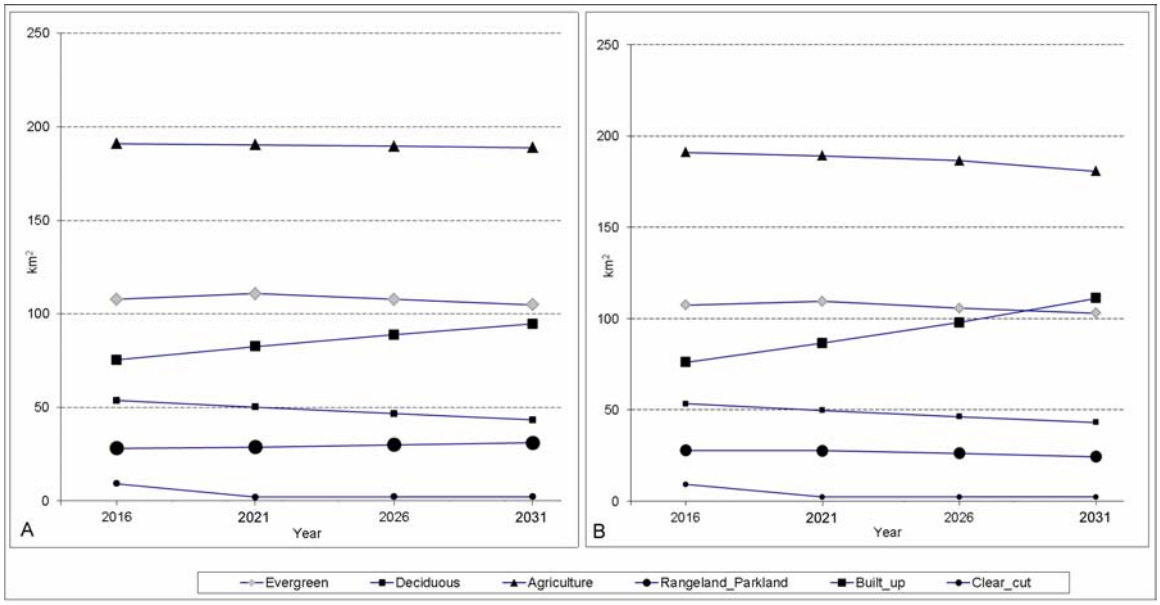

Figure 3.4: Simulated land-use changes during the period 2016-2031 in the east sub-catchment of the Elbow River watershed based on Scenarios BAU, RV-LUC, BC-LUC (A) and Scenario P-LUC (B)

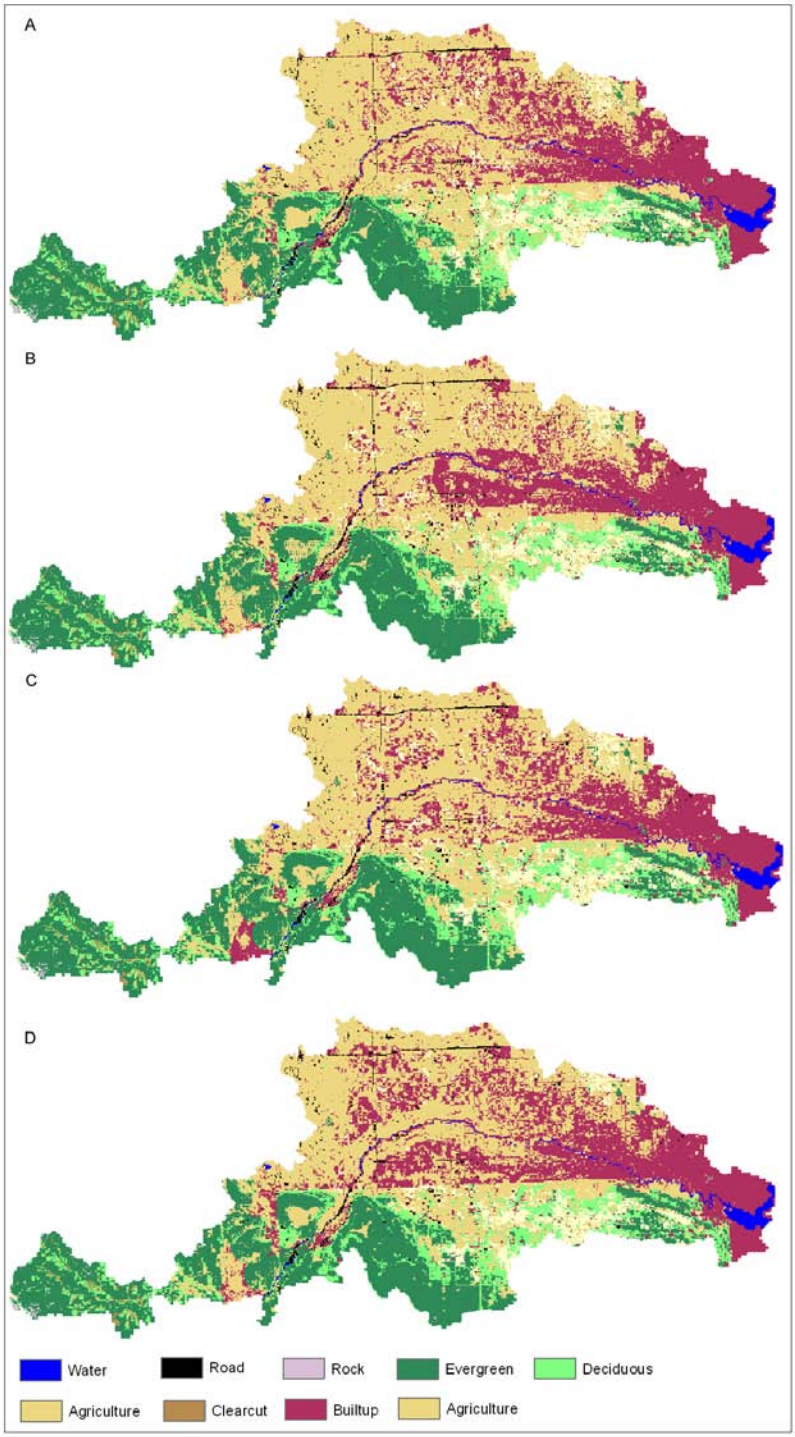

Figure 3.5: Forecasted land-use maps for the year 2031 in the east sub-catchment of the Elbow River watershed according to the scenarios BAU (A), RV-LUC (B), BC-LUC (C), and P-LUC (D)

The unique spatial patterns generated from the land-use maps affect the spatial patterns of each land-use based data and parameters (e.g., surface roughness). The non land-use based data and parameters (e.g., slope of the terrain) interact with these land-use based parameters in a complex way to influence the hydrological processes. Fig. 3.6 shows the impact of the land-use changes on each hydrological process for the period 2016-2031 within the east part of the watershed. The scenario P-LUC generated the highest OL value (average of 306 mm) while the scenario RV-LUC generated the lowest OL value (average of 273 mm) (Table 3.6, Fig. 3.6a). This scenario also produced the lowest BF (avg: 117 mm), ET (avg: 1922 mm), and Inf (avg: 346 mm), while the RV-LUC scenario produced the highest BF (avg: 118 mm), and Inf (avg: 362 mm) (Fig. 3.6b, 19c, and 19d).

Table 3.6: Average impact of each land-use change scenario on each hydrological process expressed in storage depth (mm) calculated by taking the average of the land-use change impact values on each hydrological process corresponding to the land-use changes for the years: 2016, 2021, 2026, and 2031

Scenarios	OL (mm)	BF (mm)	ET (mm)	Inf (mm)
BAU	289.5	117.7	1948.5	333.0
RV-LUC	273.5	118.0	1941.7	362.0
BC-LUC	277.5	118.2	1940.0	360.5
P-LUC	305.7	117.5	1922.0	346.2

Although the scenarios BAU, RV-LUC, and BC-LUC generate the same land-use changes over the years, their influence on the hydrological processes is different, e.g., the average value of OL is the highest for BAU, is high for BC-LUC and is the lowest for the RV-LUC scenario (Fig. 3.6a). This is due to their unique spatial land-use change patterns (Fig. 3.5). The scenarios with

similar land-use change patterns (P-LUC and BAU) also show a different impact on the hydrological processes. This is due to more built-up areas appearing in scenario P-LUC compared to the BAU scenario. Furthermore, the scenarios with the same type of constraints and the same land-use change rate (RV-LUC and BC-LUC) also generate different impacts on the hydrological process, e.g., OL (Fig. 3.6a), mainly due to their unique location of concentrated development. This clearly shows that the land-use change area, spatial distribution, and location (for concentrated developments) of a land development play an important role on the hydrological processes.

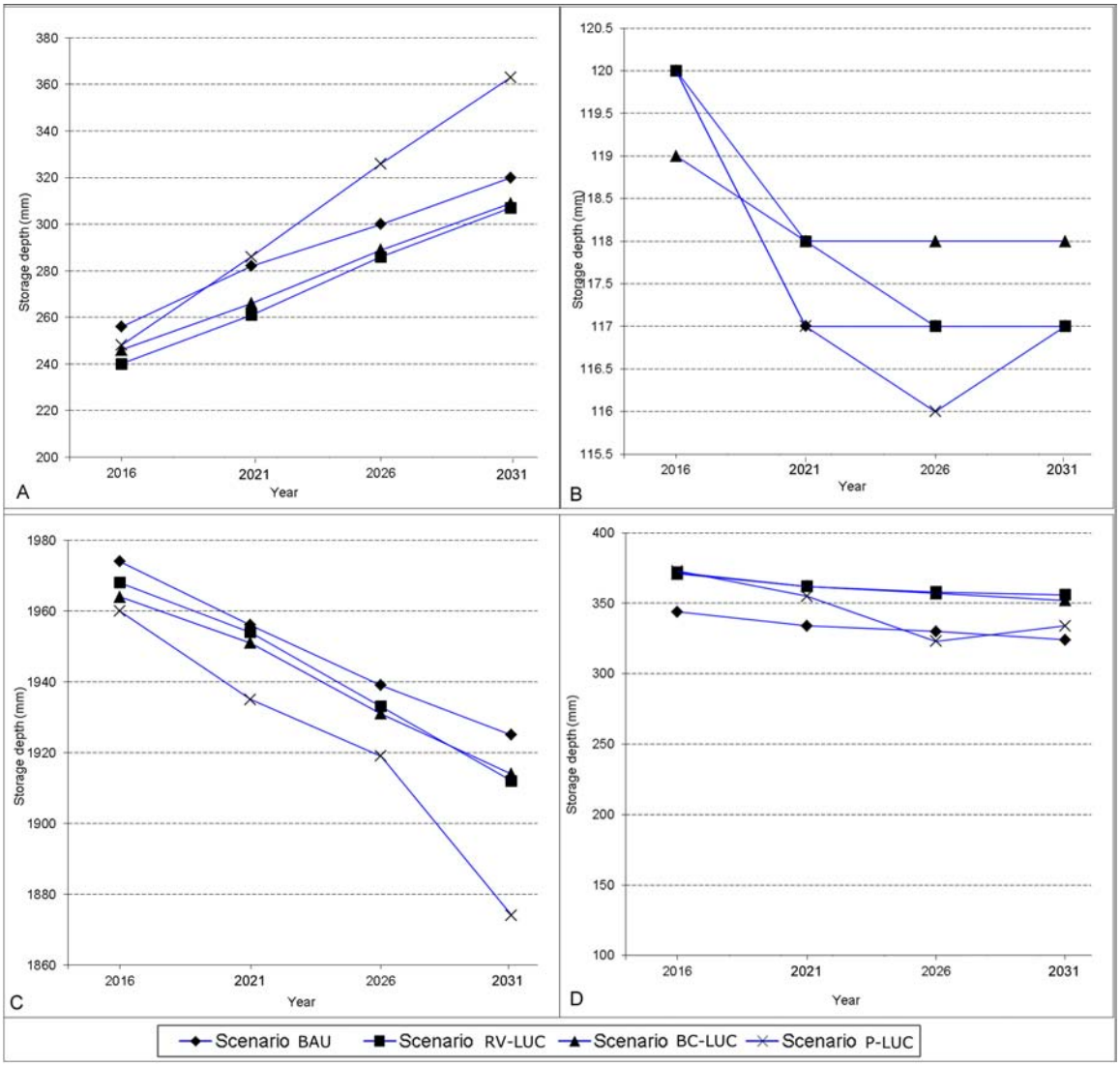

Figure 3.6: Variation of OL (A), BF (B), ET (C), and Inf (D) over time as a result of the land-use change scenarios BAU, RV-LUC, BC-LUC, and P-LUC in the east sub-catchment during the period 2016-2031

Figure 3.7 shows the percentage increase or decrease for each hydrological process over time for the four scenarios. The highest rate of increase for OL over the years occurs with the scenario P-LUC (46%) while the other scenarios generate almost equal rates of increase of OL. Furthermore, the highest rate of decrease of ET and Inf is produced with the scenario P-LUC while the highest rate of decline of BF occurs with the scenarios BAU, RV-LUC and P-LUC.

The lowest rate of decline of BF, ET, and Inf happens with the scenarios BC-LUC, BAU and RV-LUC, respectively.

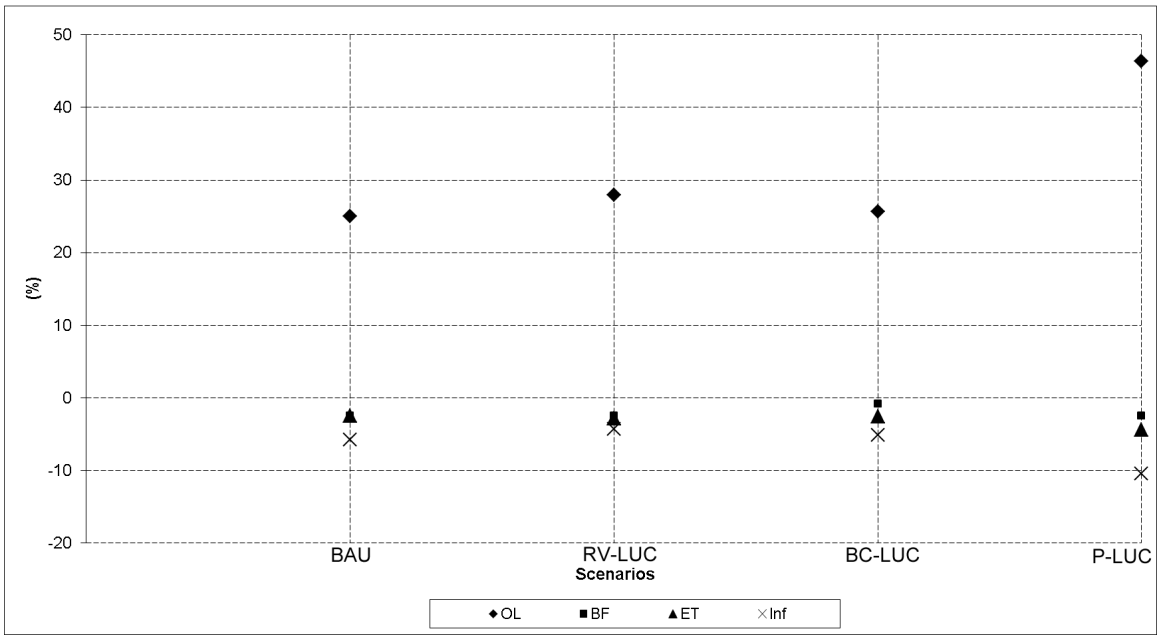

Figure 3.7: Increase/decrease percentage rate of the impact on each hydrological process based on the land-use change scenarios BAU, RV-LUC, BC-LUC, and P-LUC during the period 2016-2031, within the east sub-catchment. Positive values denote percentage increase while negative values denote percentage decrease. These percentages are calculated based on increase/decrease in value in the year 2031 relative to the year 2016, e.g., percentage increase of OL = (OL at 2031 – OL at 2016)/(OL at 2016) X 100

3.3.1 Evaluating the preferability of future land-use change scenarios

More overland flow in a watershed means that the water does not retain on the surface for infiltration and evaporation but drains away through the channels. This is caused by land uses such as built-up areas of relatively low detention storage, surface roughness, leakage coefficient, and saturated hydraulic conductivity along with high paved runoff coefficient. Less infiltration produces less nourishment to the groundwater storage, which results in low contribution to the rivers through baseflow during the dry season. Thereby, the availability of the water in the rivers

gets affected. When the rate of increase or decrease for each process is high, the accumulated effect due to each hydrological process increases in magnitude. For an example, in our study, the scenario P-LUC can drain out more water over the years than the scenario BAU (Fig. 3.6 and 3.7) resulting in less groundwater storage and baseflow.

A scenario that results in a relative low ET indicates that the vegetative cover has been reduced due to deforestation or land-use conversion into built-up areas (causing less transpiration and evaporation). Less ET produces less atmospheric vapor within the catchment and has the potential to affect the long-term precipitation cycle, which can in turn affect the long-term water availability in the Elbow River watershed. Evapotranspiration is known to be the main driving force in landscape sustainability, and known to be instrumental in temperature and water distribution in time and space. Adequate evapotranspiration is crucial mainly to keep the balance of the hydrologic cycle, dissipate/re-distribute solar heat energy, and helps to reduce the loss of organic matter that enriches the soil (Eiseltová *et al.* 2012). Therefore, a reduction of ET as a result of a certain land-use change is undesirable and the higher rate of decrease of ET can result in more adverse effect to the environment.

Table 3.7 shows the impact within a five year simulation period on each hydrological process after 50 years as a result of each land-use change scenario assuming that the same trend of land-use change corresponding to each scenario persists. The scenario BC-LUC appears to be preferable when considering both overland flow and baseflow. The scenario RV-LUC is more preferable in terms of infiltration, while the scenario BAU is preferable considering the total evapotranspiration. Overall, the scenario BC-LUC is more preferable than the other three

scenarios. The impacts of the scenario RV-LUC on the hydrological processes can be considered similar to the impacts created by BC-LUC. From being the most preferable to the least preferable, the scenarios are ranked as follow: BC-LUC, RV-LUC, BAU, and P-LUC.

Table 3.7: Impact of each land-use scenario on each hydrological process after 50 years from the initial value in the year 2016. Highlighted values are the most preferred values for each hydrological process in terms of preferability.

Scenario	OL (mm)	BF (mm)	ET (mm)	Inf (mm)
BAU	454.0	110.0	1809.3	276.1
RV-LUC	445.4	109.9	1779.6	318.0
BC-LUC	440.3	115.7	1795.9	306.6
P-LUC	584.1	110.0	1669.4	243.3

Chapter 4: Conclusion

The Elbow River watershed in Southern Alberta is located in one of the driest regions in southern Canada. The Elbow River is the source of the Glenmore reservoir, which provides drinking water to the City of Calgary. Due to the rapid population growth and urbanization in the Calgary region, the Elbow River watershed is under considerable pressure for development. It has been predicted that along with the effects of climate change and the rapidly increasing human activities, water availability in this area will become a critical issue in the near future. Therefore, investigating the future possible land-use changes in the watershed and their impact on the hydrological processes and water availability is becoming a crucial issue.

To achieve this objective, three dynamic models were chosen: 1) a cellular automata (CA) to simulate land-use changes, 2) MIKE-SHE, a physical based, distributed watershed hydrological model, and 3) MIKE-11, a physical based channel model, to simulate the impact of land-use changes on hydrologic processes in the study area. This thesis describes the coupling of these models to study the impact of historical land-use changes and four future land-use change scenarios on the hydrological processes in the Elbow River watershed.

For calibrating the land-use change CA model, historical land-use maps acquired in the summer of the years 1985, 1992, 1996, 2001, 2006, and 2010 were classified into nine land covers/ land uses (water, road, rock, evergreen forest, deciduous forest, agriculture, rangeland/parkland, built-up, and clear-cut areas) using Landsat TM imagery at the spatial resolution of 30 m. Maps showing the distance to a main river, the distance to downtown Calgary, the distance to a main road, and ground slope were prepared and used to represent the influence of external driving

factors on land use. Analyses were first conducted to assess the sensitivity of the CA model to different parameters, including the cell size, neighborhood configuration, and selection of external driving factors and their values. The land-use CA model was then calibrated at the scale of 60 m using a semi-interactive calibration procedure using historical land-use maps of the years 1985, 1992, 1996, 2001, and validated against the reference land-use maps of 2006 and 2010. The validation results indicated a good performance of the CA model.

The MIKE-SHE and MIKE 11 models were configured (and named ERWHM) with a 2-dimensional surface water component and a 3-dimensional groundwater component to simulate the complex surface-groundwater interactions existing in the watershed. The methods used for these components were both physically based and fully distributed. The modified degree-day and two-layer water balance method were used to simulate snowmelt, evapotranspiration, and unsaturated flow, respectively. In calibrating the ERWHM, an exhaustive sensitivity analysis was carried out for surface water parameters (detention storage, snowmelt parameters, riverbed leakage coefficient, and riverbed resistance) and geological parameters separately. The values of these parameters were further refined during the calibration.

The quality of the calibration and validation was evaluated by comparing observed and simulated snow storage, and stream flow data. The correlation coefficient was used to compare observed and simulated total snow storage data while the coefficient of determination, the Nash and Sutcliffe coefficient of efficiency (NSE), the logarithmic NSE, and the relative NSE were used to compare observed and simulated stream flow data.

The impact of land-use changes on hydrological processes was evaluated based on the historical land-use changes and future land-use changes. Future land-use changes were simulated for the years 2016, 2021, 2026, and 2031 based on four scenarios relevant to the Elbow River watershed (BAU: Business as usual, following trends detected from the historical land-use maps, RV-LUC: new centralized development within the Rocky View county, BC-LUC: new centralized development in the area of Bragg Creek, P-LUC: development based on projected population growth). A total of 21 simulations were run for evaluating the impact of land-use changes on the hydrological processes. For each simulation, the distribution of land-use based parameters such as: surface roughness, leaf area index (LAI)/root depth (RD), paved coefficient, detention storage, leakage coefficient, and soil saturated conductivity were extracted from the corresponding land-use maps. Each simulation of ERWHM based on each land-use change was run for five years. After each simulation, the total water balance error, total overland flow (OL), total ET, total infiltration (Inf), and baseflow (BF) were derived and tabulated for the east and west sub-catchments of the watershed.

The preferability of each scenario was evaluated using the impact of land-use changes on each hydrological process after 50 years from the initial value corresponding to the year 2016 assuming that the same trend of land-use change corresponding to each scenario persists. This was done by extrapolating the impact of land-use changes on each hydrological process using linear regression analysis considering the corresponding magnitude and the rate of change. When this value is relatively high for the overland flow, and low for infiltration, evapotranspiration and baseflow, the corresponding land-use change scenario is considered less preferable; it is more preferable when the opposite is true.

A NSE value of 0.74 was obtained during both calibration and validation against observed and simulated monthly stream flow data. Furthermore, the analysis of relative and logarithmic NSE showed that ERWHM performs well in simulating high and low (mainly contributed by the baseflow) stream flows. An average correlation coefficient of 0.86 and 0.80 was respectively achieved for the calibration and validation of ERWHM against total snow storage.

The analysis of the historical impact of land-use changes on the hydrological processes within the east sub-catchment characterized by considerable growth in built-up areas reveals an increase of runoff and reduced baseflow, infiltration, and evapotranspiration. The west sub-catchment is dominated by forest and rangeland/parkland areas that have a higher water retention capacity compared to built-up areas. Therefore the impact of the land-use changes on the hydrological processes was found minimal in that sub-catchment. The impact of land-use changes on the hydrological processes particularly in the east sub-catchment varies with the land-use changes rate, their spatial patterns, and the location of concentrated land development if any. Furthermore, based on the criterion used for evaluating the preferability, the scenario BC-LUC was considered the most preferable compared to the other scenarios while P-LUC is considered the least preferable.

4.1 Thesis contribution

This study is the first of this nature carried out in the Elbow River watershed. Compared to previous studies, this research contains the following unique features.

The modeling system that was developed incorporates three comprehensive models that fully represent land-use changes and the hydrological processes of the Elbow River watershed. The land-use change model and the hydrological model are connected through a complete set of land-use based parameters that are spatially distributed. Furthermore, the framework of the modeling system offers the flexibility of altering the data, parameters and system configuration so that a variety of water related sustainability issues can be investigated within the Elbow River watershed with a minimal amount of modifications. As an example, the integrated modeling system can serve as a tool to find the location of a land development plan that will contribute to water resource sustainability. It could be used to explore a wide variety of land-use change scenarios from urban expansion to deforestation. Furthermore, the model configuration is flexible enough to extend the range of questions that could be investigated, e.g., to quantify the total stream flow at various spatial locations, to examine the fluctuations of the groundwater table as a result of land-use changes, or to assess the impact of removing/adding new water licenses on groundwater storages.

4.2 Limitations of the study

Some limitations were identified in this study. Firstly, in simulating groundwater component it was found that the MIKE-SHE model required extensive computational power to complete simulations within a reasonable time period. Therefore, hydrologic simulations at a spatial resolution finer than 200 m could not be implemented to capture the finer details of land-use changes that occur at 60 m. Second, adequate and valid data could not be obtained to complete the calibration and validation of the groundwater component against groundwater levels. As a result, the impact of land-use change on the groundwater table could not be evaluated. Finally, a

full integration (programmed integration between the models so that land-use based data extraction and transfer can be done programmatically) between the land-use CA and ERWHM could not be achieved due to the fact that the source code of MIKE-SHE/MIKE-11 was not available and a generic application program interface was not available.

4.3 Future work

The modeling systems presented in this study can be easily extended to add components that are critical within the Elbow River watershed. For example, with the existing interface of MIKE-SHE, it is possible to consider predicted changes in the climate conditions and jointly consider land-use and climate changes impacts on the sustainability of water resources. The current modeling system can act as a foundation for a comprehensive decision support system where the inter-relationship of many aspects that have an impact on the water sustainability can be investigated by decision makers to guide future planned activities in the Elbow River watershed. Work is underway for integrating predicted climate change data to simulate the combined impact of land-use and climate changes on the hydrological processes of the watershed. Furthermore, collaboration is established with DHI, the developers of MIKE-SHE, to design a framework to tightly couple the models, so that the entire modeling system can be operated without manual intervention. This framework will also provide a programmable interface to link additional environmental models to fulfill the needs of decision makers.

References

Abbott, M.B. and Ionescu, F.,1967, On the numerical computation of nearly-horizontal flows, *Journal of Hydraulic Research*, 5: 97–117.

AEP, 1991, Alberta Vegetation Inventory: Standards Manual, Alberta Environmental Protection (AEP), Resource Data Division, Data Acquisition Branch, 58 pages

Allen, R. G., Pereira, L. S., Raes, D., Smith, M., 1998, Crop evapotranspiration - Guidelines for computing crop water requirements - FAO Irrigation and drainage paper 56, FAO - Food and Agriculture Organization of the United Nations, Rome (Report).

Almeida, C. M., Gleriani, J. M., Castejon, E. F., and Soares-Filho, B. S., 2008, Using neural networks and cellular automata for modelling intra-urban land-use dynamics, *International Journal of Geographical Information Science*, 22(9):. 943-963.

Andersen, J., Refsgaard, J. C., and Jensen, K. H., 2001, Distributed hydrological modeling of the Senegal River Basin – model construction and validation, *Journal of Hydrology*, 247: 200–214.

AquaResource Inc., 2011, Integrated surface and groundwater model review and technical guide, Prepared for Ontario Ministry of Natural Resources, 116 pages.

Barredo, J. I., Kasanko, M., McCormick, N., and Lavalle, C., 2003, Modelling dynamic spatial processes: simulation of urban future scenarios through cellular automata, *Landscape and Urban Planning*, 64(3):145-160

Benenson, I., 2007, Warning! The scale of land-use CA is changing! Computers, *Environment and Urban Systems*, 31(2): 107-113.

Bow River Basin Council, 2010, Bow River Basin: State of the watershed summary, Calgary, Alberta, Bow River Basin Council, URL: http://wsow.brbc.ab.ca/reports/BRBCWSOWBookletV2-Dec28.pdf

Camp Dresser and McKee, 2001, Evaluation of Integrated Surface Water and Groundwater Modelling Tools, Water Resources Research & Development Program, 35 pages.

Chen, Q., and Mynett, A. E., 2003, Effects of cell size and configuration in cellular automata based prey-predator modeling, *Simulation Modelling Practice and Theory*, 11(7-8): 609-625.

Chen, Z., Grasby, S. E., Osadetz, K. G., and Fesko, P., 2006, Historical climate and stream flow trends and future water demand analysis in the Calgary region, Canada, *Water Science and Technology*, 53 (10): 1-11.

Christiaens, K., and Feyen, J., 2001, Analysis of uncertainties associated with different methods to determine soil hydraulic properties and their propagation in the distributed hydrological MIKE-SHE model, *Journal of Hydrology*, 246(1-4): 63-81.

Chu, H. J., Lin, Y. P., Huang, C. W., Hsu, C. Y., and Chen H. Y., 2010, Modeling the hydrologic effects of dynamic land-use change using a distributed hydrologic model and a spatial land-use allocation model, *Hydrological Processes*, 24 (2538-2554), doi: 10.1002/hyp.7667.

Claudia R., Calidonna, C. R., Di Napoli, C., Giordano, M., Furnari, M. M., and Di Gregorio, S., 2001, A network of cellular automata for a landslide simulation, *Proceedings of the 15th international conference on Supercomputing*, Sorrento, Italy: 419-426.

Coote, D. R., and Gregorich, L. J., 2000, The health of our water, Towards sustainable agriculture in Canada, Research branch, Agriculture and Agri-Food Canada,

Pulication 2020/E, Minister of Public Works and Government Services Canada. Ottawa, 188 pages.

DeFries, R., and Eshleman, K. N., 2004, Land-use change and hydrologic processes: a major focus for the future, *Hydrological Processes*, 18(2183–2186), doi:10.1002/hyp.5584.

DHI, 2009. MIKE SHE User Manual Volume 2: Reference Guide

DHI Water and Environment, 2010, Elbow River watershed hydrological modeling – final report, Report prepared for Alberta Environment, 85 pages.

Du, J., Qian, L., Rui, H., Zuo, T., Zheng, D., Xu, Y., and Xu, C. Y., 2012, Assessing the effects of urbanization on annual runoff and flood events using an integrated hydrological modelling system for Qinhuai River basin, China, *Journal of Hydrology*, 464-465, Pages 127–139, doi: 10.1016/j.jhydrol.2012.06.057

Eiseltová, M., Pokorny´ , J., Hesslerová, P., Ripl, W., 2012. Evapotranspiration—a driving force in landscape sustainablility. In: Evapotranspiration—Remote Sensing and Modeling, Irmak, A. (Ed.),, Intech Publisher, pp. 305–328.

ESRI (2006). ArcGIS 9.1 reference manual.

Elfert, S., and Bormann, H., 2010, Simulated impact of past and possible future land use changes on the hydrological response of the Northern German lowland 'Hunte'catchment, *Journal of Hydrology*, 383(3): 245-255.

Engelen, G., White, R., Uljee, I., and Drazan, P., 1995, Using cellular automata for integrated modeling of socio-environmental systems, *Environmental Monitoring and Assessment*, 34: 203-214.

Engelen, G., White, R., and Nijs, T., 2003, Environment Explorer: Spatial Support System for the Integrated Assessment of Socio-Economic and Environmental Policies in the Netherlands, *Integrated Assessment*, 4(2): 97 – 105.

ERWP (2012) Elbow River Watershed Partnership. http://www.erwp.org/

Fang, S., Gertner, G. Z., Sun, Z., and Anderson, A.A., 2005, The impact of interactions in spatial simulation of the dynamics of urban sprawl, *Landscape and Urban Planning*, 73: 294-306.

Feyen, L., Va´zquez, R., Christiaens, K., Sels, O., and Feyen, J., 2000, Application of a distributed physically-based hydrological model to a medium size catchment, Hydrology and Earth System Sciences, 4(1): 47–63.

Fohrer, N., Haverkamp, S., and Frede, H. G., 2005, Assessment of the effects of land use patterns on hydrologic landscape functions, development of sustainable land use concepts for low mountain range areas, *Hydrological Processes*,19: 659-675.

Gan, T. Y., 2000, Reducing vulnerability of water resources of Canadian prairies to potential droughts and possible climatic warming, *Water Resources Management*, 14(2): 111-135.

Gustard, A. and Wesselink, A. J., 1993, Impact of land-use change on water resources: Balquhidder catchments, *Journal of Hydrology*,145: 389-401.

Hagen, A., 2003, Fuzzy set approach to assessing similarity of categorical maps, *International Journal of Geographical Information Science*, 17(3): 235-249.

Haith, D. A. and Shoemaker, I. L., 1987, Generalized watershed loading functions for stream flow nutrients, *Water Resources Bulletin*,107: 121–137.

Harbor, J. M., 1994, A practical method for estimating the impact of land-use change on surface runoff, groundwater recharge and wetland hydrology, *Journal of the American Planning Association,* 60(1): 95-108.

Hargrove, W. W., Gardner, R. H., Turner, M. G., Romme, W. H., and Despain, D. G., 2000, Simulating fire patterns in heterogeneous landscapes, *Ecological Modeling,* 135: 243–263.

Hasbani, J-G, 2008, Semi-automated calibration of a cellular automata model to simulate land-use changes in the Calgary region. Unpublished M.Sc. thesis, Department of Geomatics Engineering, University of Calgary.

Hasbani, J-G, Wijesekara N, and Marceau, D. J., 2011, An Interactive Method to Dynamically Create Transition Rules in a Land-use Cellular Automata Model, Cellular Automata - Simplicity Behind Complexity, Dr. Alejandro Salcido (Ed.). ISBN: 978-953-307-230-2. *InTech*. http://www.intechopen.com/books/cellular-automata-simplicity-behind-complexity/an-interactive-method-todynamically-create-transition-rules-in-a-land-use-cellular-automata-model

Heritage Community Foundation, 2002, Alberta's Resource Inventory, http://www.abheritage.ca/abresources/inventory/resources_soil_agriculture_today_crops.html (web article).

Holtan, H. N., Stiltner, G. F., Hensen, W. H., and Lopez, N. C., 1975, USDAHL-74 revised model of watershed hydrology, Technical Bulletin No. 1518, Agricultural Research Service, US Department of Agriculture, Washington, DC, USA, 108 pages.

Hu, X., Muzy, A., and Ntaimo, L., 2005, A hybrid agent-cellular space modeling approach for fire spread and suppression simulation, *Proceedings of 2005 Winter simulation conference*, December 3-6: 248-255

Im, S., Kim, H., Kim, C., and Jang, C., 2009, Assessing the impacts of land use changes on watershed hydrology using MIKE SHE, *Environmental geology*, 57(1): 231-239.

Jantz, C. A., and Goetz, S. J., 2005, Analysis of scale dependencies in an urban land-use-change model, *International Journal of Geographical Information Science* 19(2): 217-241.

Jasper, K., Gurtz, J., and Lang, H., 2002, Advanced flood forecasting in Alpine watersheds by coupling meterological observations and forecasts with a distributed hydrological model, *Journal of Hydrology*, 267: 40–52.

Jayatilaka, C. J., Storm, B., and Mudgway, L. B.,1998, Simulation of water flow on irrigation bay scale with MIKE-SHE, *Journal of Hydrology*, 208: 108-130

Jenerette, D. G., and Wu, J., 2001, Analysis and simulation of land-use change in the central Arizona – Phoenix region, USA, *Landscape Ecology*, 16: 611-626.

Johnson, M. S., Coon, W. F., Mehta, V. K., Steenhuis, T. S., Brooks, E. S., and Boll, J., 2003, Application of two hydrologic models with different runoff mechanisms to a hillslope dominated watershed in the northern US: a comparison of HSPF and SMR, *Journal of Hydrology*, 284: 57–76.

Kim, S. H., Park, J. H., Woo, C. S., Lee, K. S., 2005, Analysis of Temporal Variability of MODIS Leaf Area Index (LAI) Product over Temperate Forest in Korea, *Proceedings of International Geoscience and Remote Sensing Symposium (IGARSS) 6*: 4343-4346, 25-29 July 2005, Seoul, South Korea.

Kocabas, V., and Dragicevic, S., 2006, Assessing cellular automata model behaviour using a sensitivity analysis approach, *Computers, Environment and Urban Systems*, 30: 921-953.

Krause, P., Boyle, D. P., and Bäse, F., 2005, Comparison of different efficiency criteria for hydrological model assessment, *Advances in Geosciences*, 5: 89-97.

Kuusisto, E., 1980, On the Values and Variability of Degree-Day Melting Factor in Finland , *Nordic hydrology*, 11: 235-242.

Legates, D. R., and McCabe Jr, G. J., 1999, Evaluating the use of" goodness-of-fit" measures in hydrologic and hydroclimatic model validation, *Water Resources Research*, 35(1): 233-241.

Li, L., Sato, Y., and Zhu, H., 2003, Simulating spatial urban expansion based on a physical process, *Landscape and Urban Planning*, 64(1-2): 67-76

Li, X., and Yeh, A. G.-O., 2000, Modelling sustainable urban development by the integration of constrained cellular automata and GIS, *International Journal of Geographical Information Science*, 14(2): 131-152.

Li, X., and Yeh, A. G.-O., 2002. Neural-network-based cellular automata for simulating multiple land use changes using GIS, *International Journal of Geographical Information Science*, 16(4): 323-343.

Lin. Y. P., Hong, N. M., Wu, P. J., Wu, C. F., and Verburg, P. H., 2007, Impacts of land use change scenarios on hydrology and land use patterns in the Wu-Tu watershed in Northen Taiwan, *Landscape and Urban Planning*, 80(1-2): 111-126.

Liu, Y., and Phinn, S. R., 2003, Modelling urban development with cellular automata incorporating fuzzy-set approaches, *Computers, Environment and Urban Systems*, 27: 637-658.

Malamud, B. D., and Turcotte, D. L., 2000, Cellular-automata models applied to natural hazards, *Computing in Science & Engineering*, 2 (3): 42-51.

Manwell, B. R., and Ryan, M. C., 2006, Chloride as an indicator of non-point source contaminant migration in a shallow alluvial aquifer, *Water Quality Research Journal of Canada*, 41(4): 383-397.

Marceau, D.J., F. Wang, and ijesekara, N., 2012, Investigating land-use dynamics at the periphery of a fast-growing city with cellular automata at two spatial scales. In: Cities and Nature, I. Benenson, D. Malkinson, and Daniel Czamanski, eds, *Springer*. Submitted on October 1, 2012.

Mathey, A.-H., Krcmar, E., Dragicevic, S., and Vertinsky, I., 2008, An object-oriented cellular automata model for forest planning problems, Ecological Modelling, (212): 359-371.

Ménard, A., and Marceau, D. J., 2005, Exploration of spatial scale sensitivity in geographic cellular automata, *Environment and Planning B*, 32: 693-714.

Ménard, A., and Marceau, D. J., 2007, Simulating the impact of forest management scenarios in an agricultural landscape of southern Quebec, Canada, using a geographic cellular automaton, *Landscape and Urban Planning*, 79(3-4): 253-265.

Meyboom, P., Groundwater resources of the City of Calgary and vicinity, Research Council of Alberta, 1961, 82 pages.

Moreno, N., Wang, F., and Marceau, D.J., 2009, Implementation of a dynamic neighborhood in a land-use vector-based cellular automata model, Computers, *Environment and Urban Systems*, 33: 44-54.

Moreno, N., Wang, F., and Marceau, D. J., 2010, A geographic object-based approach in cellular automata modeling, *Photogrammetric Engineering and Remote Sensing*, 76(2): 183-191.

Moriasi, D. N., Arnold, J. G., Van Liew, M. W., Bingner, R. L., Harmel, R. D., and Veith, T. L., 2007, Model evaluation guidelines for systematic quantification of accuracy in watershed simulations, *Transactions of the ASABE*, 50(3): 885-900.

Municipal District of Rocky View, 2012, Rocky View 2060, Growth management strategy, http://www.rockyview.ca/2060/reports/Final_GMS_Document.pdf

Niehoff, D., Fritsch, U., and Bronstert, A., 2002, Land-use impacts on storm-runoff generation, scenarios of land-use change and simulation of hydrological response in a meso-scale catchment in SW-Germany, *Journal of Hydrology*, 267(1-2): 80-93.

Oogathoo, S., 2006, Runoff Simulation in the Canagagigue Creek Watershed using the MIKE-SHE Model, Unpublished M.Sc. thesis, Department of Bioresource Engineering, McGill University, Montreal, Canada.

Pan, Y., Roth, A., Yu, Z., and Doluschitz, R., 2010, The impact of variation in scale on the behavior of a cellular automata used for land-use change modeling, *Computers, Environment and Urban Systems*, 34:400-408.

Pijanowski, B. C., Brown, D.G., Shellito, B.A., and Manik, G.A., 2002, Using neural networks and GIS to forecast land use changes: a land transformation model, *Computers, Environment and Urban Systems*, 26: 553-575.

Puliafito, J. L., 2006, A transport model for the evolution of urban systems, *Applied Mathematical Modelling*, 31(11): 2391-2411.

Quan-Xing, L. and Zhen, J., 2005, Cellular automata modelling of SEIRS, *Chinese Physics*, 14: 1370-1377.

Refsgaard, J., 1996, Chapter 2: Terminology, modeling protocol and classification of hydrological model codes, *Distributed Hydrological Modeling*, Abbott M, Refsgaard J (eds); Kluwer Academic Publisher: Dordrecht: 16-39.

Refsgaard, J. C., 1997, Parameterization, calibration and validation of distributed hydrological models, *Journal of Hydrology*, 198: 69–97.

Refsgaard, J. C., Thorsen, M., Jensen, J. B., Kleeschulte, S., and Hansen, S., 1999, Large scale modeling of groundwater contamination from nitrate leaching, *Journal of Hydrology*, 221: 117–140.

Romano, N., and Palladino, M., 2002, Prediction of soil water retention using soil physical data and terrain attributes, *Journal of Hydrology*, 265: 56–75.

Rood, S. B., Samuelson, G. M., Weber, J. K., and Wywrot, K. A., 2005, Twentieth-century decline in streamflows from the hydrographic apex of North America, *Journal of Hydrology*, 306(1): 215-233.

Rood, S. B., Pan, J., Gill, K. M., Franks, C. G., Samuelson, G. M., and Shepherd, A., 2008, Declining summer flows of Rocky Mountain rivers: Changing seasonal hydrology and probable impacts on floodplain forests, *Journal of Hydrology*, 349(3): 397-410.

Samat, N., 2006, Characterizing the scale sensitivity of the cellular automata simulated urban growth, A case study of the Seberang Perai Region, Penang State, Malaysia Computers, *Environment and Urban Systems*, 30(6): 905-920.

Scurlock, J. M. O., Asner, G. P., and Gower, S. T., 2001, Worldwide Historical estimates of Leaf Area Index, 1932–2000, DOE Scientific and Technical Information, http://www.osti.gov/bridge/ (Article), 34 pp.

Sahoo, G. B., Ray, C., and De Carlo, E. H., 2006, Calibration and validation of a physically distributed hydrological model MIKE-SHE to predict stream flow at high frequency in a flashy mountainous Hawaii stream, *Journal of Hydrology*, 327(1-2): 94-109.

Santé. I., García, A. M., Miranda, D., and Crecente, R., 2010, Cellular automata models for the simulation of real-world urban processes, A review and analysis, *Landscape and Urban Planning*, 96: 108-122.

Schindler, D. W., and Donahue, W. F., 2006, An impending water crisis in Canada's western prairie provinces, *Proceedings of the National Academy of Sciences of the United States of America*, 103(19): 7210–7216.

Schindler, D. W., and Donahue, W. F., 2005, A case study of the Saskatchewan River system, *Rosenburg conference on managing upland watersheds in an era of global change, Banff, Alberta*, 6-11 Sept, 2005

Shen, Z., Kawakami, M., and Kawamura, I., 2009, Geosimulation model using geographic automata for simulating land-use patterns in urban partitions, *Environment and Planning B*, 36: 802-823.

Shepherd, A., Gill, K. M., and Rood, S. B., 2010, Climate change and future flows of Rocky Mountain rivers: converging forecasts from empirical trend projection and down scaled global circulation modeling, *Hydrological Processes*, 24(26): 3864-3877.

Singh, R., Subramanian, K., and Refsgaard, J. C., 1999, Hydrological modeling of a small watershed using MIKE-SHE for irrigation planning, *Agricultural Water Management*, 41 (3): 149-166.

Sirakoulis, G. C., Karafyllidis, I., and Thanailakis, A., 2000, A cellular automaton model for the effects of population movement and vaccination on epidemic propagation, *Ecological Modeling*, 133: 209–223.

Sittner, W. T., Schanss, C. E., and Monro, J. C., 1969, Continuous hydrograph synthesis with an API-type hydrologic model, *Water Resources Research*, 5: 1007-1022.

Statistics Canada, 2012, 2011 Census Profile, Calgary, http://www12.statcan.gc.ca/census-recensement/index-eng.cfm

Stevens, D., Dragicevic, S., and Rothley, K., 2007, iCity: A GIS–CA modelling tool for urban planning and decision making, *Environmental Modelling and Software*, 22(6): 761-773.

Syphard, A. D., Clarke, K. C., and Franklin, J., 2005, Using a cellular automaton model to forecast the effects of urban growth on habitat pattern in southern California, *Ecological Complexity*, 2 (2): 185-203.

Task Committee on Hydrology Handbook of Management Group D of the American Society of Civil Engineers, 1996, Hydrology Handbook, ASCE, New York.

Thanapakpawin, P., Richey, J., Thomas, D., Rodda, S., Campbell, B., and Logsdon, M., 2006, Effects of landuse change on the hydrologic regime of the Mae Chaem river basin, NW Thailand, *Journal of Hydrology*, 334: 215– 230.

The City of Calgary, 2012, Fall 2012: Calgary & Region Economic Outlook 2012-2017 with long-term Economic Trends 2018-2042,

http://www.calgary.ca/CA/fs/Documents/Corporate-Economics/Calgary-and-Region-Economic-Outlook/Calgary-and-Region-Economic-Outlook-2012-Fall.pdf

Thorpe, A. J., 2005, Climate Change Prediction, A challenging scientific problem, Institue of physics, http://www.iop.org/publications/iop/archive/file_52051.pdf

The City of Calgary, 2010, 2010 Civic Census Results, http://www.calgary.ca/CA/city-clerks/Documents/Election-and-information-services/Census/2010_census_result_book.pdf

The City of Calgary, 2011, Economic Outlook: 2011 – 2021, Calgary & Region, Volume 2, Calgary Economic Development 2012.

(USACE) US Army Corps of Engineers, 2000, Hydrologic Modeling System HEC-HMS: Technical REference Manual, Hydrologic Engineering Center, 157 pp.

Valeo, C., Xiang, Z., Bouchart, F. J-C., Yeung, P., and Ryan, M. C., 2007, Climate change impacts in the Elbow River watershed, *Canadian Water Resources Journal*, 32(4): 285-302.

Van Vliet, J., Bregt, A. K., and Hagen-Zanker, A., 2011, Revisiting Kappa to account for change in the accuracy assessment of land-use change models, *Ecological Modelling*, 222(8): 1367-1375.

Va´zquez, R. F., and Feyen, J., 2003, Effect of potential evapotranspiration estimates on effective parameters and performance of the MIKE-SHE code applied to a medium-size catchment, *Journal of Hydrology*, 270: 309–327.

Verburg, P. H., Soepboer, W., Veldkamp, A., Limpiada, R., Espaldon, V., and Mastura, S. S., 2002, Modeling the spatial dynamics of regional land use: the CLUE-S model. *Environmental Management*, 30(3): 391-405.

Verburg, P. H., de Nijs, T. C. M., Van Eck, J.R., Visser, H., and de Jong, K., 2004, A method to analyse neighbourhood characteristics of land use patterns, Computers, *Environment and Urban Systems*, 28(6): 667-690.

Visser, H., and de Nijs, T., 2006, The Map Comparison Kit, *Environmental Modelling and Software*, 21(3): 346-358.

Wang, F., 2012, A Cellular Automata model to simulate land-use changes at fine spatial resolution, Published Ph.D. thesis, Department of Geomatics Engieering, University of Calgary.

Ward, D. P., Murray, A. T., and Phinn, S. R., 2000, A stochastically constrained cellular model of urban growth, *Computers, Environment and Urban Systems*, 24 (6): 539-558.

White, R., Engelen, G., and Uljee, I., 1997, The use of constrained cellular automata for high-resolution modelling of urban land-use dynamics, *Environment and Planning B*, 25: 323-343.

White, R., and Engelen, G., 2000, High-resolution integrated modeling of the spatial dynamics of urban and regional systems, *Computers, Environment and Urban Systems*, 24: 383-400.

Wijesekara, G. N., and Marceau, D. J., 2012, Elbow River Watershed MIKE-SHE Model: Enhancement and scenario modelling project, Report submitted to Alberta Environment and Sustainable Resource Development, Calgary, AB, 75 pp.

Wijesekara, N., Gupta, A., Valeo, C., Hasbani, J. G., Qiao, Y., Delaney, P., and Marceau, D. J., 2012, Assessing the impact of future land-use changes on hydrological processes in the Elbow River watershed in southern Alberta, Canada. *Journal of Hydrology*, 412-413: 220-232.

Wu, F., 2002, Calibration of stochastic cellular automata: the application to rural-urban land conversions, International Journal of Geographical Information Sciences, 16: 795-818.

Wu, J., and David, J. L., 2002, A spatially explicit hierarchical approach to modeling complex ecological systems: theory and applications, *Ecological Modelling*, 153 (1-2): 7-26.

Yang, D., Herath, S., and Musiake, K., 2000, Comparison of different distributed hydrological models for characterization of catchment spatial variability, *Hydrological Processes*, 14 (3): 403-416.

Appendix A: Historical land-use maps of the Elbow River watershed

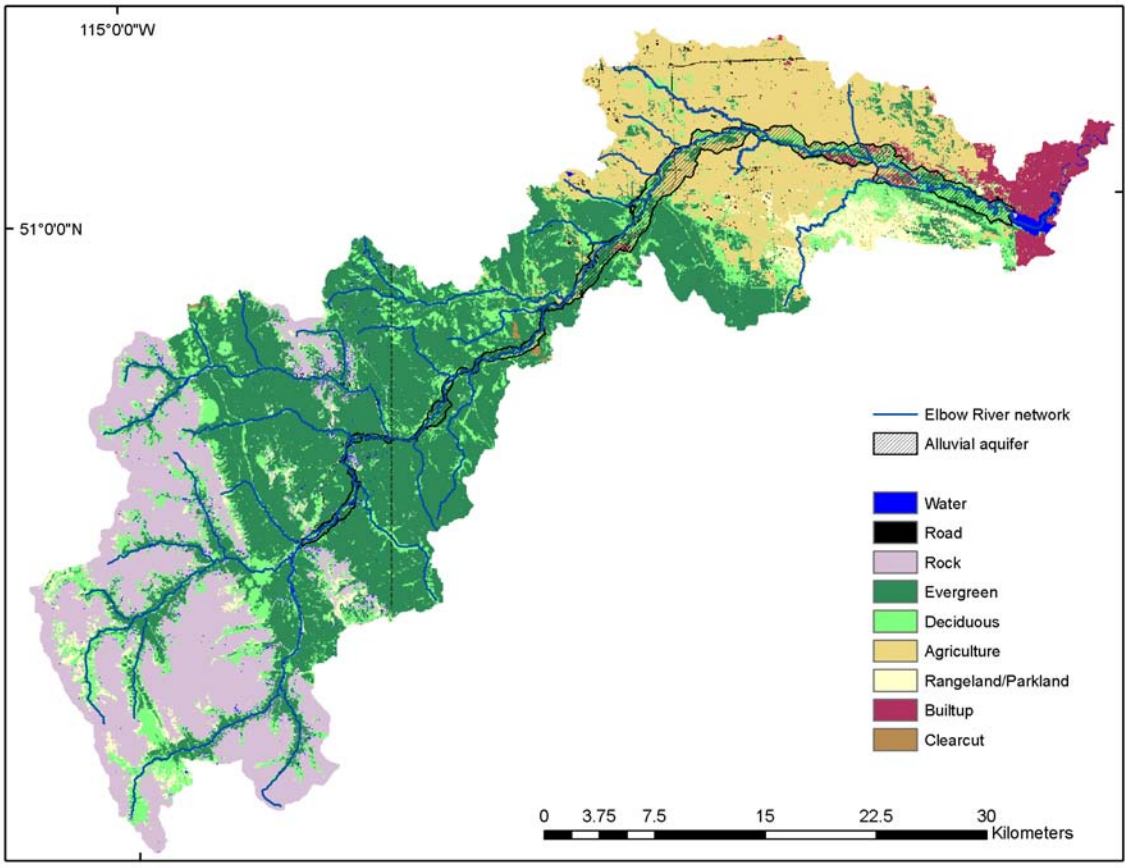

Figure A.1: Land-use map of 1985

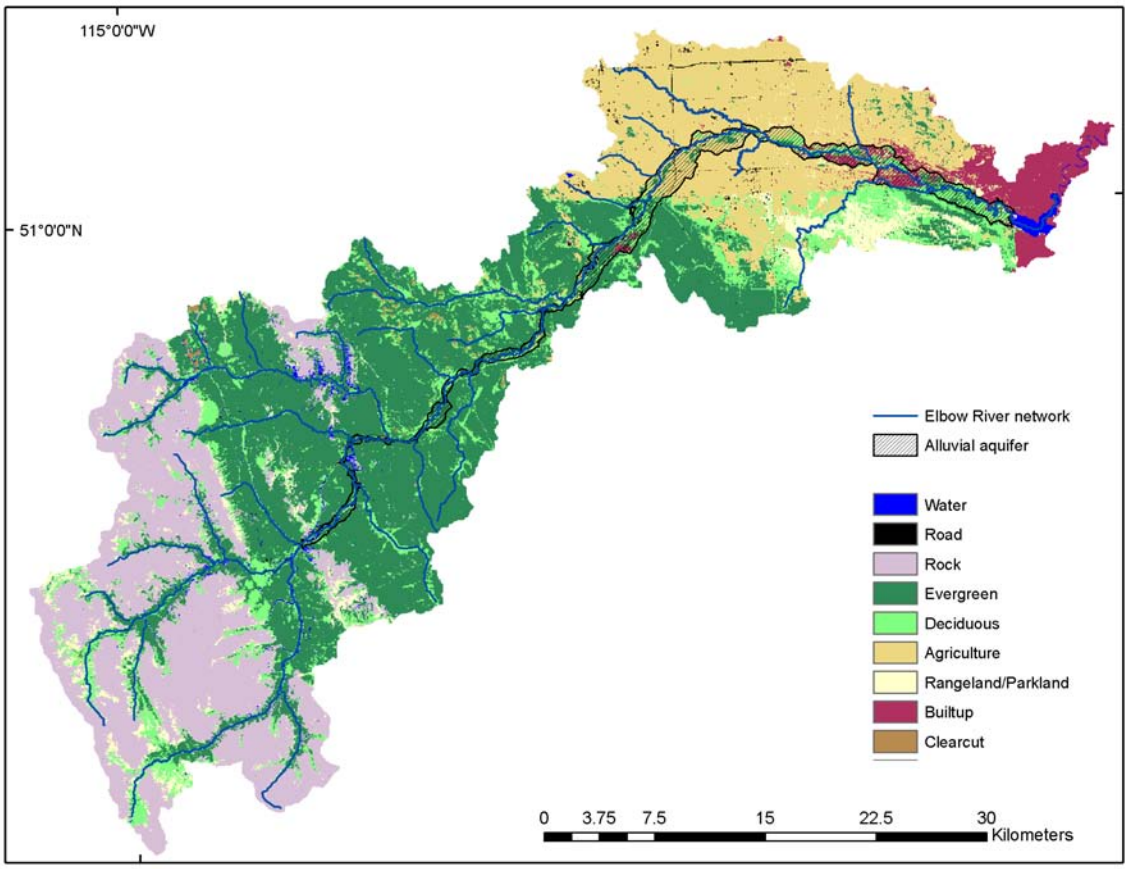

Figure A.2: Land-use map of 1992

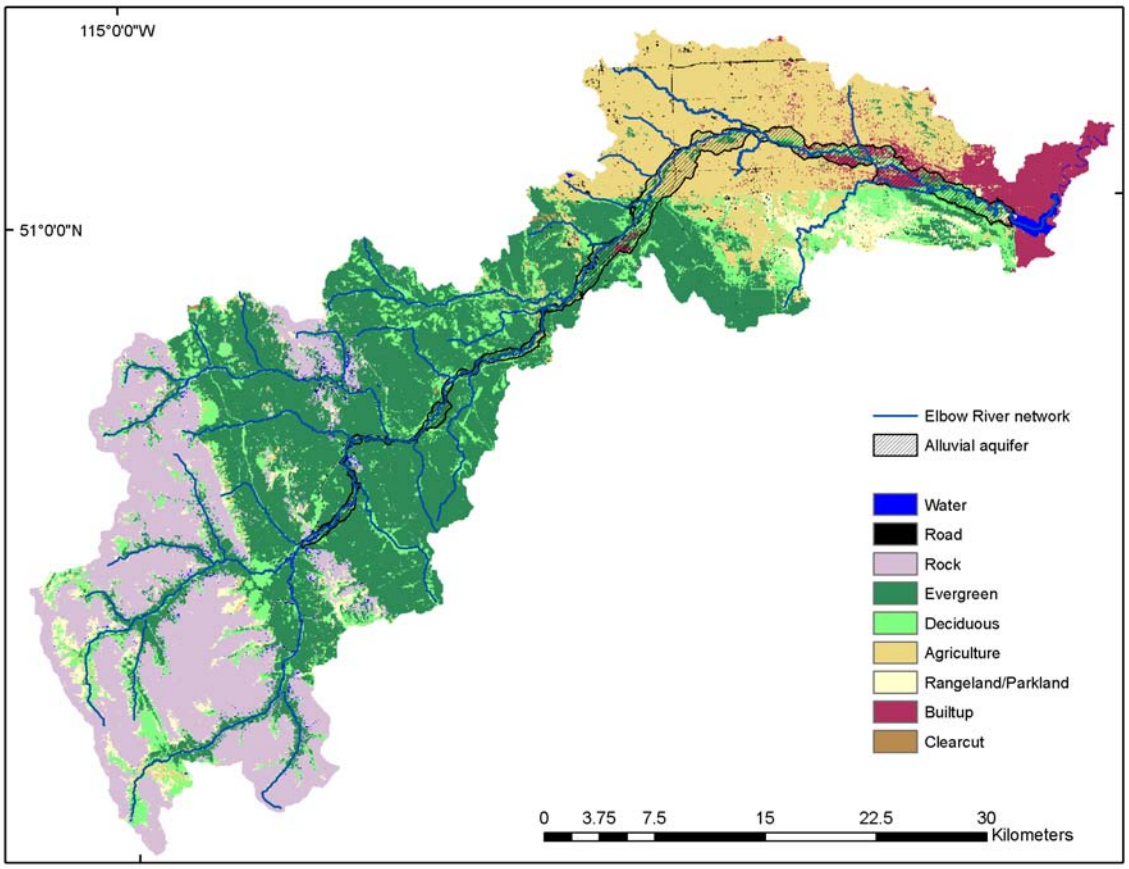

Figure A.3: Land-use map of 1996

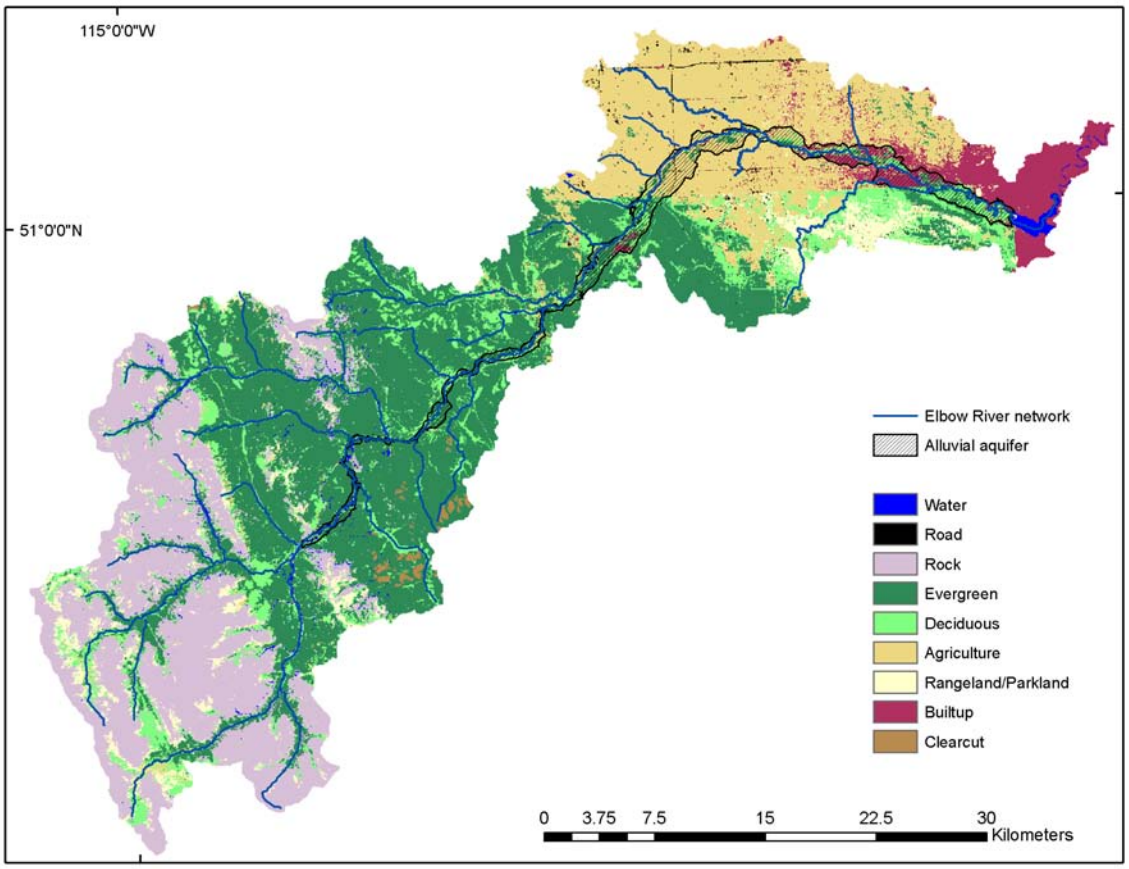

Figure A.4: Land-use map of 2001

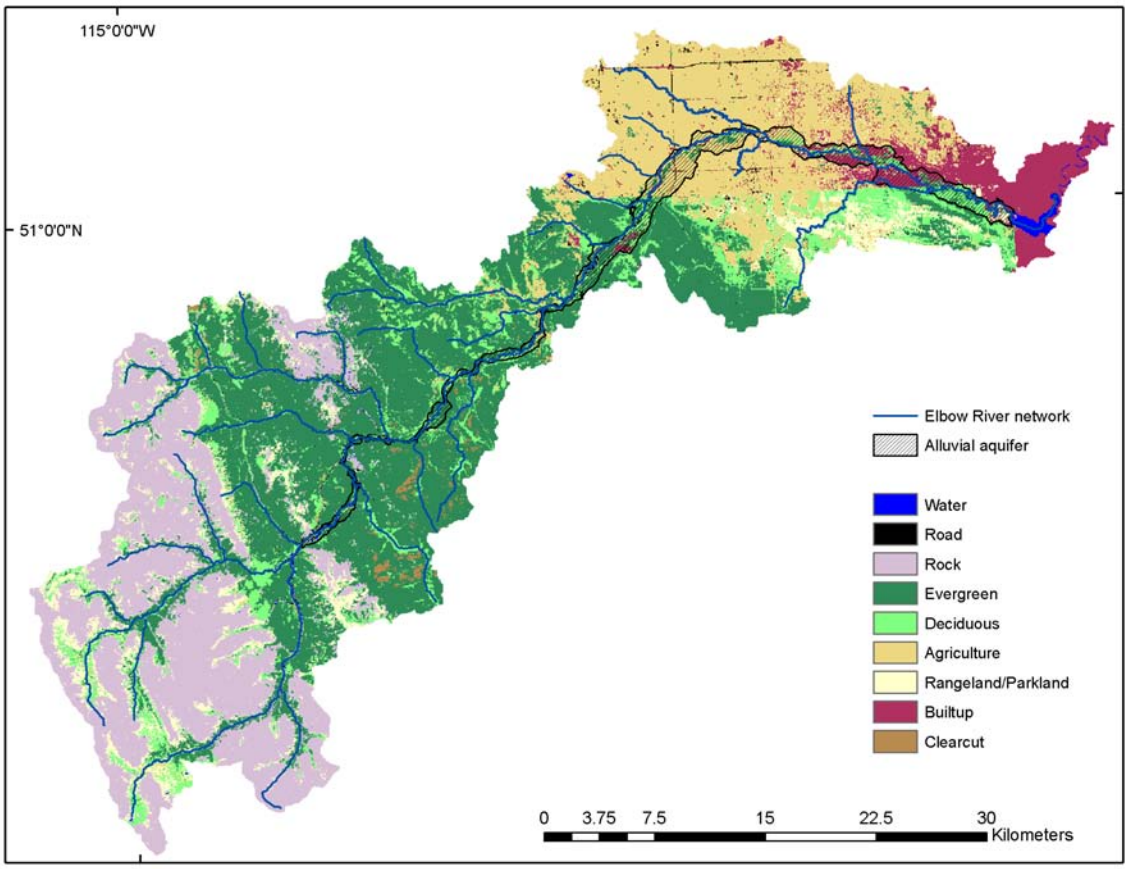

Figure A.5: Land-use map of 2006

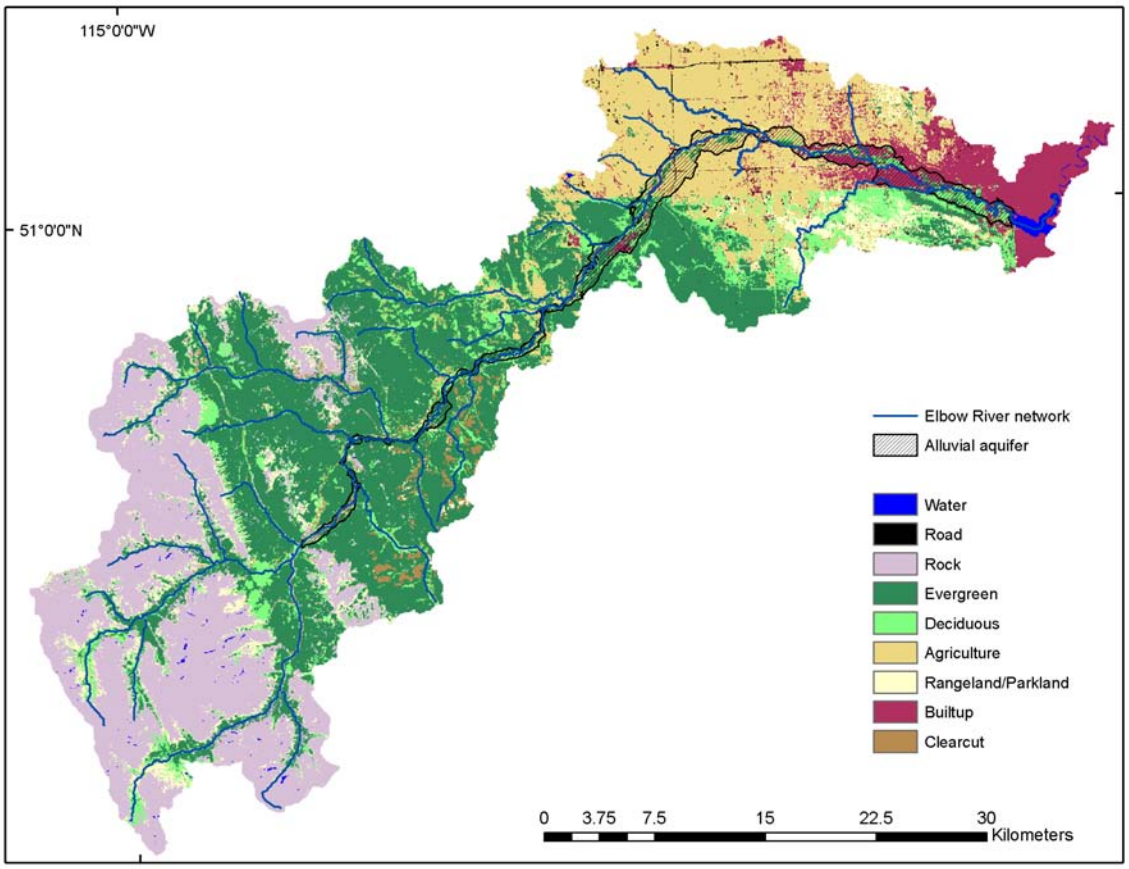

Figure A.6: Land-use map of 2010

Appendix B: Distributed surface roughness corresponding to the historical land-use maps

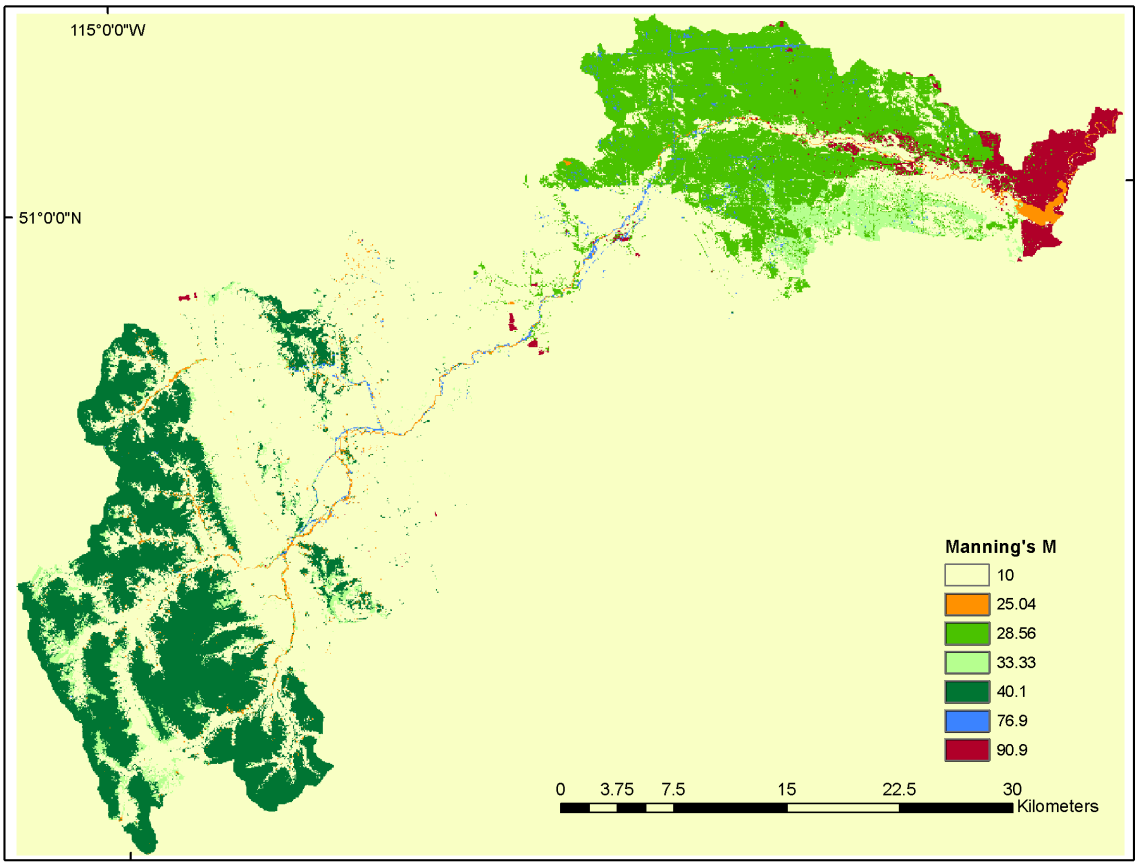

Figure B.1: Map of surface roughness for the year 1985

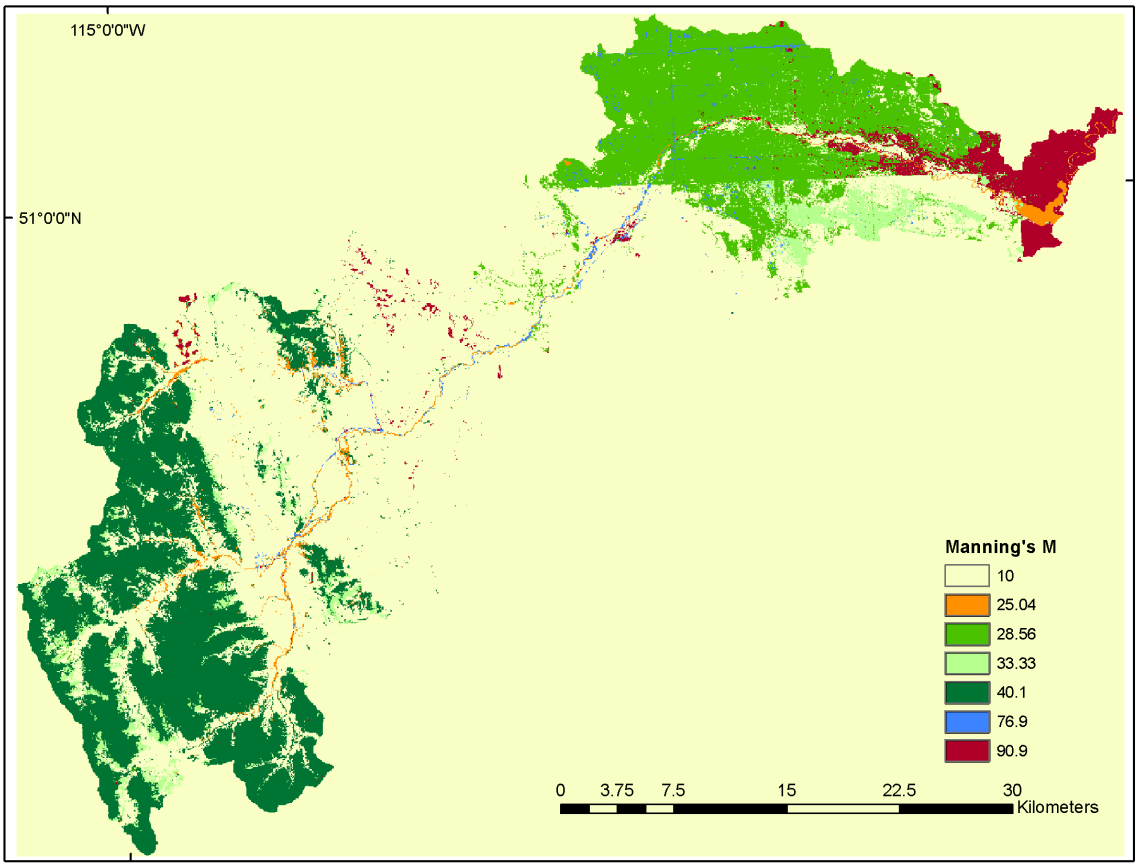

Figure B.2: Map of surface roughness for the year 1992

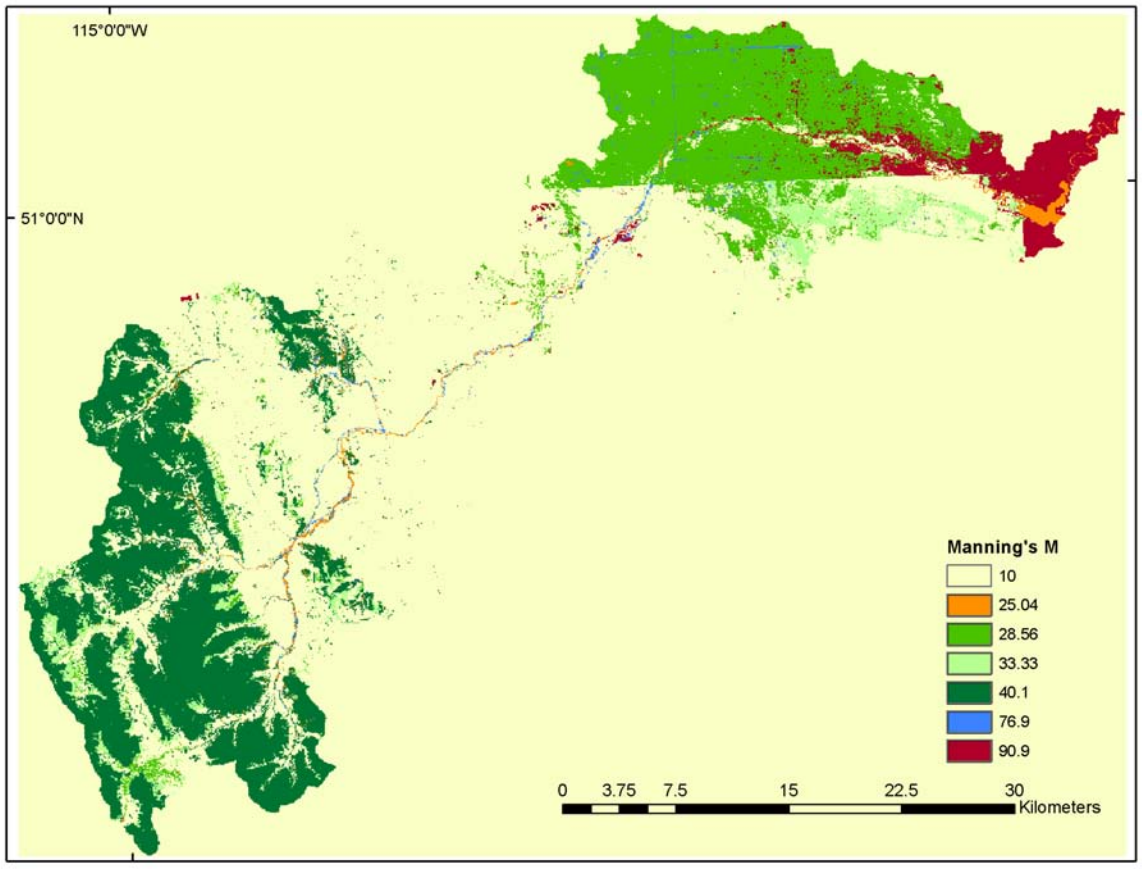

Figure B.3: Map of surface roughness for the year 1996

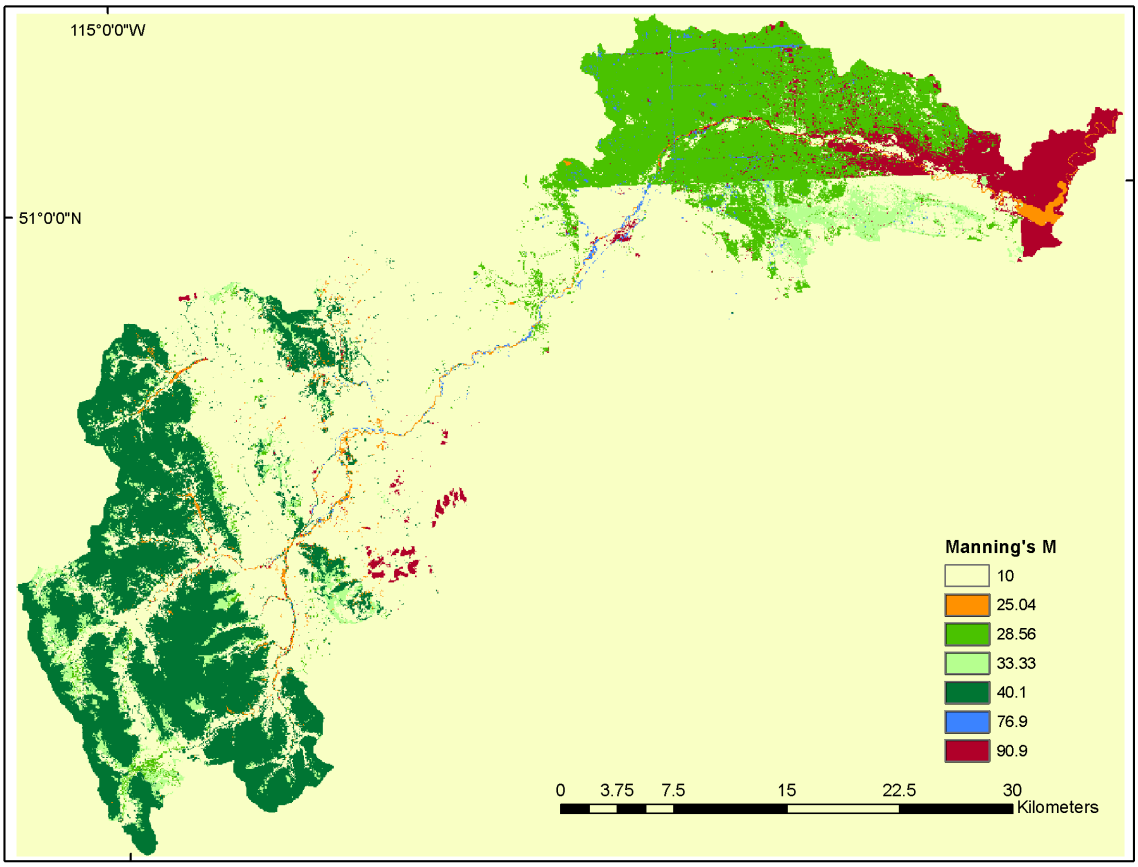

Figure B.4: Map of surface roughness for the year 2001

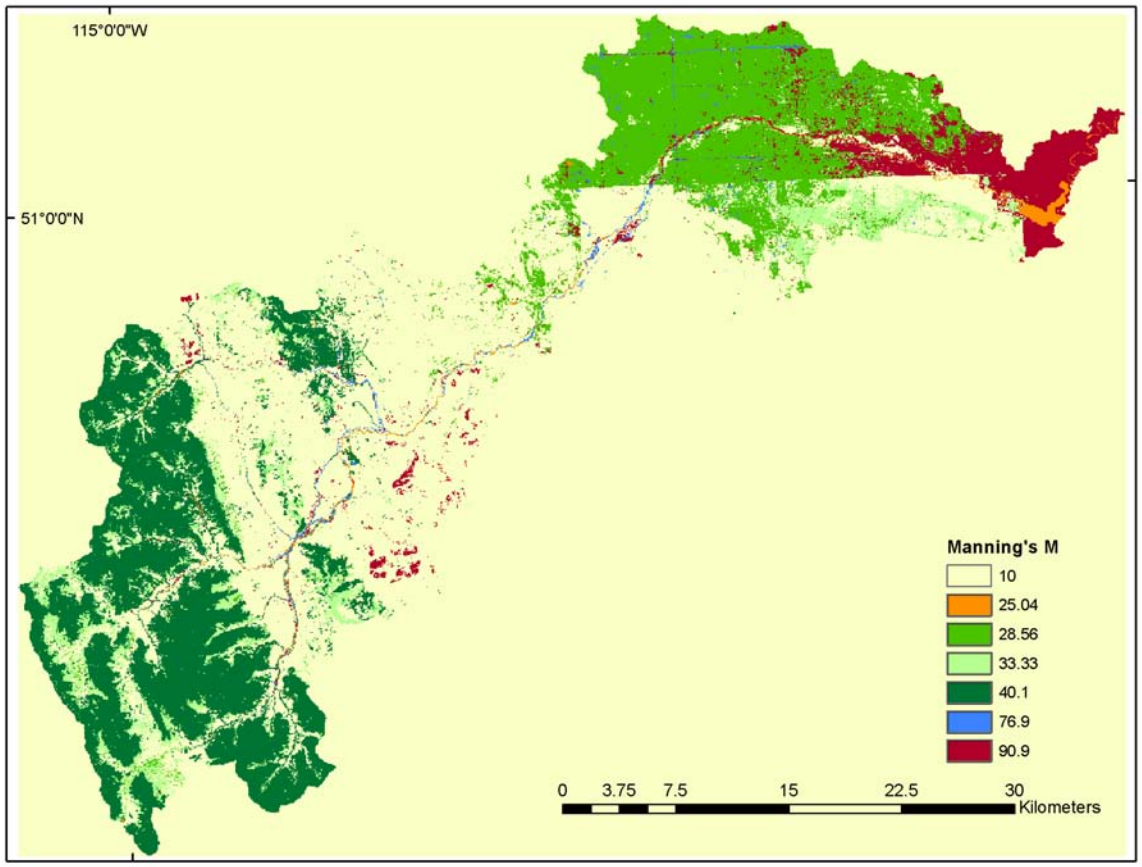

Figure B.5: Map of surface roughness for the year 2006

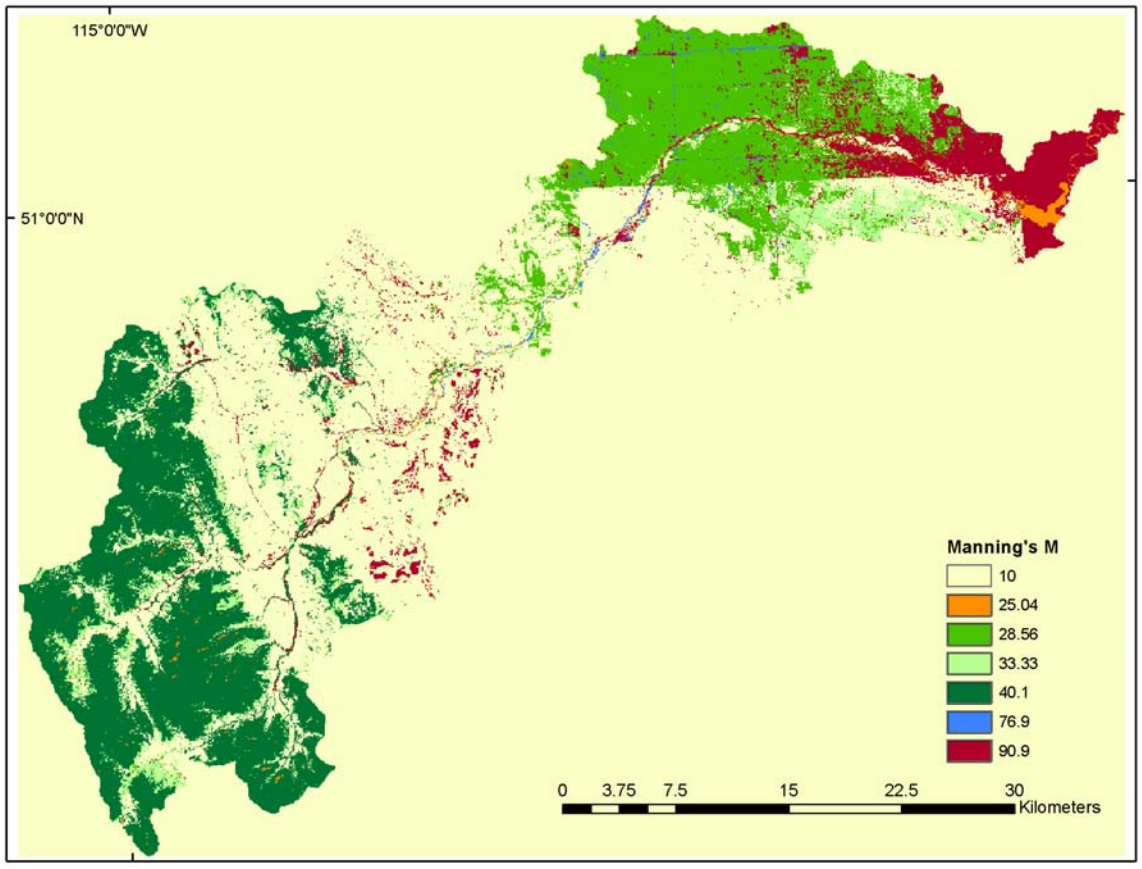

Figure B.6: Map of surface roughness for the year 2010

Appendix C: Soil distribution corresponding to each historical land-use map

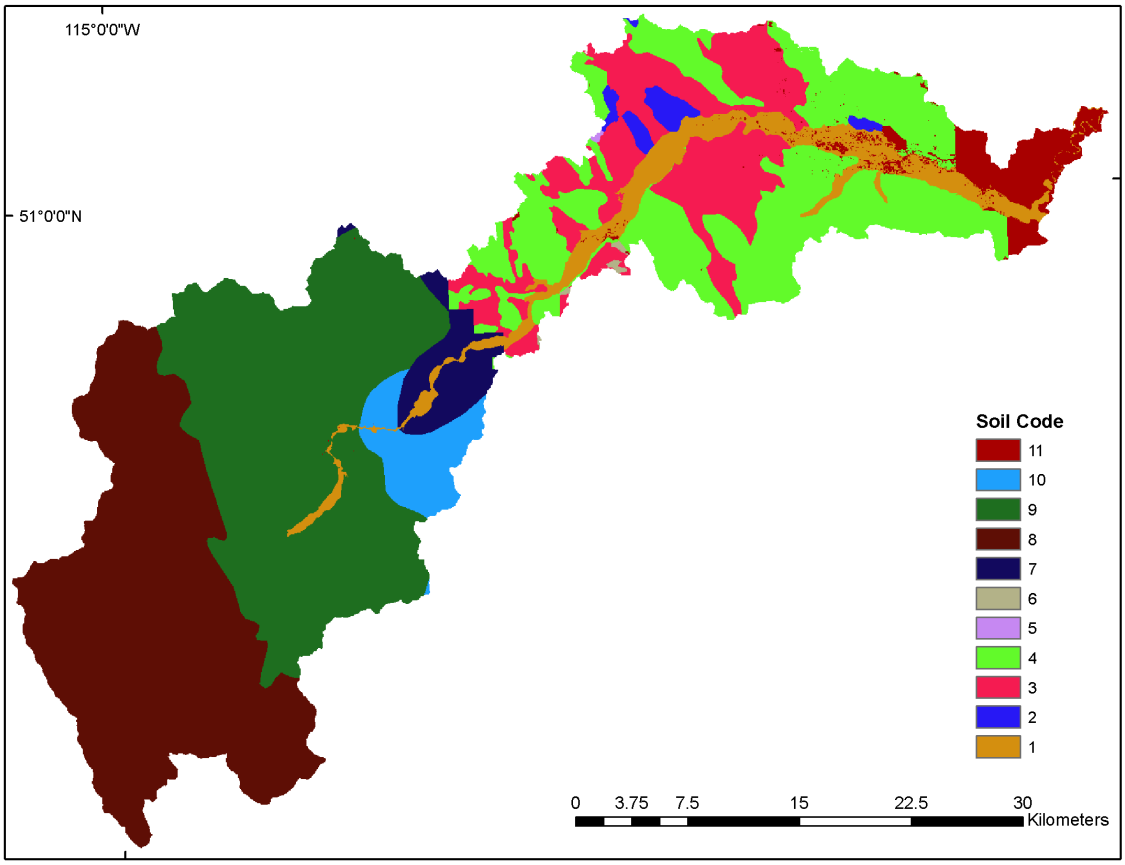

Figure C.1: Map of soil distribution for the year 1985

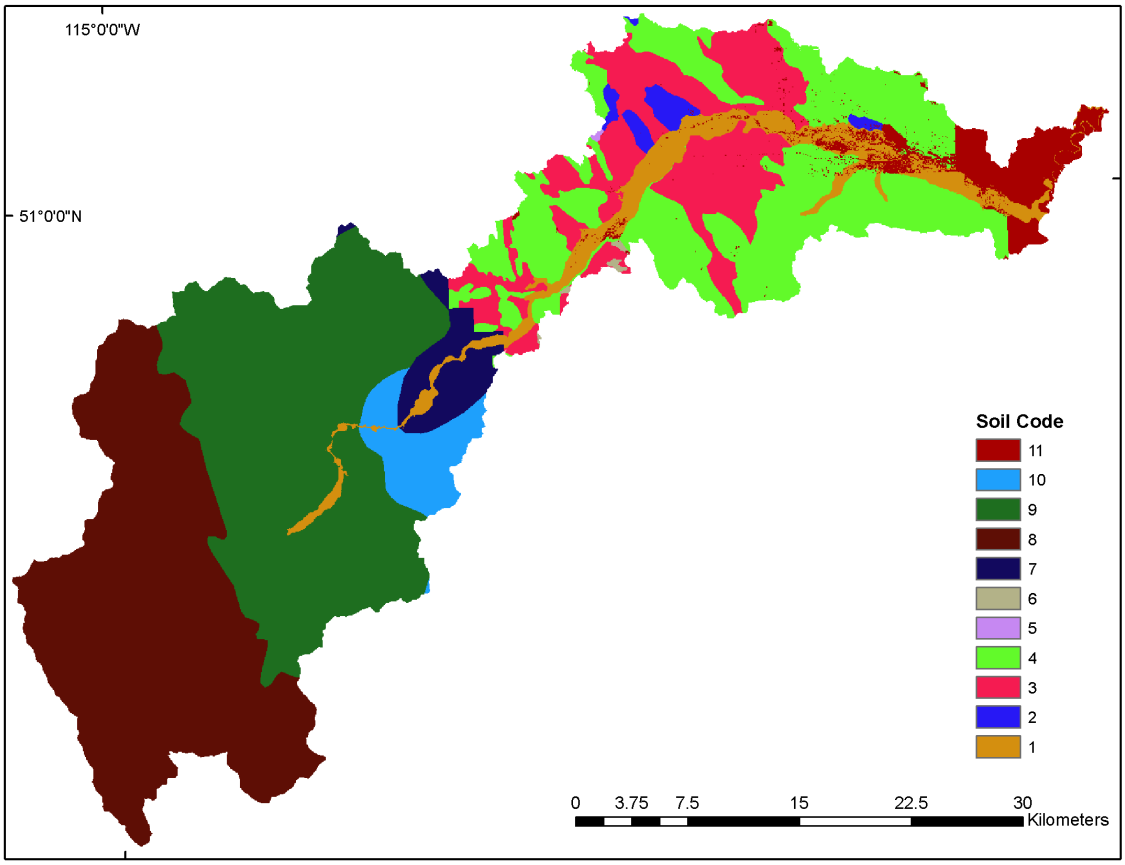

Figure C.2: Map of soil distribution for the year 1992

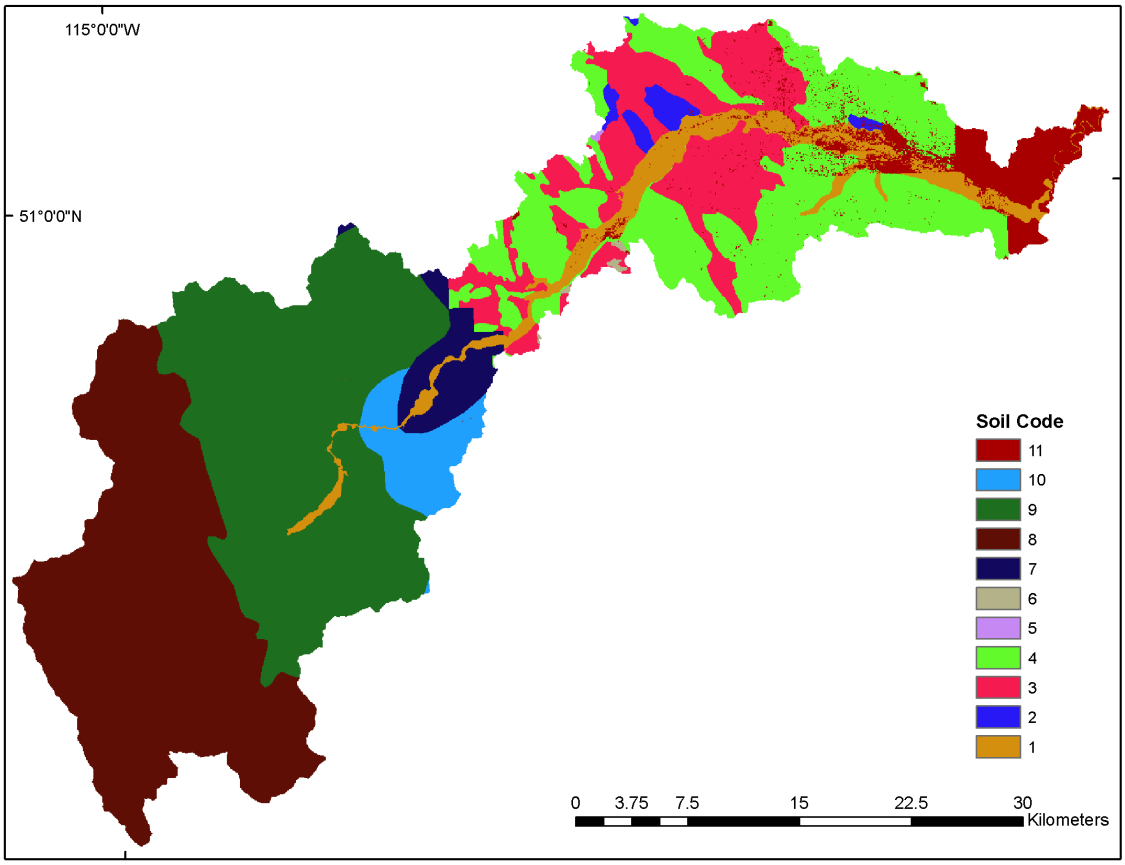

Figure C.3: Map of soil distribution for the year 1996

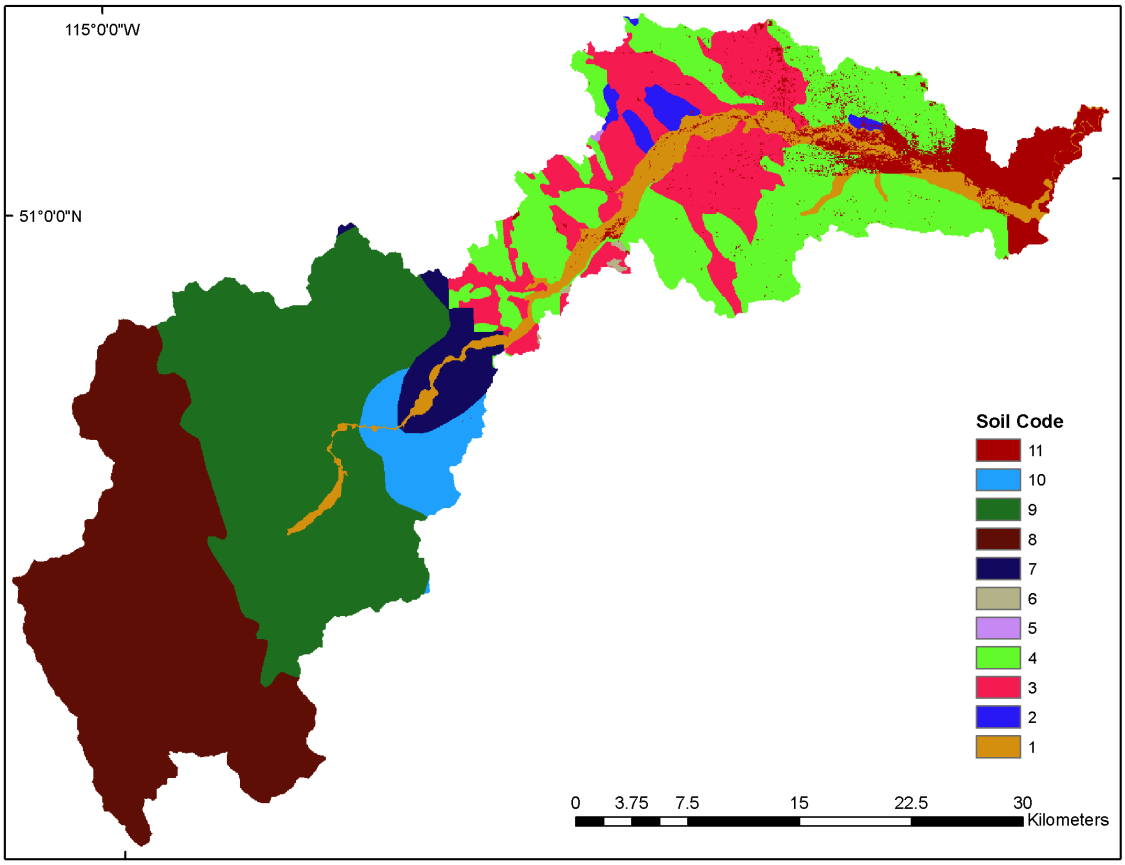

Figure C.4: Map of soil distribution for the year 2001

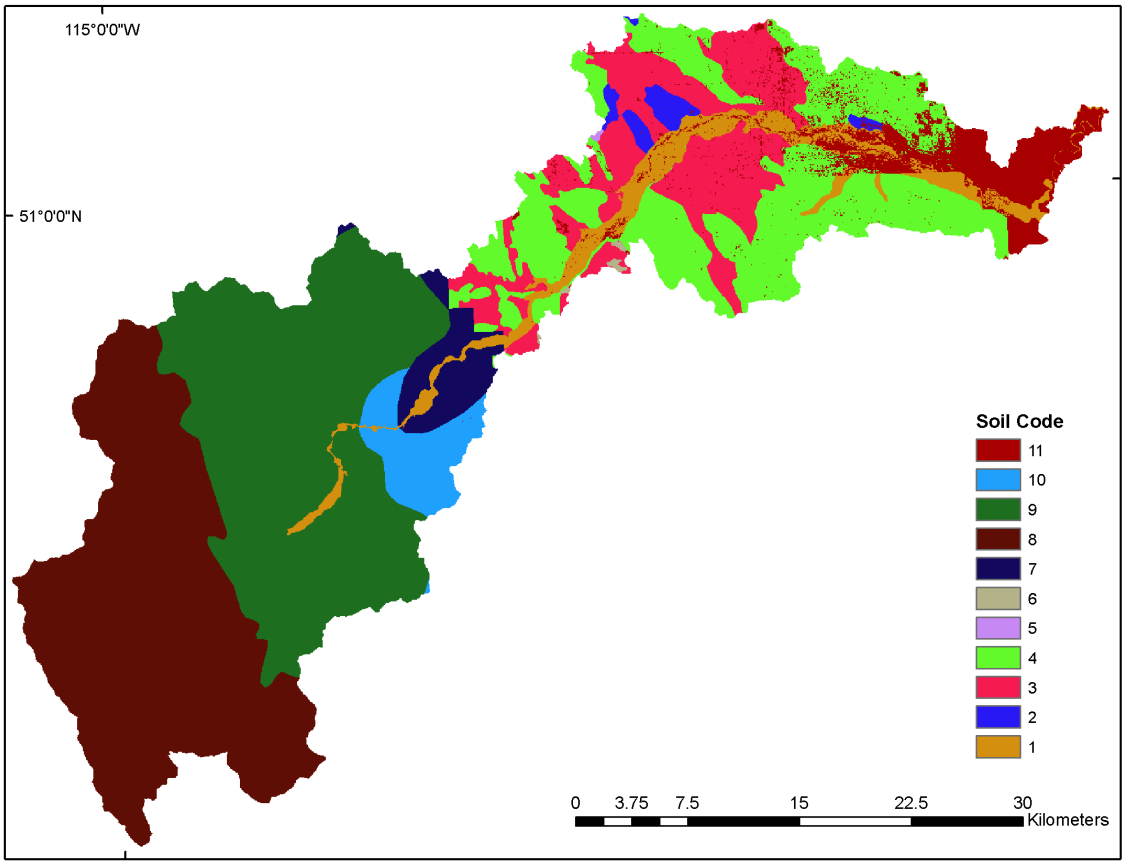

Figure C.5: Map of soil distribution for the year 2006

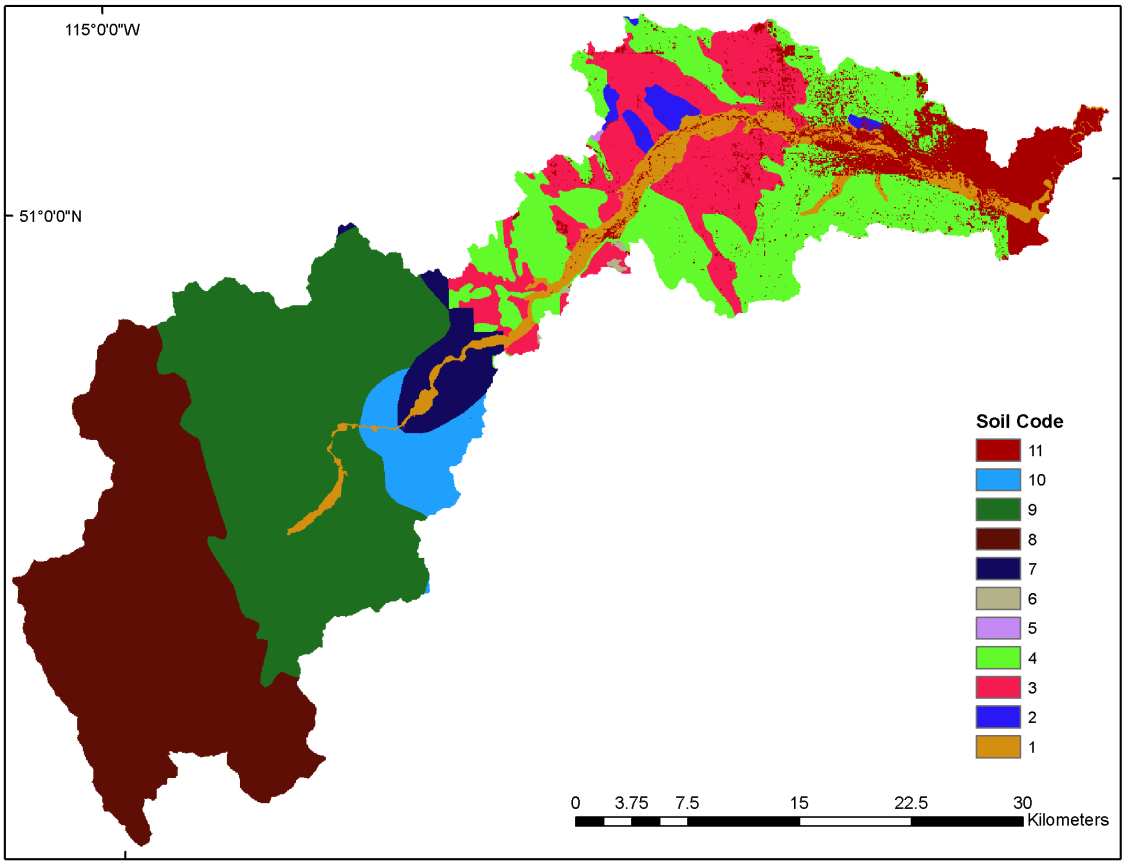

Figure C.6: Map of soil distribution for the year 2010

Appendix D: Distributed detention storage corresponding to each historical land-use map

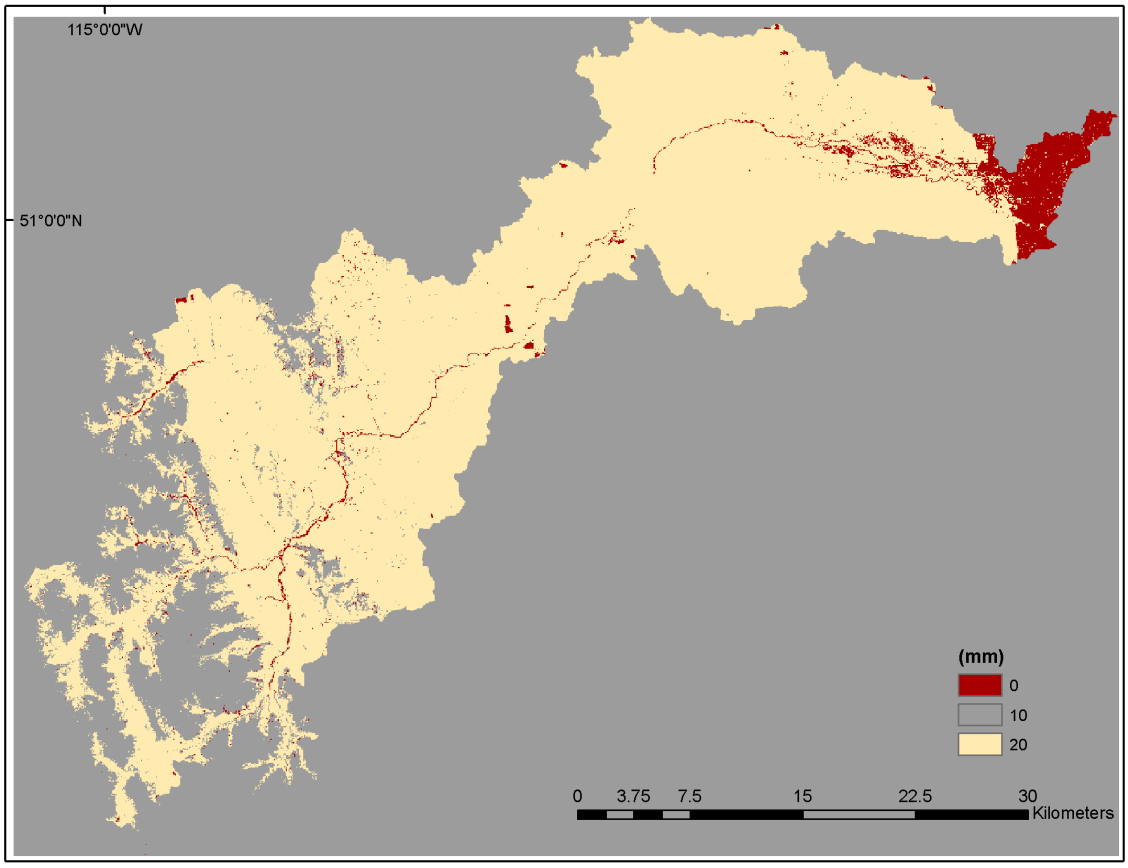

Figure D.1: Map of distributed detention storage for the year 1985

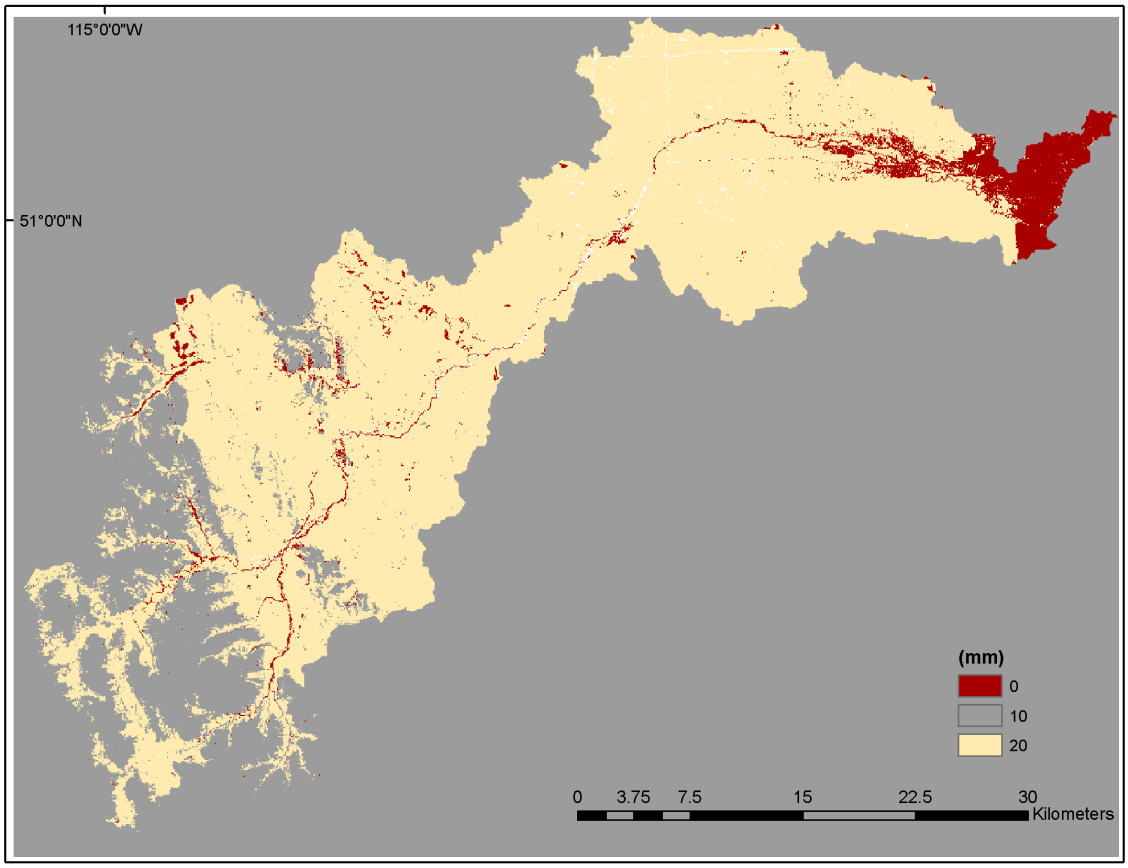

Figure D.2: Map of distributed detention storage for the year 1992

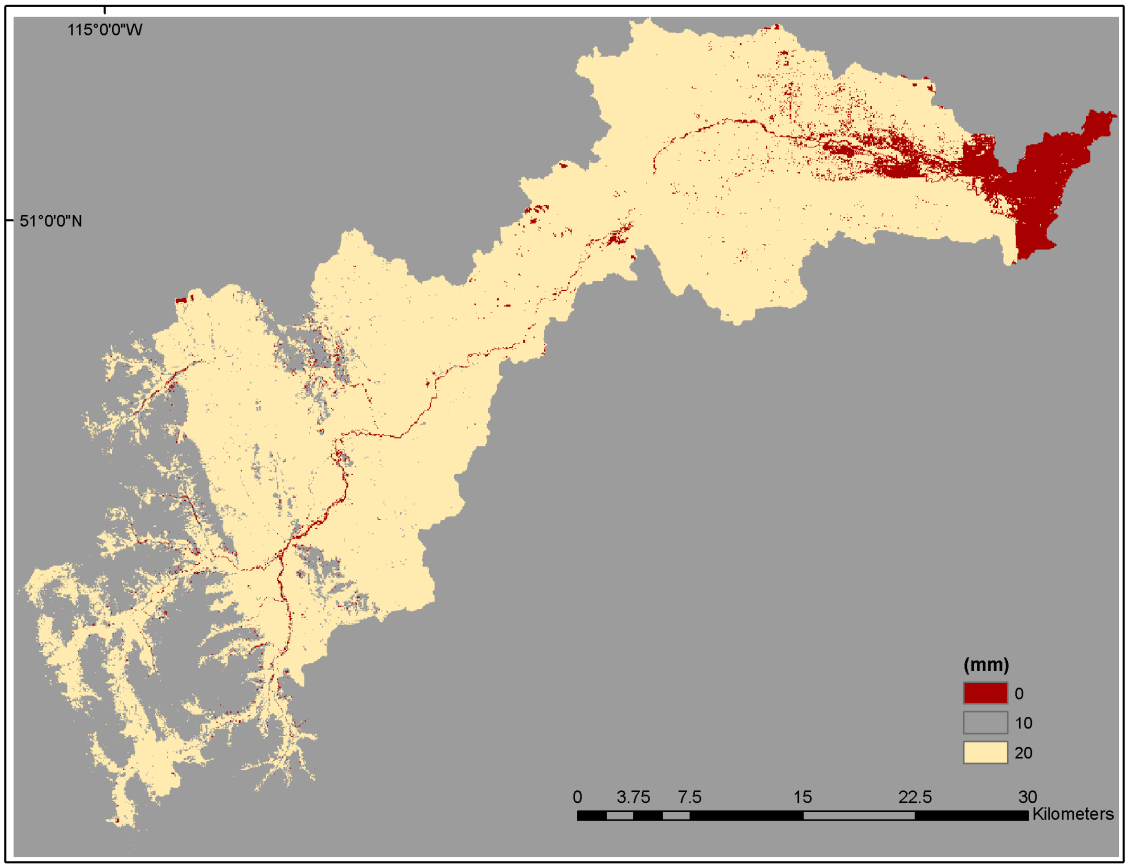

Figure D.3: Map of distributed detention storage for the year 1996

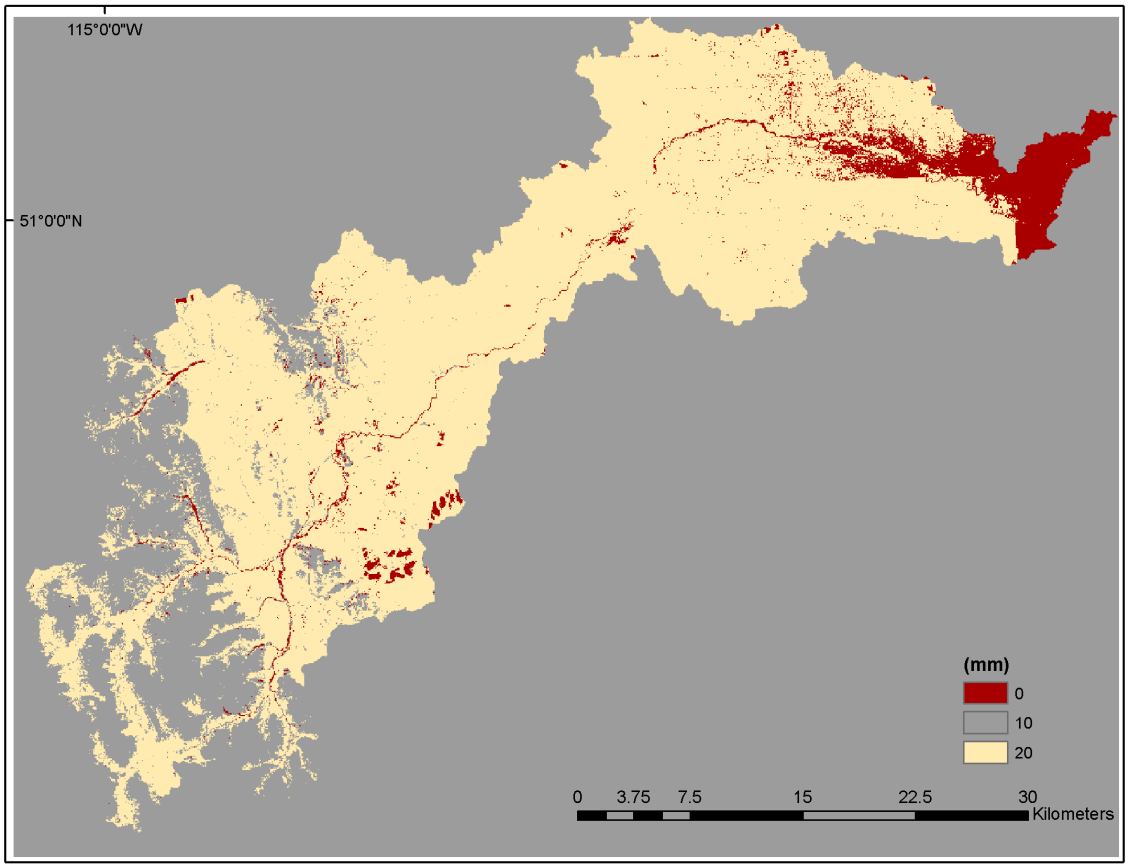

Figure D.4: Map of distributed detention storage for the year 2001

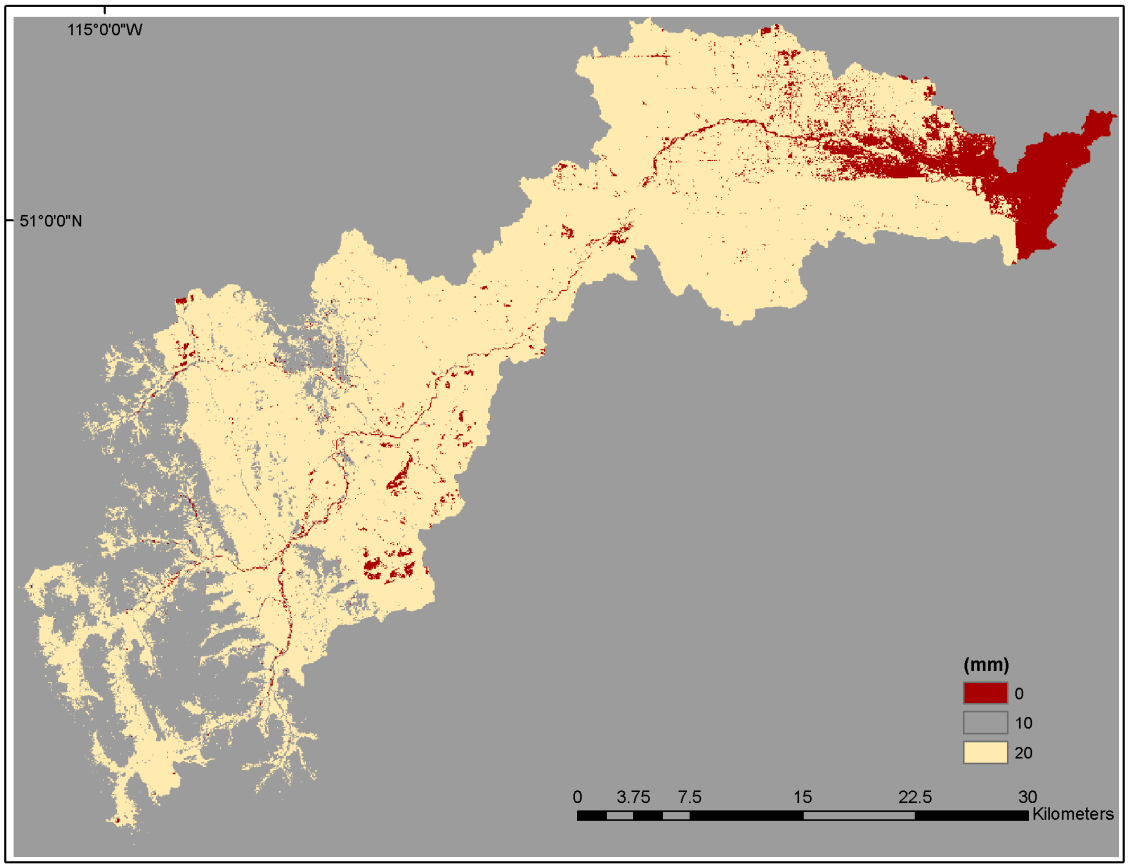

Figure D.5: Map of distributed detention storage for the year 2006

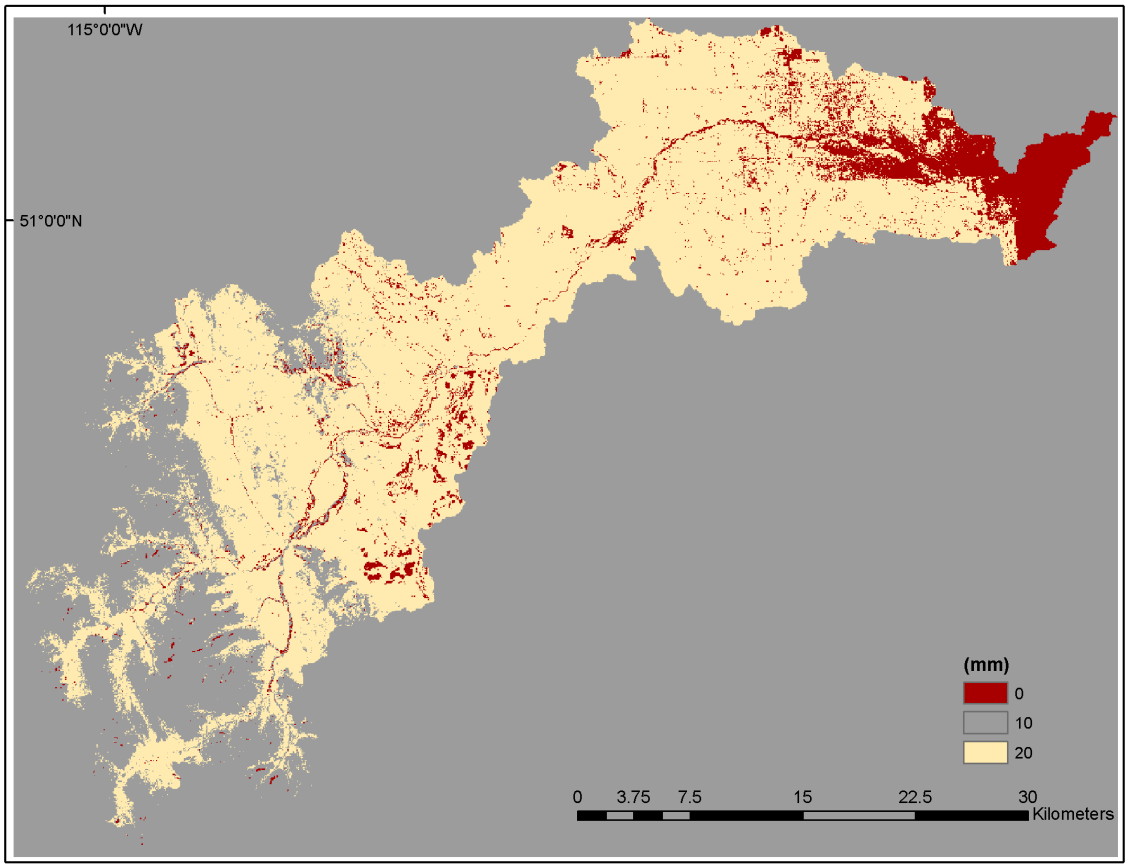

Figure D.6: Map of distributed detention storage for the year 2010

Appendix E: Distributed paved runoff coefficient and overland-groundwater leakage coefficient corresponding to each historical land-use map

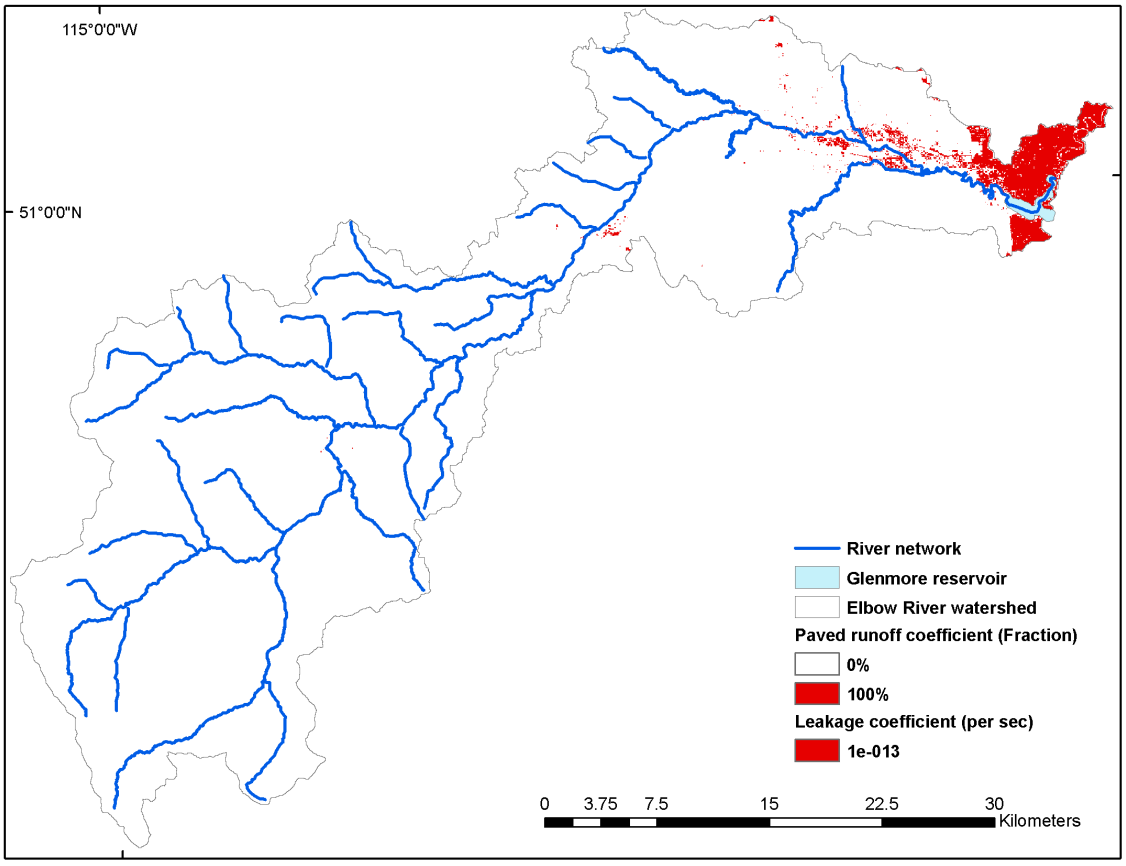

Figure E.1: Map of distributed paved runoff coefficient and overland-groundwater leakage coefficient for the year 1985

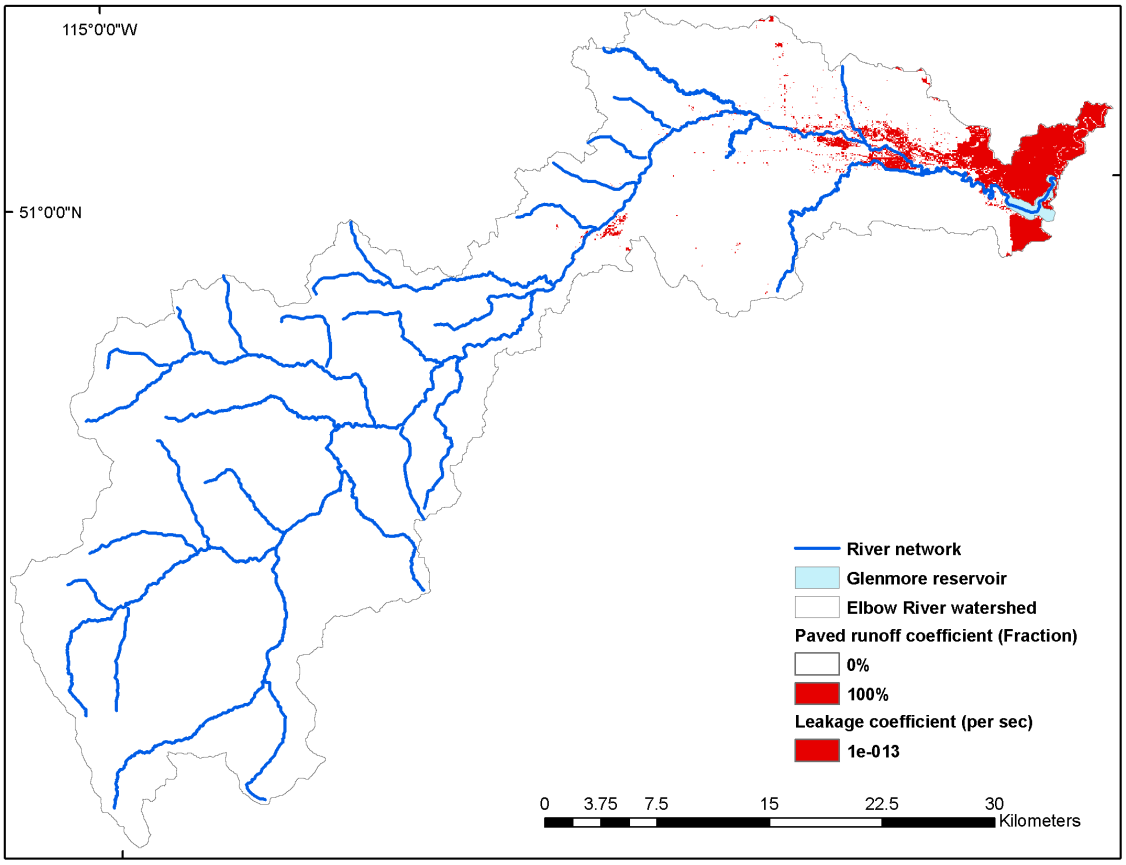

Figure E.2: Map of distributed paved runoff coefficient and overland-groundwater leakage coefficient for the year 1992

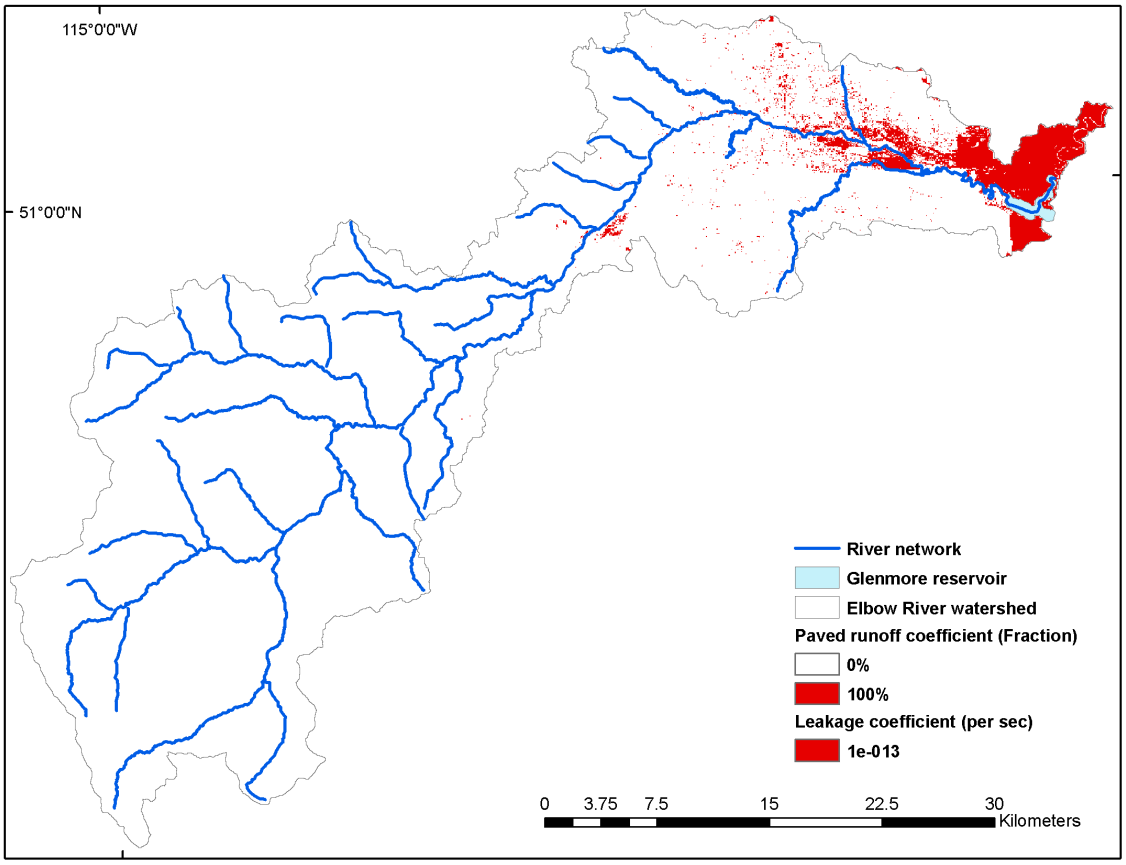

Figure E.3: Map of distributed paved runoff coefficient and overland-groundwater leakage coefficient for the year 1996

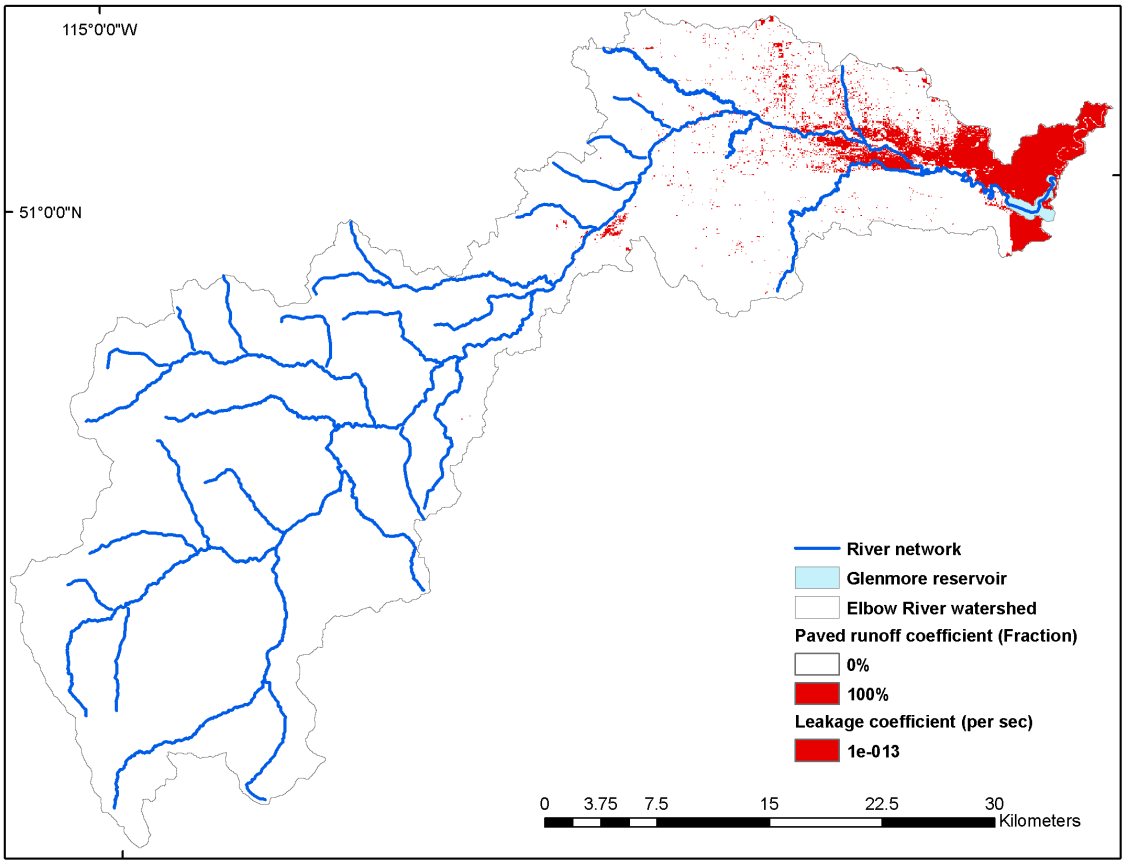

Figure E.4: Map of distributed paved runoff coefficient and overland-groundwater leakage coefficient for the year 2001

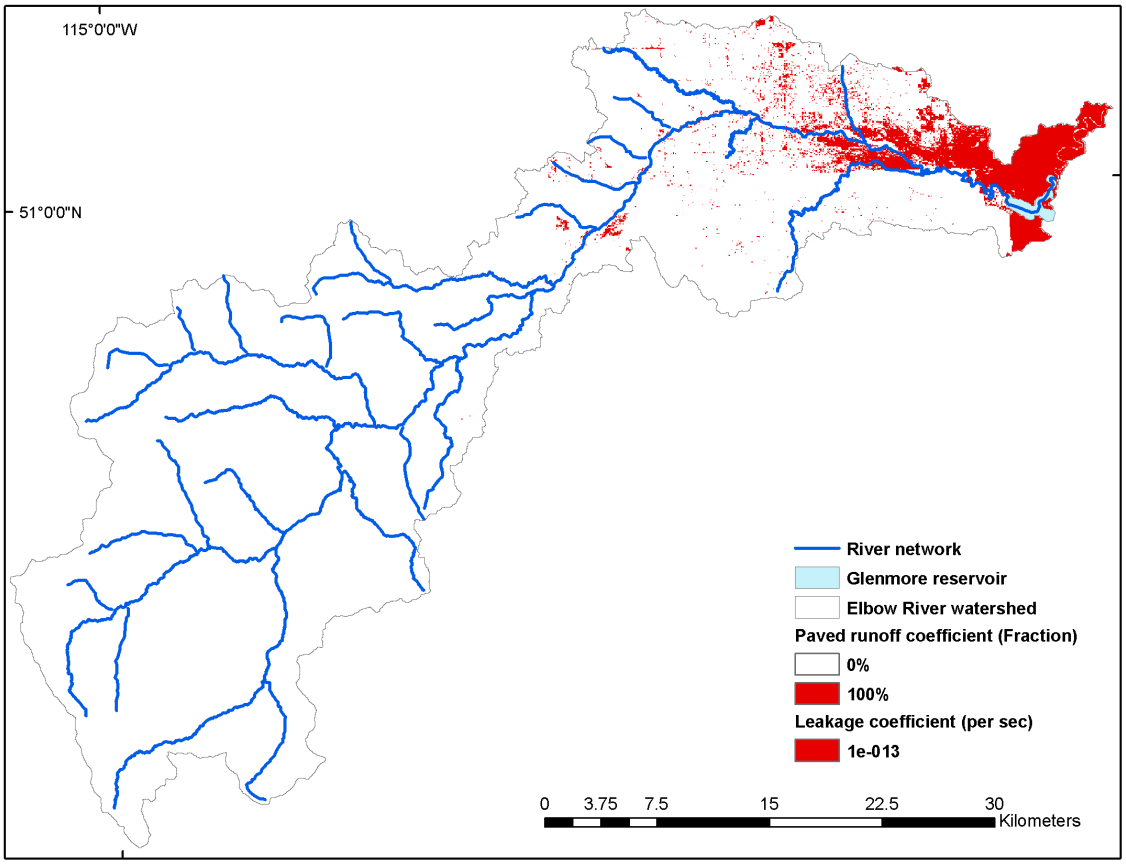

Figure E.5: Map of distributed paved runoff coefficient and overland-groundwater leakage coefficient for the year 2006

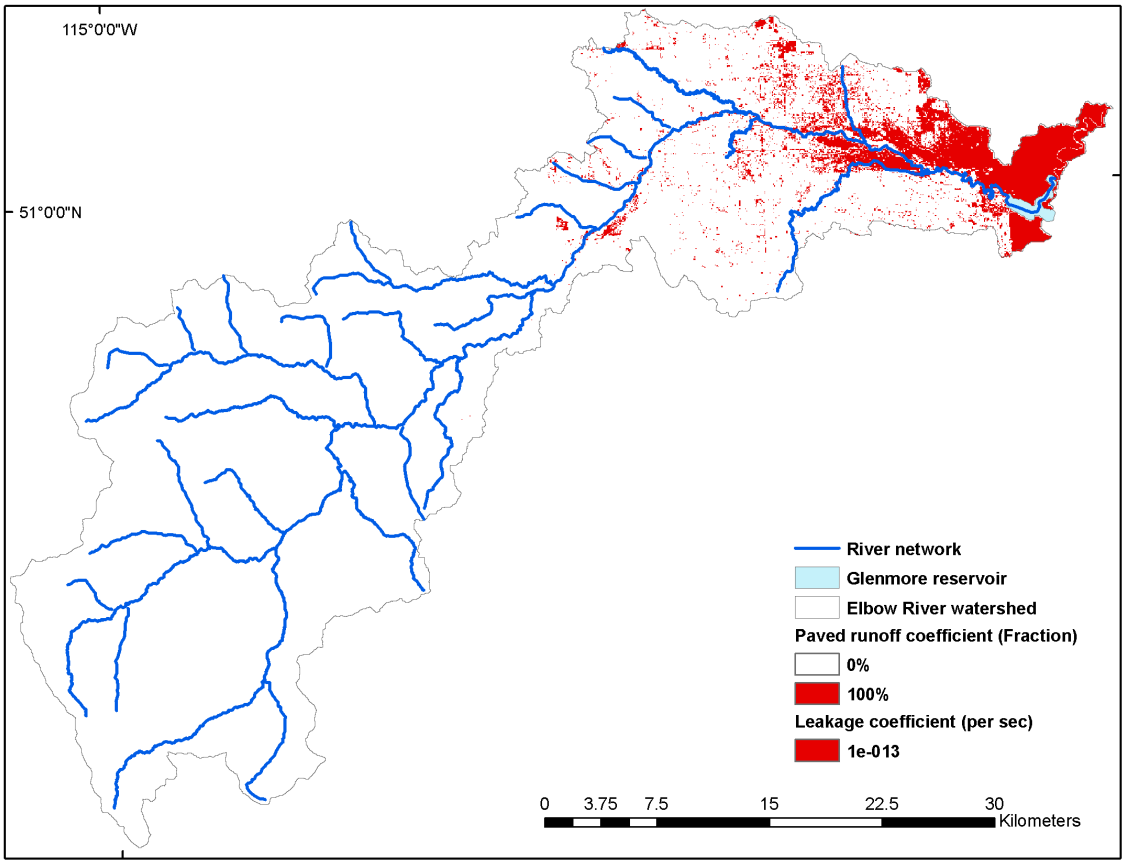

Figure E.6: Map of distributed paved runoff coefficient and overland-groundwater leakage coefficient for the year 2010

Appendix F: Results of the sensitivity analysis to cell size, neighborhood configuration, selection of external driving factors and their values from frequency histograms of the land-use CA model.

Table F.1: Values of K_{sim}, $K_{transLoc}$, and $K_{transition}$ obtained when using a cell size of 60 m and 100 m in the CA model (Hasbani *et al.* 2011)

Cell size	**K_{sim}**	**$K_{transLoc}$**	**$K_{transition}$**
60 m	0.058	0.140	0.411
100 m	0.038	0.093	0.409

Table F.2: Values of K_{sim}, $K_{transLoc}$, and $K_{transition}$ obtained when using different neighborhood configurations in the CA model (Hasbani *et al.* 2011)

Neighborhood Configuration	**K_{sim}**
3-5	0.015
3-5-15	0.037
5-9-14	0.044
5-9-15	0.045
5-9-16	0.046
5-9-17	0.047
5-12-17	0.045
6-9-15	0.031
6-14-18	0.043
6-14-19	0.045
7-10-15	0.042
7-10-16	0.044
7-10-17	0.044

7-13-17	0.034
7-14-18	0.043
7-14-19	0.044
7-14-20	0.045
7-15-19	0.043
8-12	0.024
8-15-19	0.042

Table F.3: Values of K_{sim}, $K_{transLoc}$, and $K_{transition}$ obtained when using different grouping of parameter values from the frequency histograms for the definition of the transition rules in the CA model (Hasbani *et al.* 2011)

Selection of parameter values	**K_{sim}**	**$K_{transLoc}$**	**$K_{transition}$**
Most dominant ranges of values	0.047	0.085	0.551
Values dispersed from the mode	0.045	0.081	0.551
Values concentrated around the mode	0.069	0.126	0.551
One group of values	0.041	0.074	0.551

Table F.4: Values of K_{sim}, $K_{transLoc}$, and $K_{transition}$ obtained when using four external driving factors compared to the combinations of only three factors in the CA model (Hasbani *et al.* 2011)

Factor selection	**K_{sim}**	**$K_{transLoc}$**	**$K_{transition}$**
Distance to main road Distance to city center Distance to river Ground slope	0.058	0.140	0.411
Distance to main road Distance to city center Distance to river	0.042	0.102	0.411

Distance to main road Distance to city center Ground Slope	0.038	0.094	0.411
Distance to main road Distance to river Ground Slope	0.041	0.100	0.411
Distance to city center Distance to river Ground Slope	0.041	0.101	0.411

Appendix G: Gathering expert knowledge on historical and simulated land-use maps.

Table G.1: Participants gathered during the GEOIDE workshop conducted in 2011

Name	Organization
Gloria Wilkinson	Implementation Committee of the Elbow River Basin Water Management Plan
Sarah Hamza	Elbow River Partnership
Anil Gupta	Alberta Environment
Tom Tang	Alberta Environment
Ellen Pond	UBC
Shawn Marshall	University of Calgary, Geography
Danielle Marceau	University of Calgary, Geomatics Eng.
Caterina Valeo	University of Calgary, Civil Eng.
Michael Barry	University of Calgary, Geomatics Eng.
Liz Breakey	Action for Agriculture
Rob Dunn	Agriculture and Food
Sillah Kargbo	Land-use framework
Ed Kulcsar	Spray Lakes Sawmills
Darrell Burgess	Calgary Regional Partnership
Rick Butler	Calgary Regional Partnership
Colleen Sheppard	Calgary Regional Partnership
Diane Coleman	Elbow River Partnership
Jennifer Dick	Rocky View Municipal District

Kent Berg	Alberta Environment
Stephen Sheppard	UBC
Scott Heckbert	Portland State University
Jamie Dixon	City of Calgary Water Resources
Gord Lehn	Spray Lakes Sawmills
Chad Wilms	Rocky View Municipal District
Chris Wolfe	Rocky View Municipal District
Axel Anderson	Sustainable Resource Development
Niandry Moreno	Alberta Environment
Roger White	Memorial University
Vince Diot	Rocky View Municipal Engineering Technologist
Linda Ratzalff	Rocky View Policy & Land Use Manager

Appendix H: Maps of simulated land-use changes based on different scenarios for the east sub-catchment.

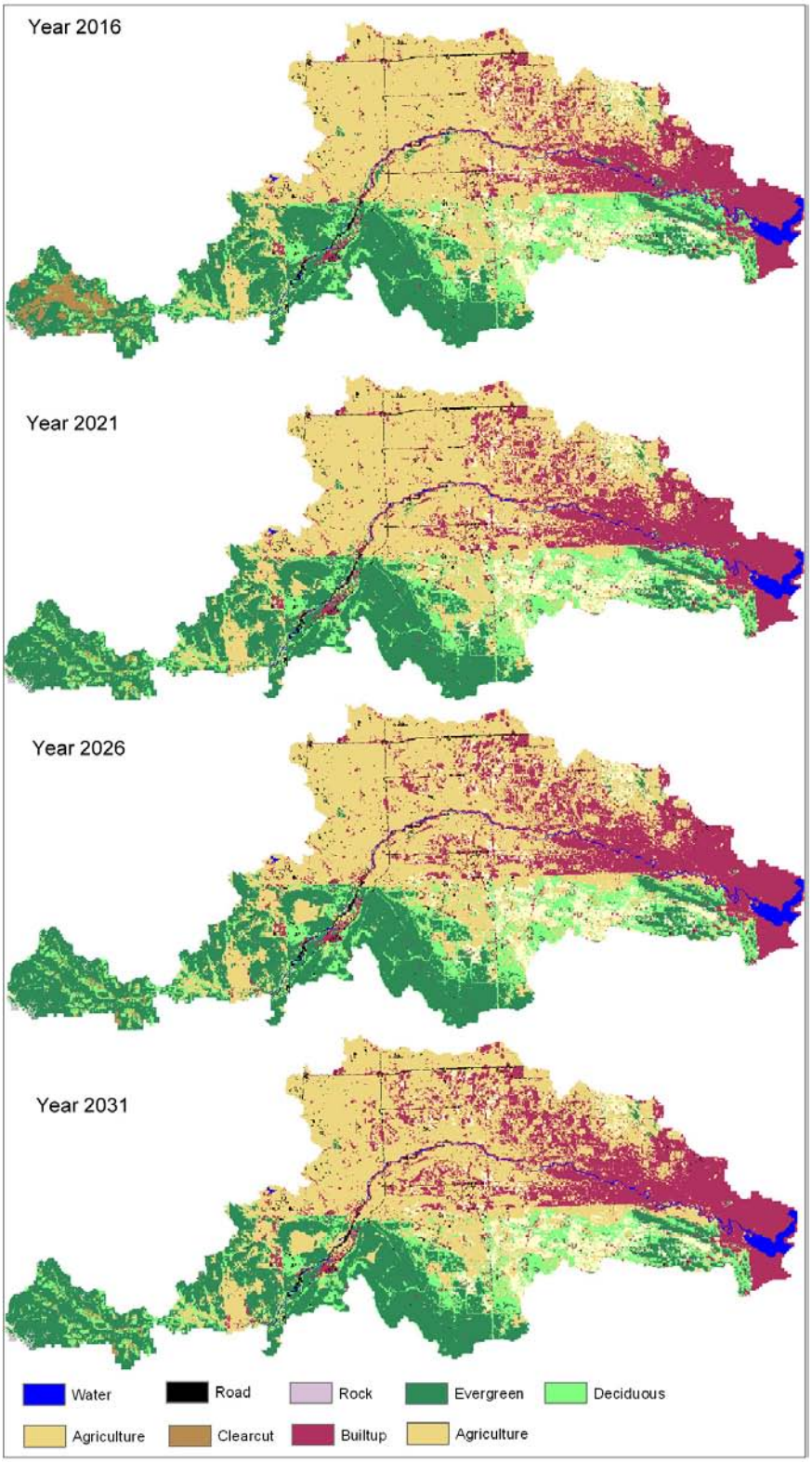

Figure H.1: Simulated maps based on the scenario BAU within the east sub-catchment of the watershed

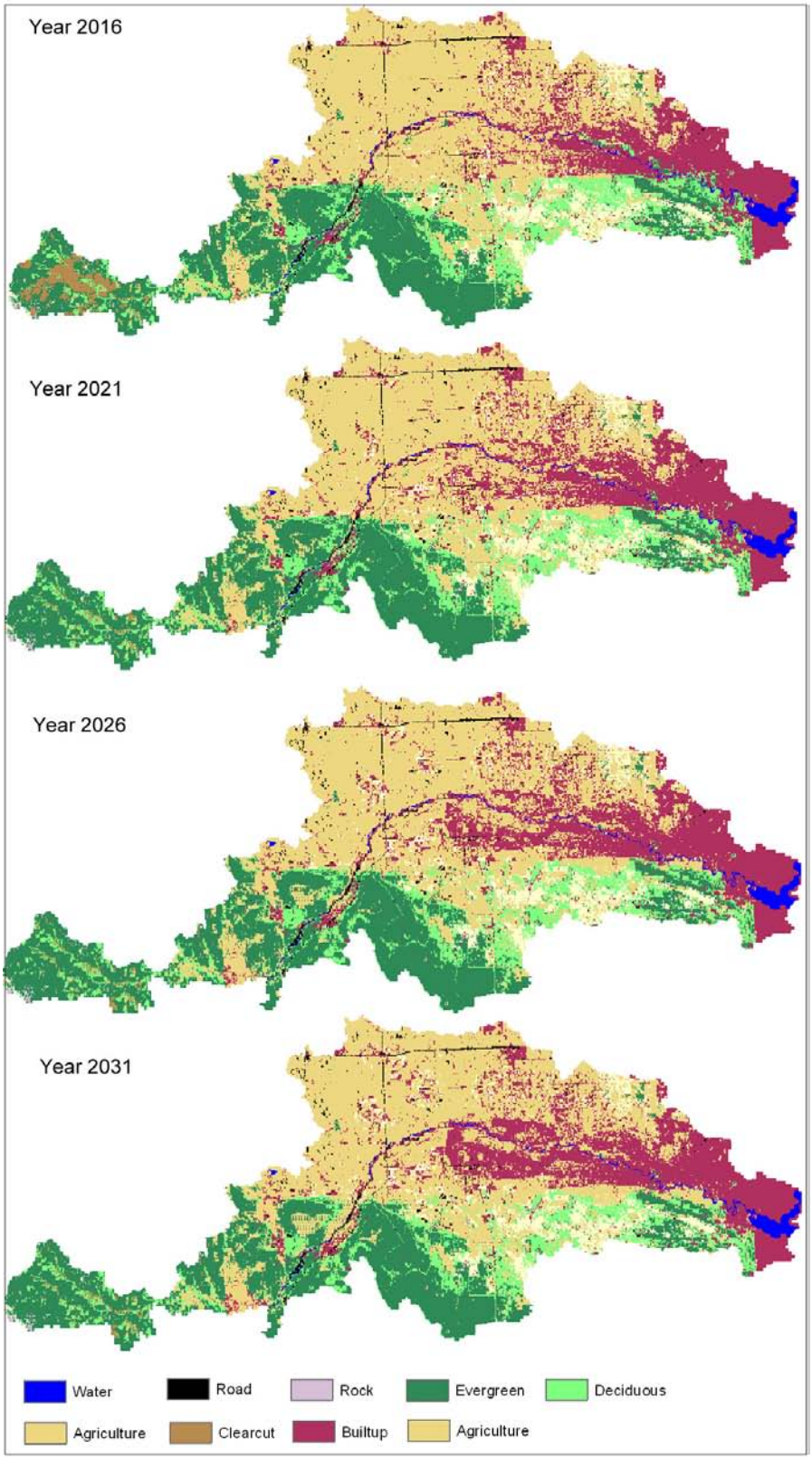

Figure H.2: Simulated maps based on the scenario RV-LUC within the east sub-catchment of the watershed

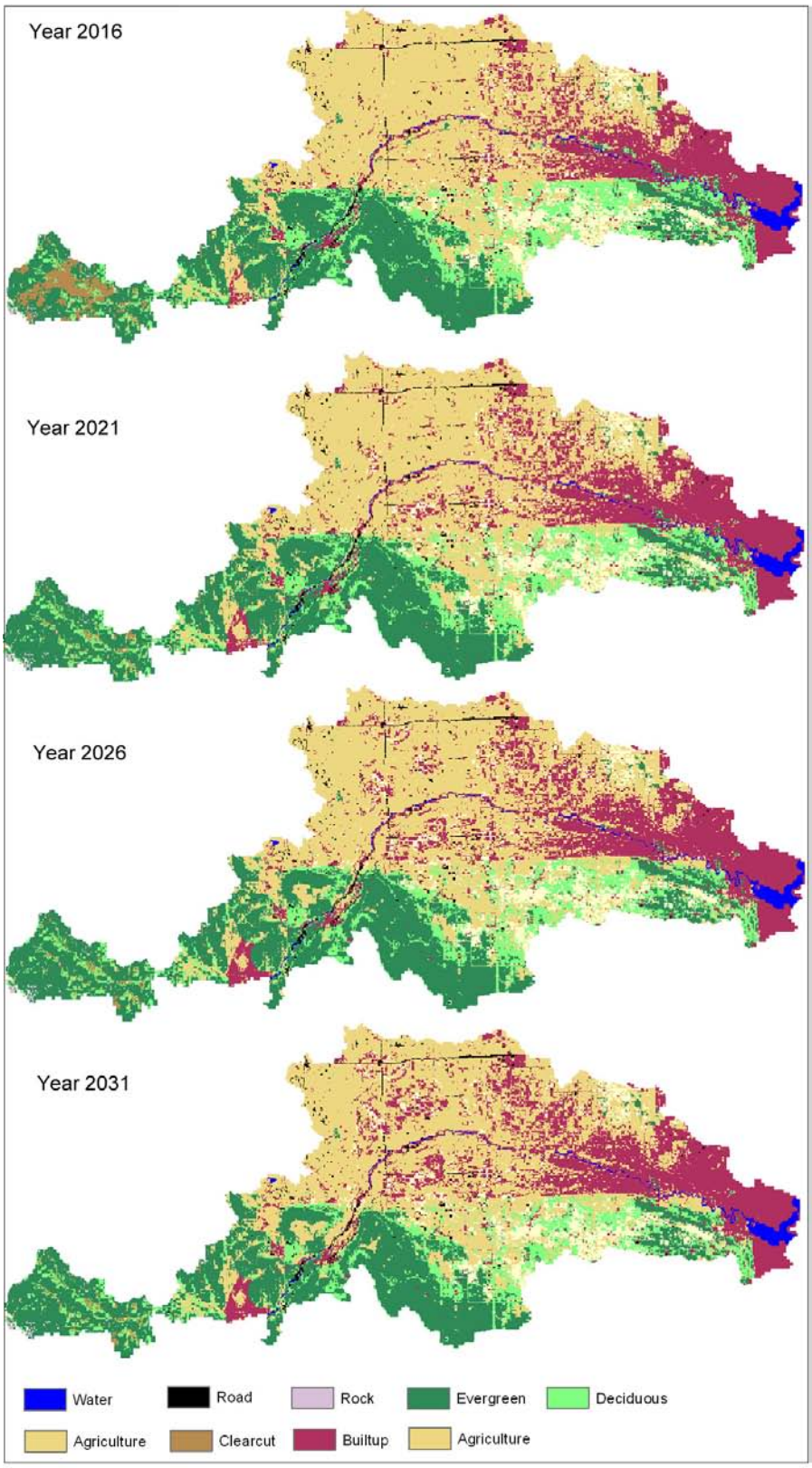

Figure H.3: Simulated maps based on the scenario BC-LUC within the east sub-catchment of the watershed

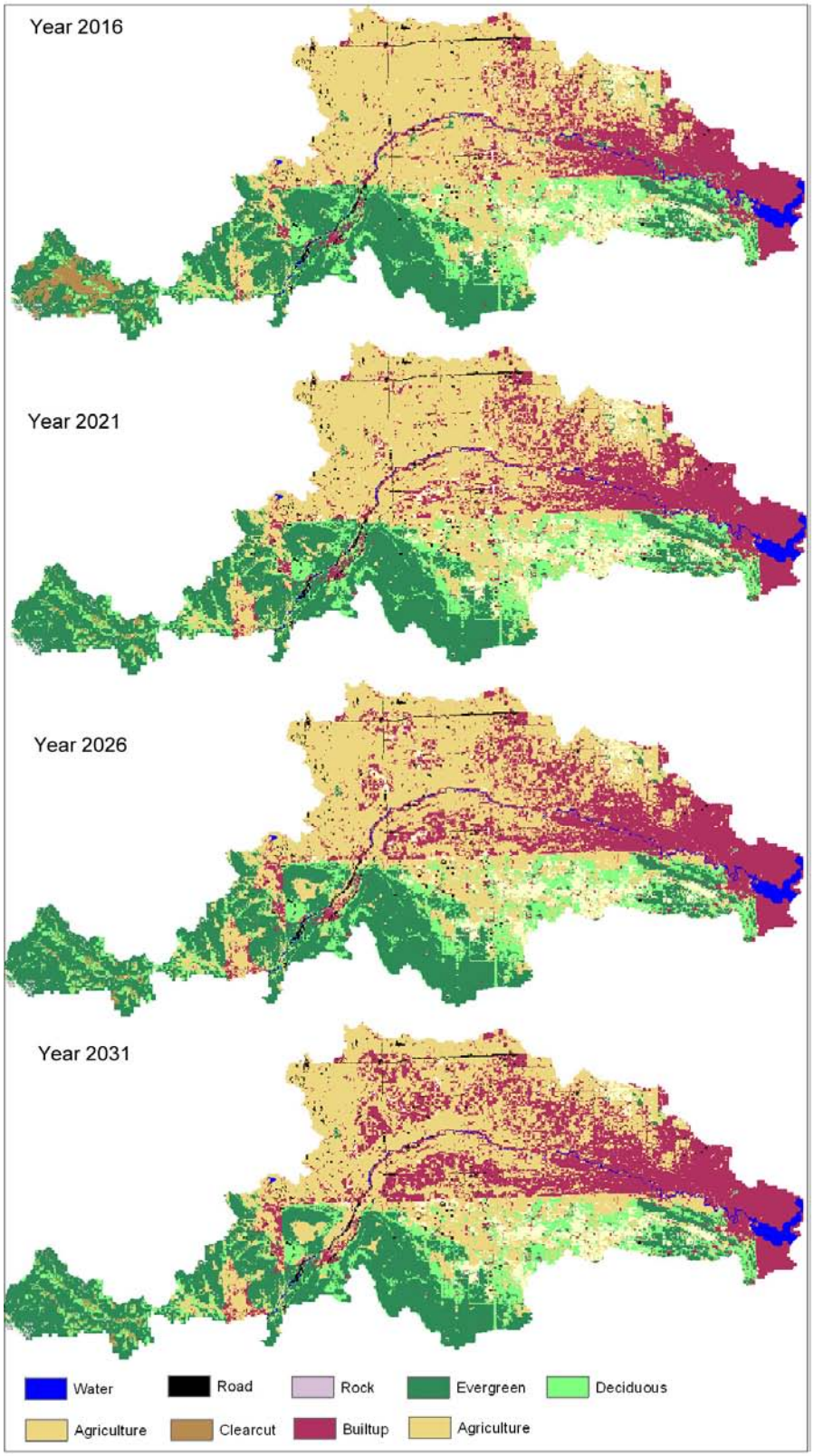

Figure H.4: Simulated maps based on the scenario P-LUC within the east sub-catchment of the watershed

Appendix I: Topographical data used to setup ERWHM

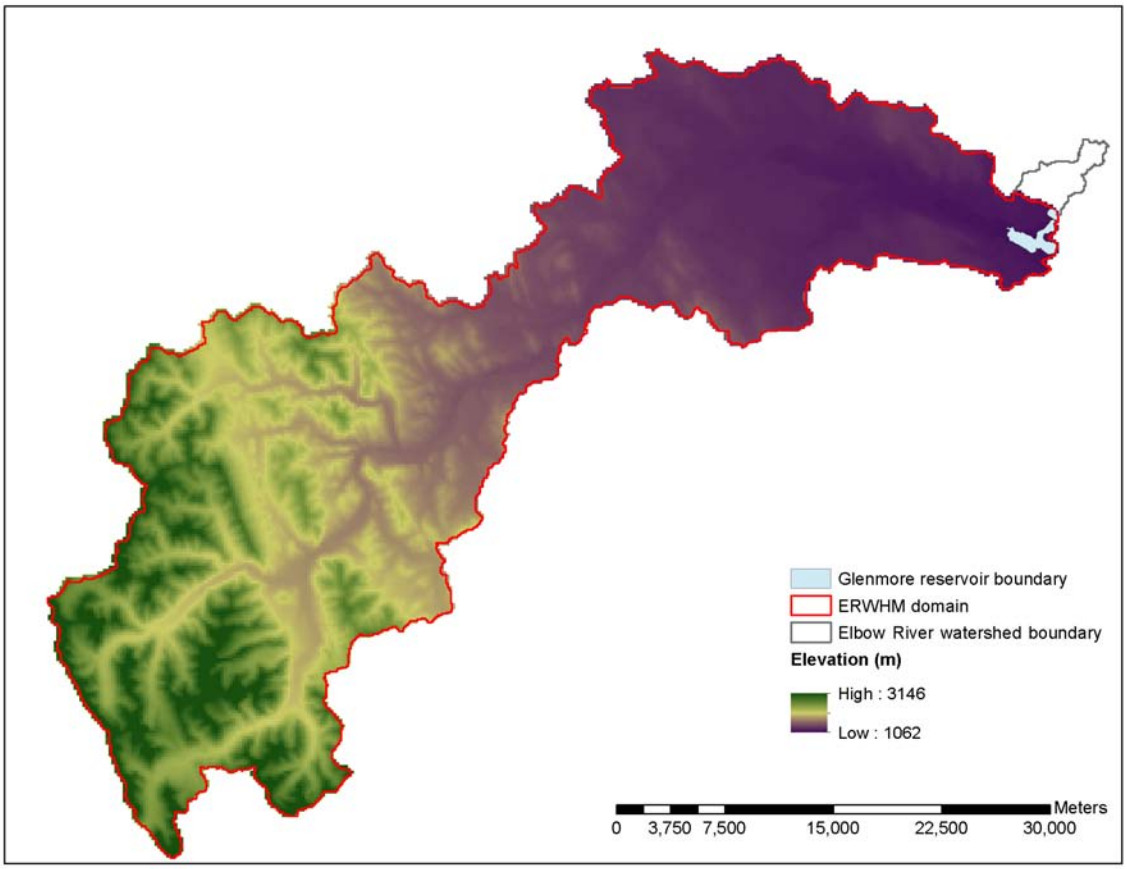

Figure I.1: Elevation map of the Elbow River watershed

Appendix J: Linear reservoir method to simulate groundwater flow

In the linear reservoir method, the entire catchment is subdivided into a number of sub-catchments; within each sub-catchment, the saturated zone is represented by a series of interdependent, shallow interflow reservoirs, plus a number of separate, deep groundwater reservoirs that contribute to the stream baseflow (Fig. J.1).

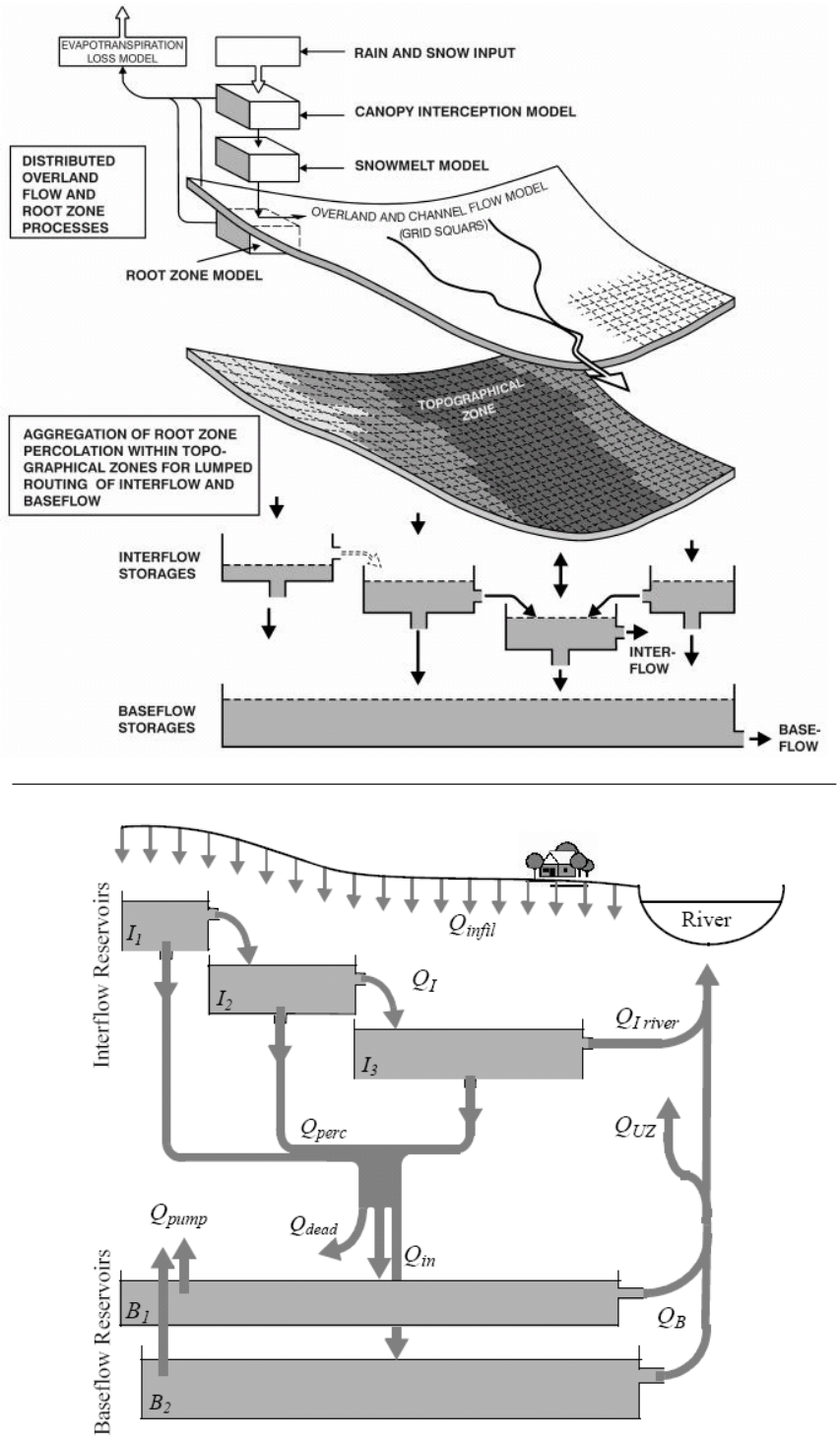

Figure J.1: Model structure of the linear reservoir method in MIKE-SHE for the saturated zone (DHI 2009)

This method is based on the linear reservoir theory in which the storage of the reservoir is linearly related to the output by a storage constant or time constant (Equation J.1).

$S = kQ$ Equation J.1

In the context of our study, the linear reservoir method routes the water to the river as interflow and baseflow (Fig. J.1: Q_{Iriver} and Q_B) through the appropriate river links. The water being infiltrated from the unsaturated zone may either contribute to the baseflow or move laterally as interflow towards the stream, and hence, within the linear reservoir model, the interflow reservoirs have two outlets (Fig. J.1).

Appendix K: Calibration and validation results

K.1: The following are the results obtained for the calibration and validation against total snow storage.

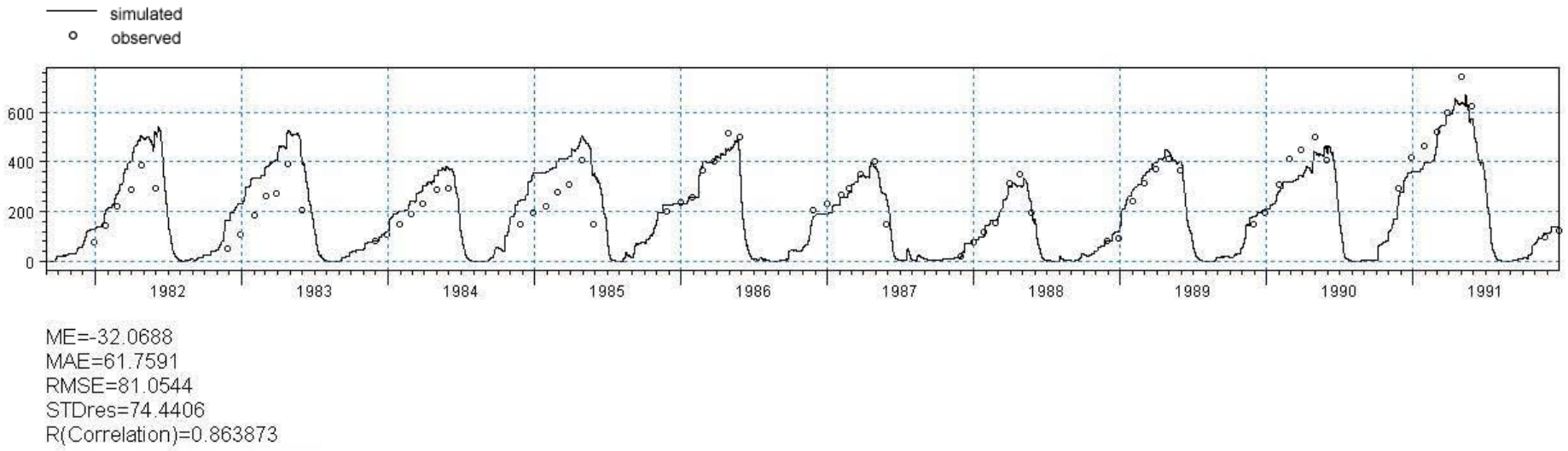

Figure K.1.1: Results of calibration against total snow storage at the Little Elbow snow station during 1981-1991

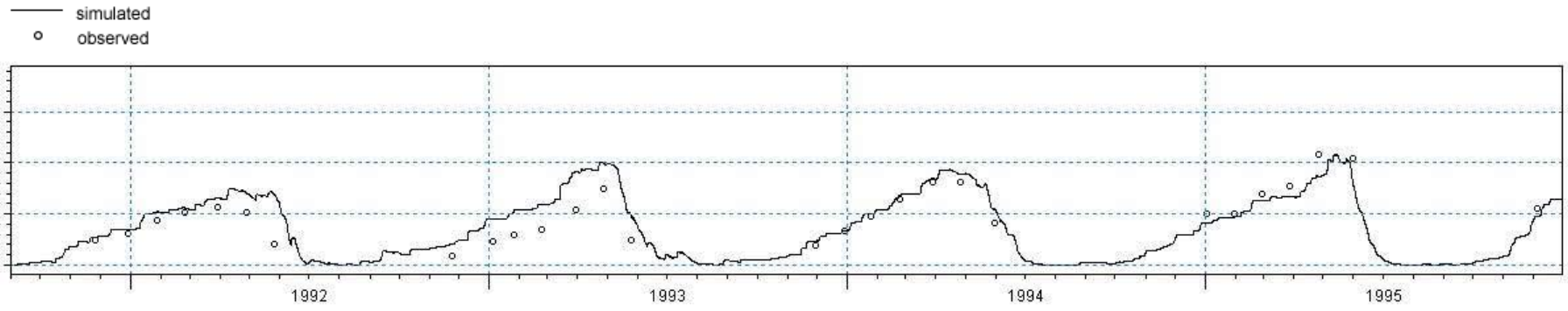

ME=-31.7661
MAE=54.1298
RMSE=71.1435
STDres=63.6577
R(Correlation)=0.772659

Figure K.1.2: Results of validation against total snow storage at the Little Elbow snow station during 1991-1995

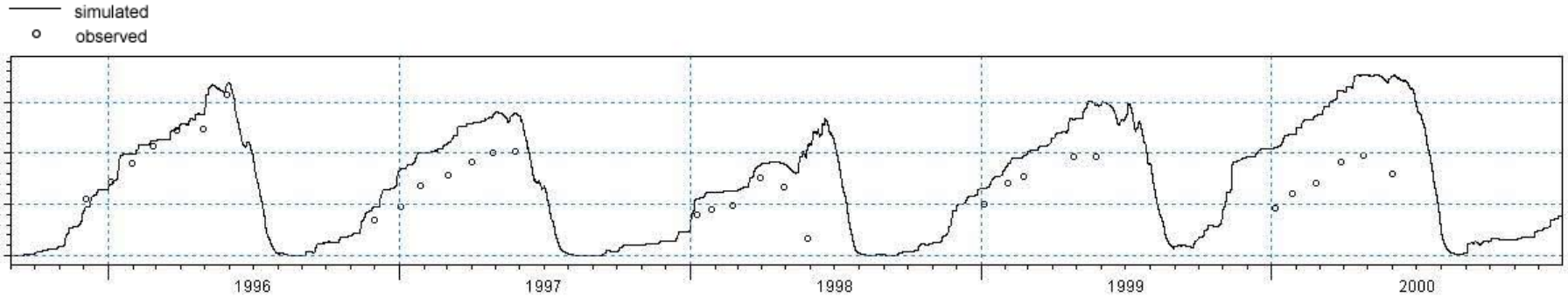

ME=-128.05
MAE=130.701
RMSE=166.654
STDres=106.663
R(Correlation)=0.694651

Figure K.1.3: Results of validation against total snow storage at the Little Elbow snow station during 1995-2000

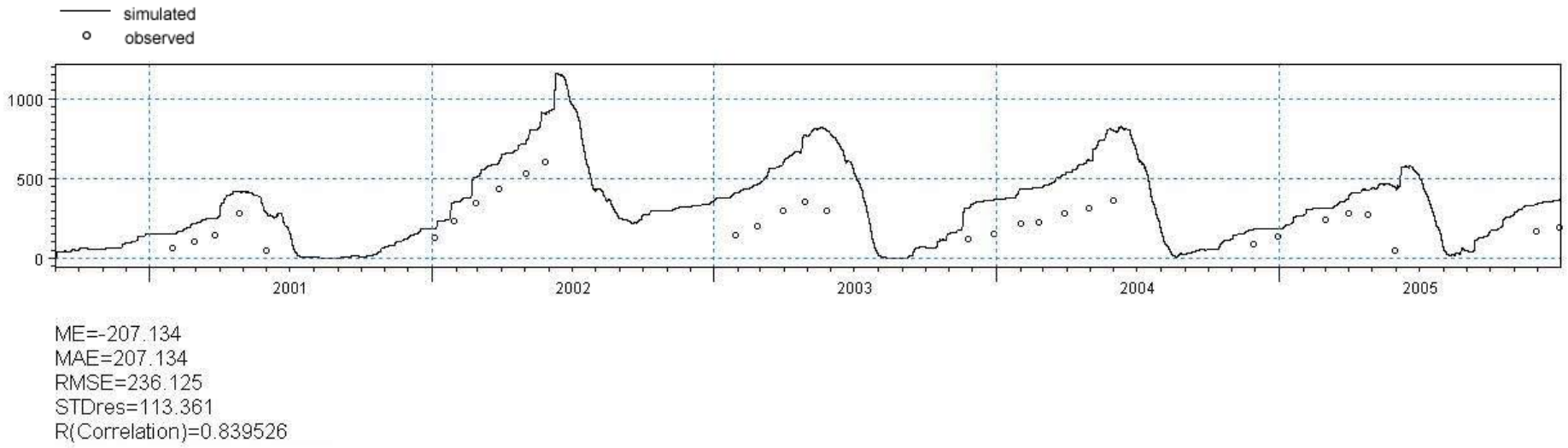

Figure K.1.4: Results of validation against total snow storage at the Little Elbow snow station during 2000-2005

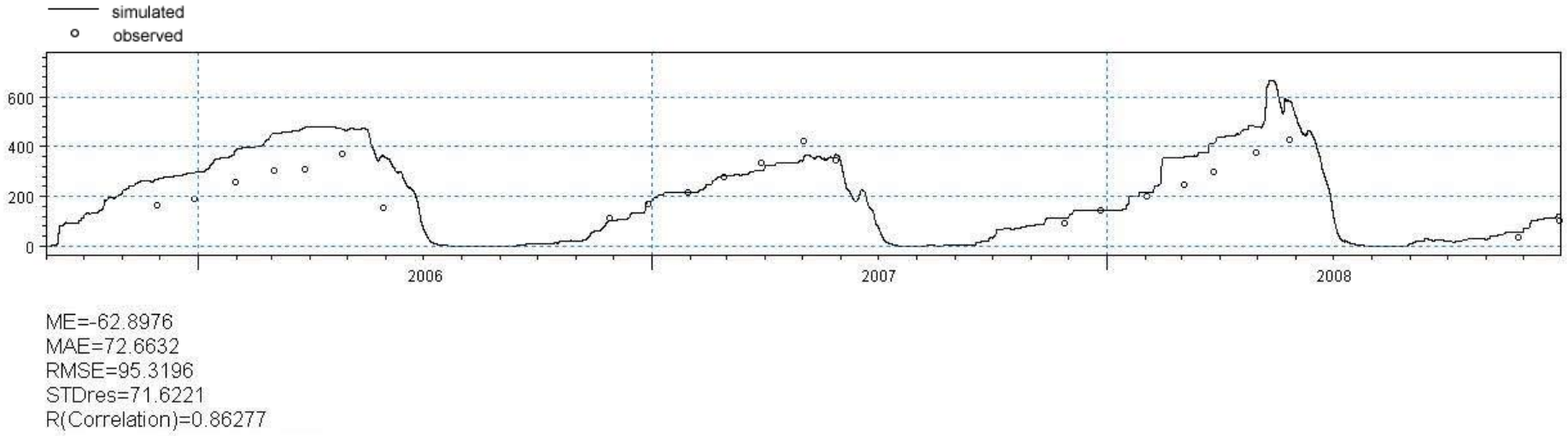

Figure K.1.5: Results of validation against total snow storage at the Little Elbow snow station during 2005-2008

K.2: The following are the results obtained for the calibration and validation against stream flow data.

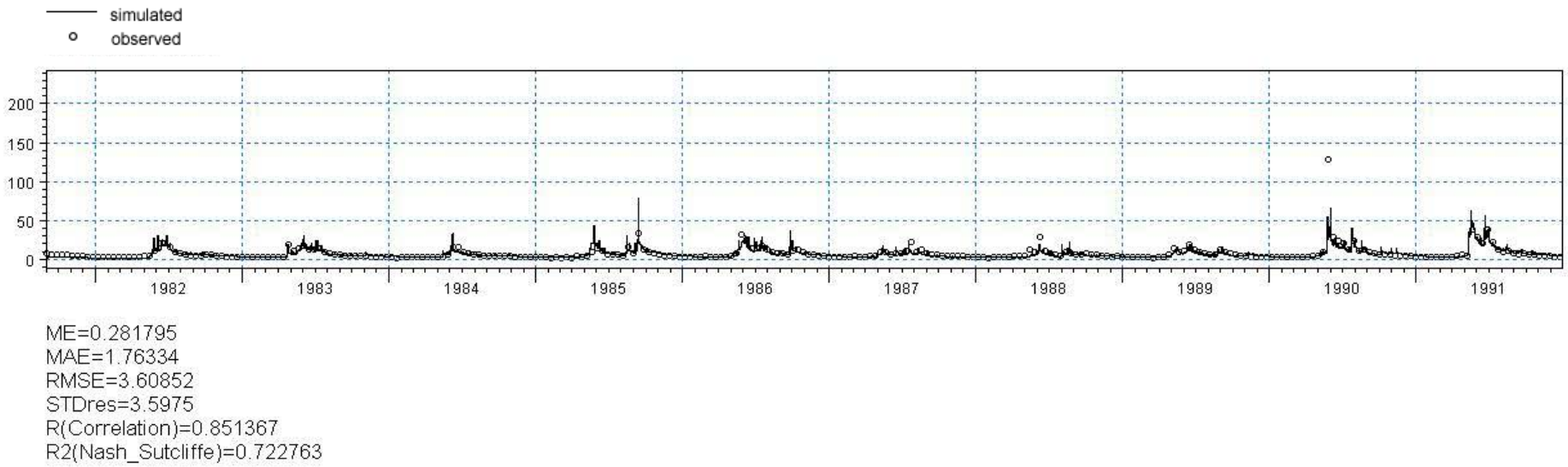

Figure K.2.1: Results of calibration against stream flow at 05BJ004 hydrometric station during 1981- 1991

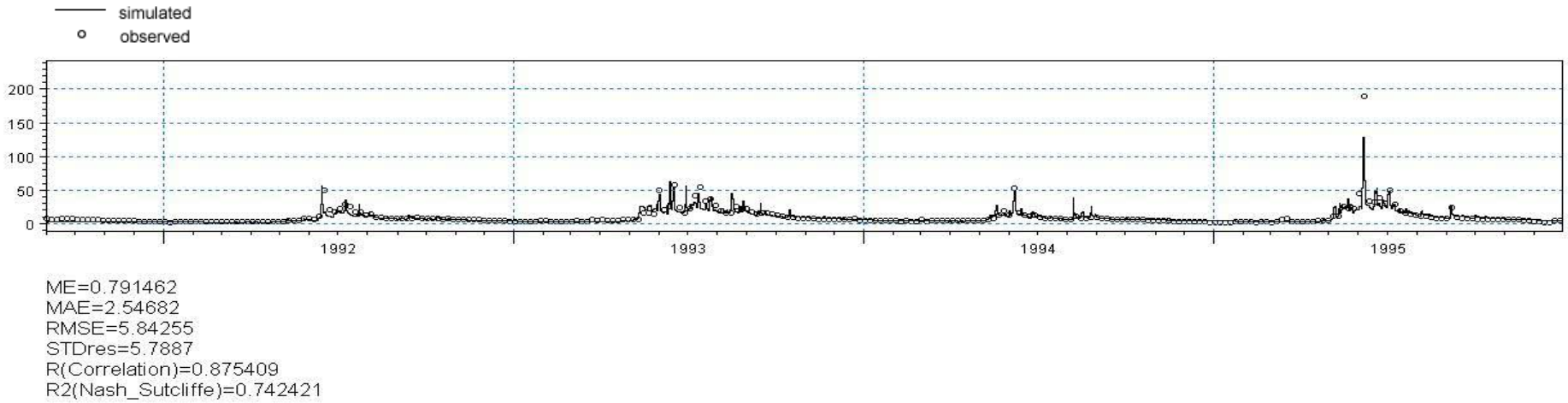

Figure K.2.2: Results of validation against stream flow at 05BJ004 hydrometric station during 1991-1995

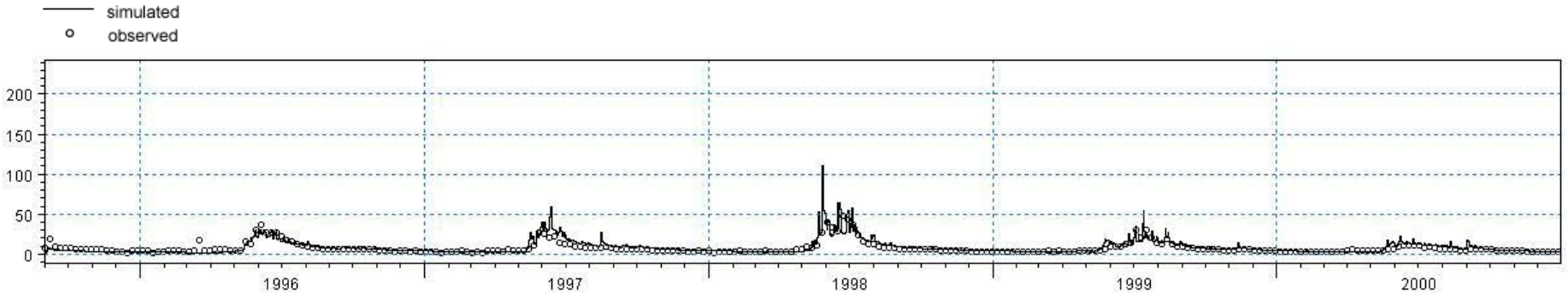

ME=-0.54674
MAE=2.33209
RMSE=3.72459
STDres=3.68425
R(Correlation)=0.901954
R2(Nash_Sutcliffe)=0.799655

Figure K.2.3: Results of validation against stream flow at 05BJ004 hydrometric station during 1995-2000

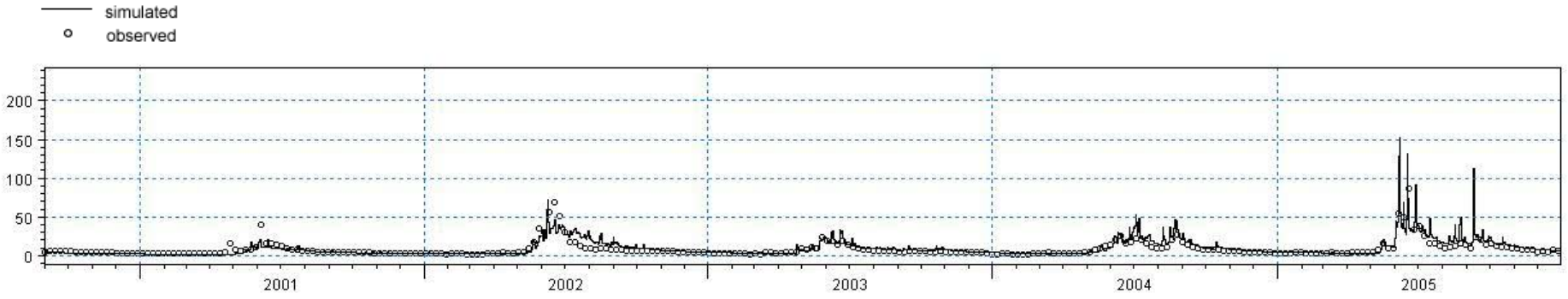

ME=-0.91647
MAE=3.05319
RMSE=6.14377
STDres=6.07503
R(Correlation)=0.861405
R2(Nash_Sutcliffe)=0.731453

Figure K.2.4: Results of validation against stream flow at 05BJ004 hydrometric station during 2000-2005

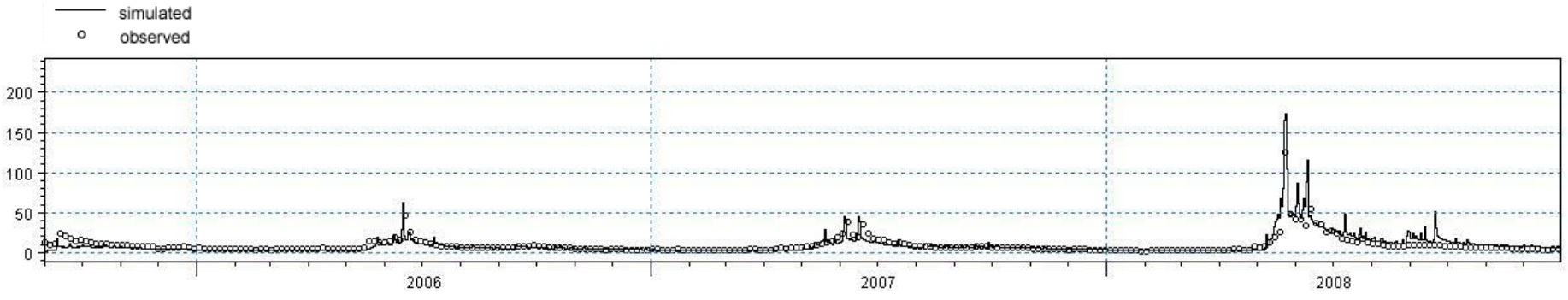

ME=-0.0269113
MAE=3.01792
RMSE=5.90635
STDres=5.90629
R(Correlation)=0.882127
R2(Nash_Sutcliffe)=0.638016

Figure K.2.5: Results of validation against stream flow at 05BJ004 hydrometric station during 2005-2008

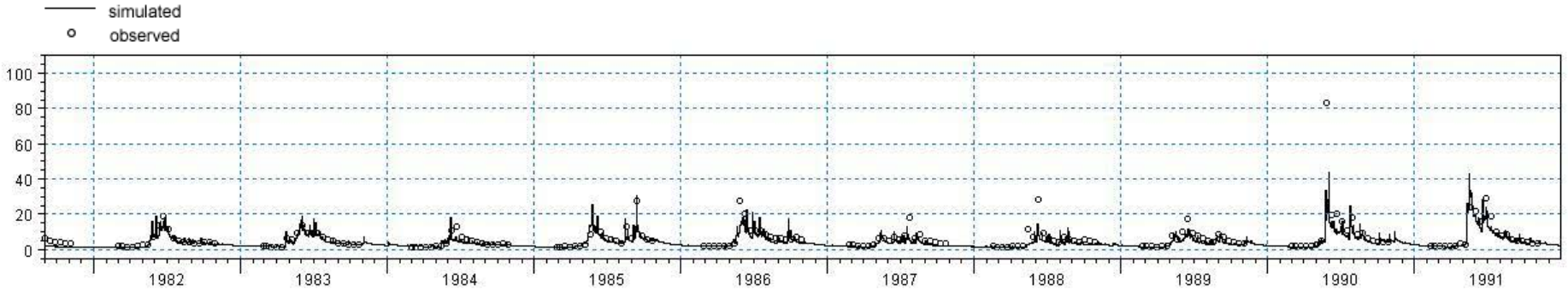

ME=1.37798
MAE=1.90506
RMSE=3.77477
STDres=3.51426
R(Correlation)=0.815519
R2(Nash_Sutcliffe)=0.603816

Figure K.2.6: Results of calibration against stream flow at 05BJ006 hydrometric station during 1981-1991

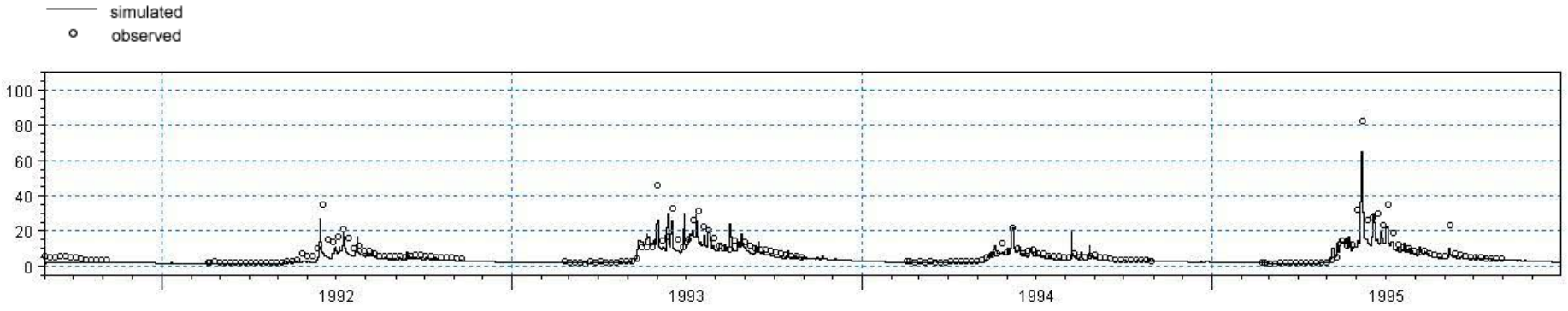

ME=2.17598
MAE=2.60276
RMSE=4.97872
STDres=4.47803
R(Correlation)=0.859783
R2(Nash_Sutcliffe)=0.619873

Figure K.2.7: Results of validation against stream flow at 05BJ006 hydrometric station during 1991-1995

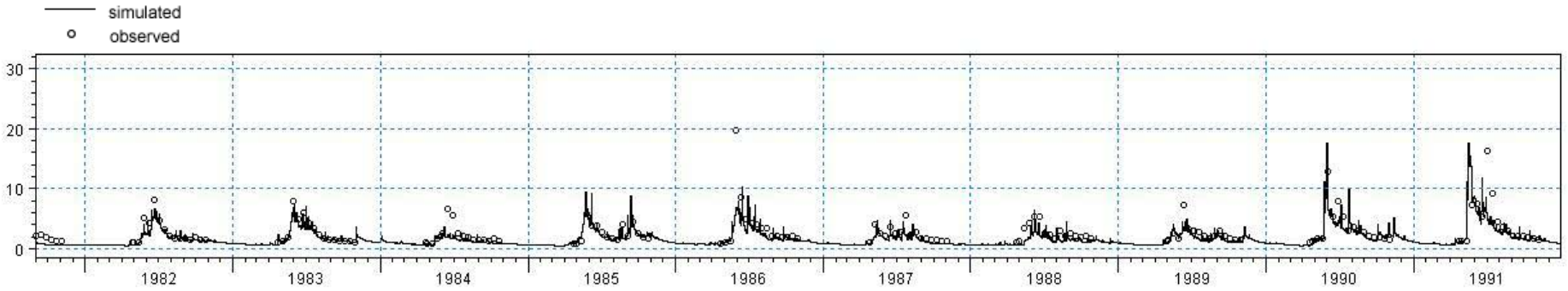

ME=0.668799
MAE=0.971079
RMSE=1.75849
STDres=1.62635
R(Correlation)=0.75769
R2(Nash_Sutcliffe)=0.501497

Figure K.2.8: Results of calibration against stream flow at 05BJ009 hydrometric station during 1981-1991

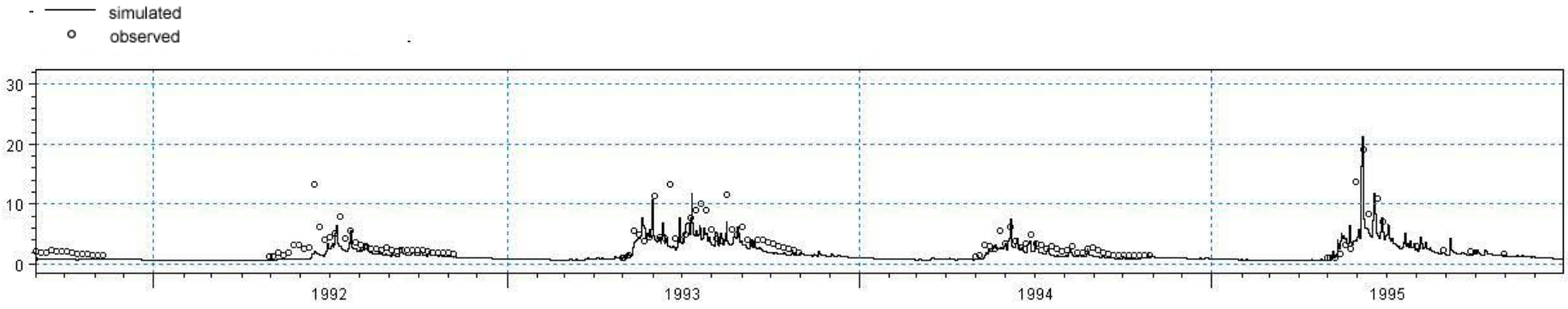

ME=1.30247
MAE=1.48645
RMSE=2.39522
STDres=2.01015
R(Correlation)=0.694181
R2(Nash_Sutcliffe)=0.257535

Figure K.2.9: Results of validation against stream flow at 05BJ009 hydrometric station during 1991-1995

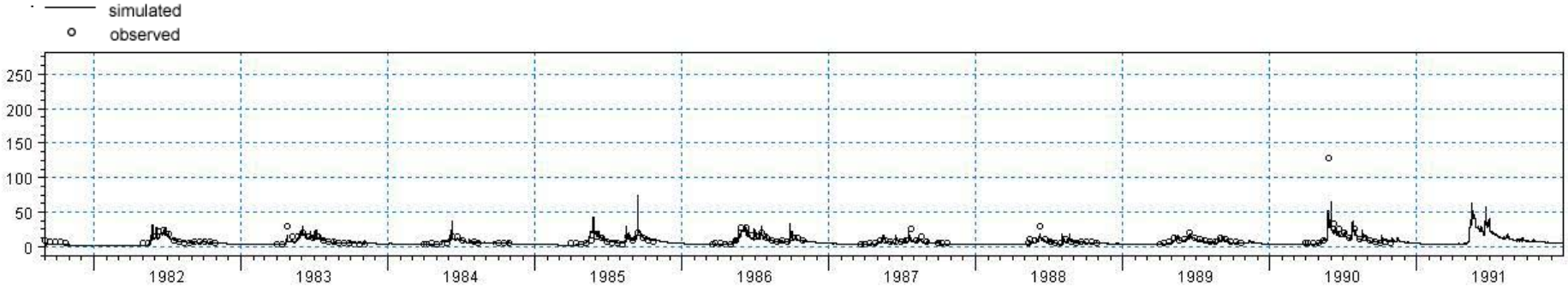

ME=1.3551
MAE=2.55128
RMSE=5.03719
STDres=4.85149
R(Correlation)=0.813444
R2(Nash_Sutcliffe)=0.627403

Figure K.2.10: Results of calibration against stream flow at 05BJ010 hydrometric station during 1981-1991

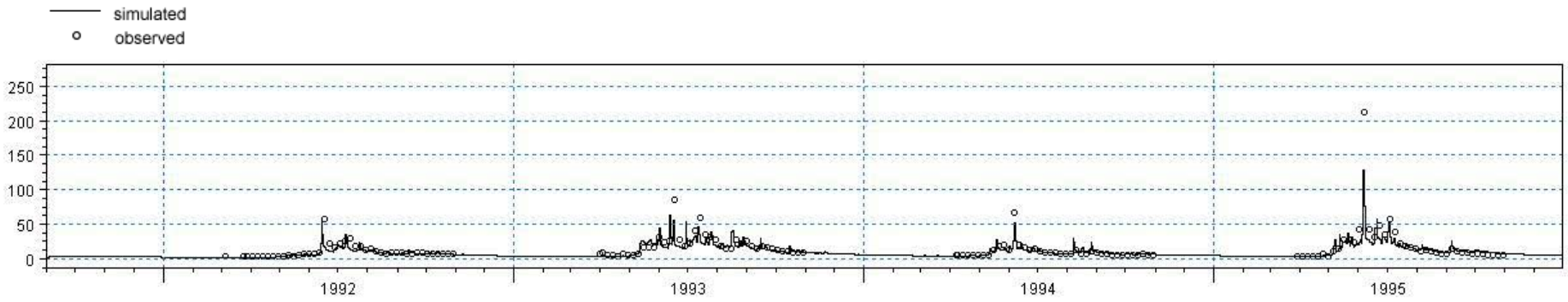

ME=2.38709
MAE=4.01245
RMSE=8.20014
STDres=7.845
R(Correlation)=0.891148
R2(Nash_Sutcliffe)=0.711604

Figure K.2.11: Results of validation against stream flow at 05BJ010 hydrometric station during 1991-1995

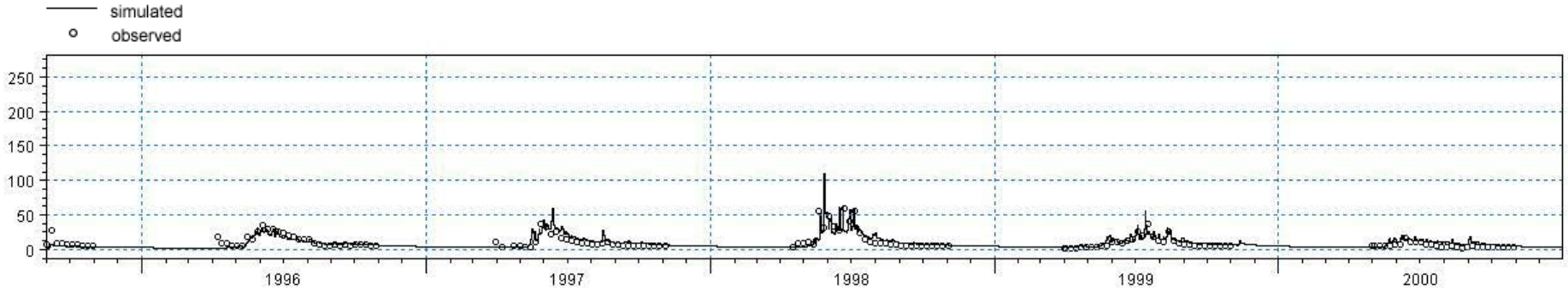

ME=-0.782608
MAE=4.35939
RMSE=6.62524
STDres=6.57886
R(Correlation)=0.841681
R2(Nash_Sutcliffe)=0.702153

Figure K.2.12: Results of validation against stream flow at 05BJ010 hydrometric station during 1995-2000

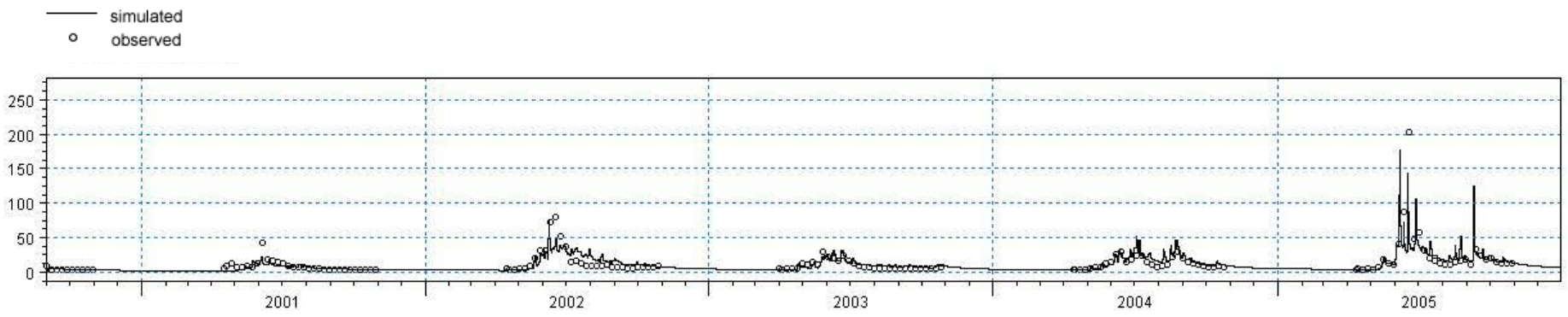

ME=-0.0697776
MAE=5.33642
RMSE=10.4989
STDres=10.4987
R(Correlation)=0.844044
R2(Nash_Sutcliffe)=0.695567

Figure K.2.13: Results of validation against stream flow at 05BJ010 hydrometric station during 2000-2005

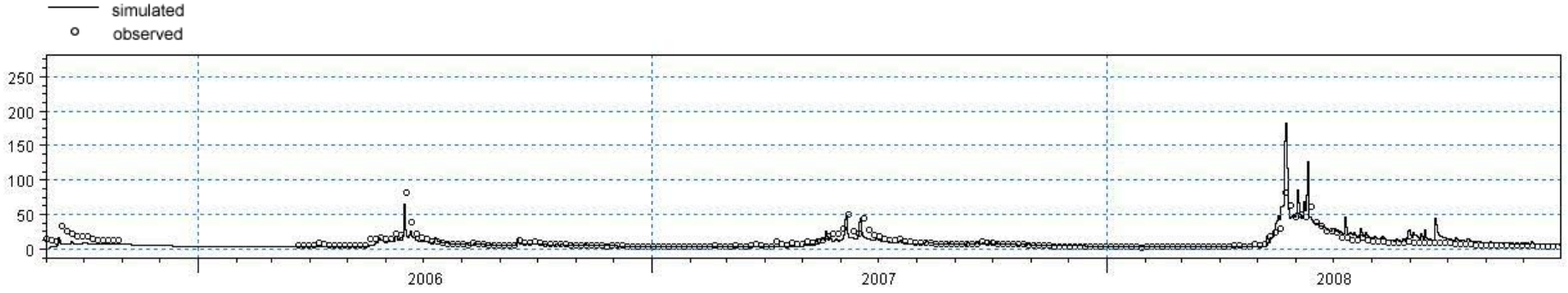

ME=0.867889
MAE=3.85858
RMSE=7.31012
STDres=7.25842
R(Correlation)=0.852004
R2(Nash_Sutcliffe)=0.709334

Figure K.2.14: Results of validation against stream flow at 05BJ010 hydrometric station during 2005-2008

Appendix L: Results of calibration and validation of ERWHM against groundwater levels

Table L.1: Results of the calibration/validation of ERWHM based on groundwater levels (Wijesekara and Marceau 2012)

Well ID	Validation period			
	1990-2005		2005-2008	
	Correlation Coefficient (R)	Mean absolute error (MAE) (m)	Correlation Coefficient (R)	Mean absolute error (MAE) (m)
Well_1	N/A	N/A	0.66	0.40
Well_2	N/A	N/A	0.17	10.93
Well_9	N/A	N/A	0.28	5.86
Well_13	N/A	N/A	0.59	1.3
Well_14	N/A	N/A	0.27	6.2
Well_29	N/A	N/A	0.82	6.4
BC-1	0.20	0.97	N/A	N/A
BC-2	0.43	1.53	N/A	N/A
BC-3	0.23	3.39	N/A	N/A
RW-1	0.08	1.42	N/A	N/A
RW-2	-0.6	0.28	N/A	N/A
RW-3	0.24	1.12	N/A	N/A
CG-1	0.73	0.34	N/A	N/A
CG-2	0.01	0.13	N/A	N/A
CG-3	-0.94	1.93	N/A	N/A
CG-4	0.16	1.40	N/A	N/A
GC-1	0.43	2.10	N/A	N/A
GC-2	-0.29	2.33	N/A	N/A
GC-3	0.10	4.80	N/A	N/A
GC-4	0.24	3.20	N/A	N/A

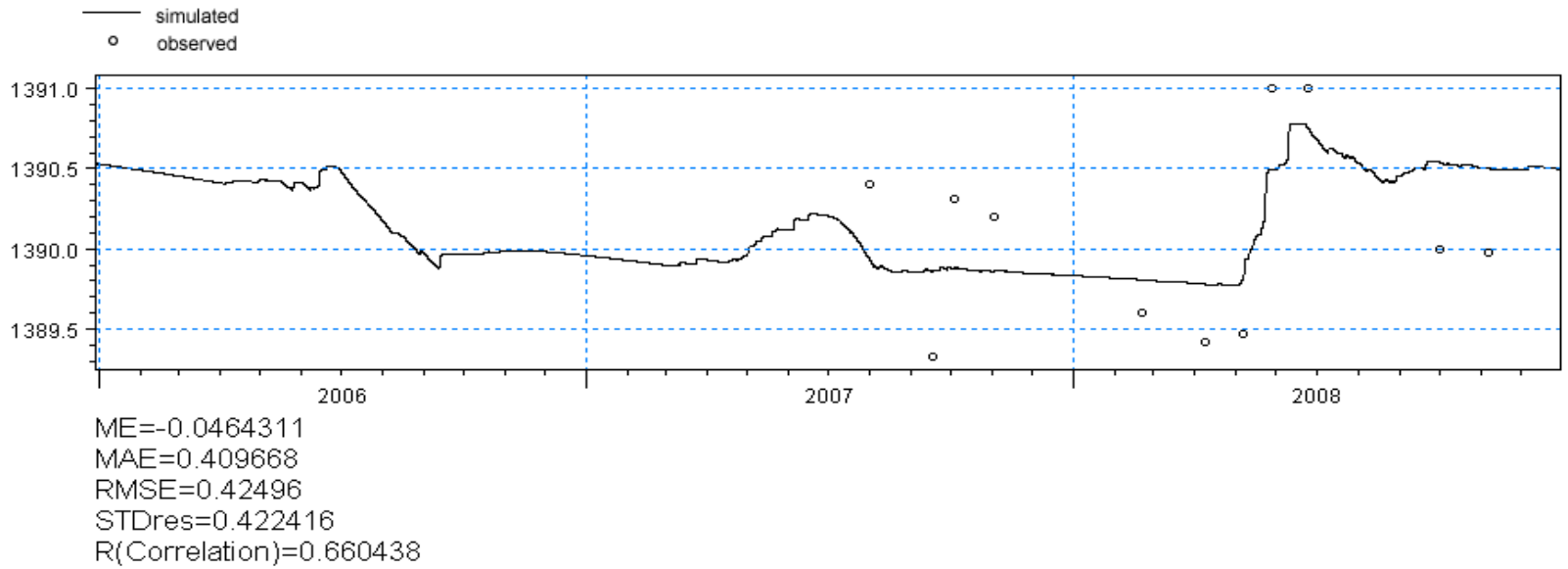

Figure L.1: Results of validation against groundwater levels at Well ID 1 during 2005-2008

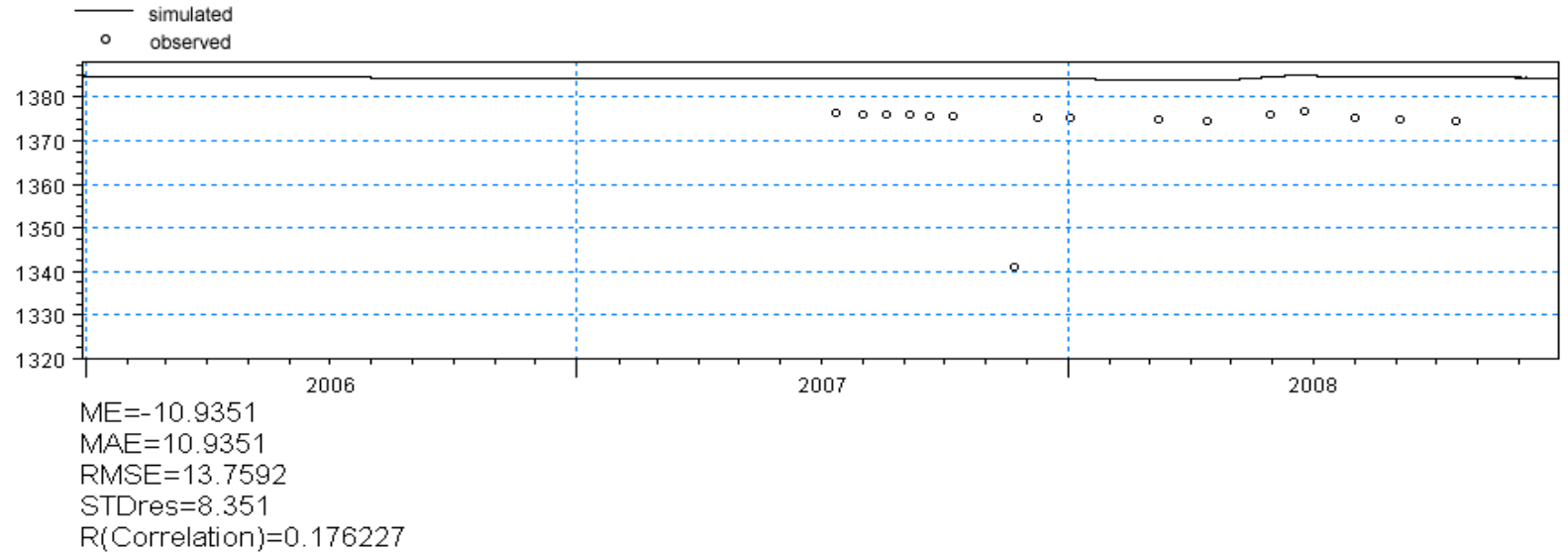

Figure L.2: Results of validation against groundwater levels at Well ID 2 during 2005-2008

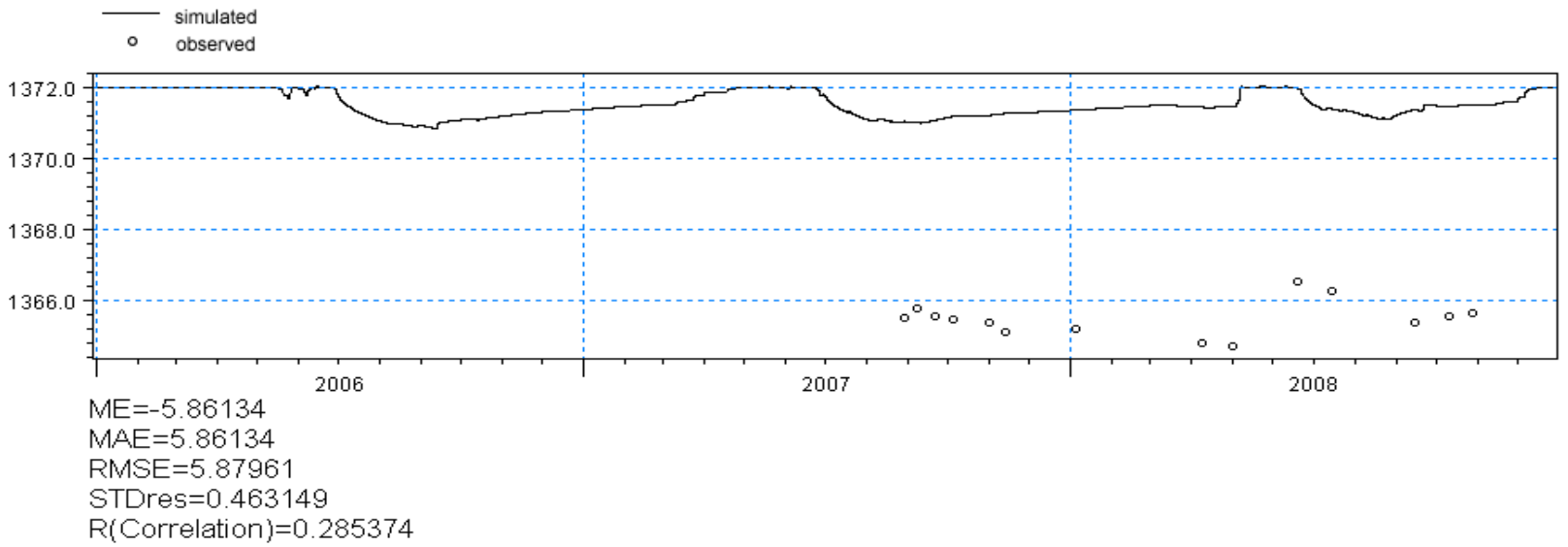

Figure L.3: Results of validation against groundwater levels at Well ID 9 during 2005-2008

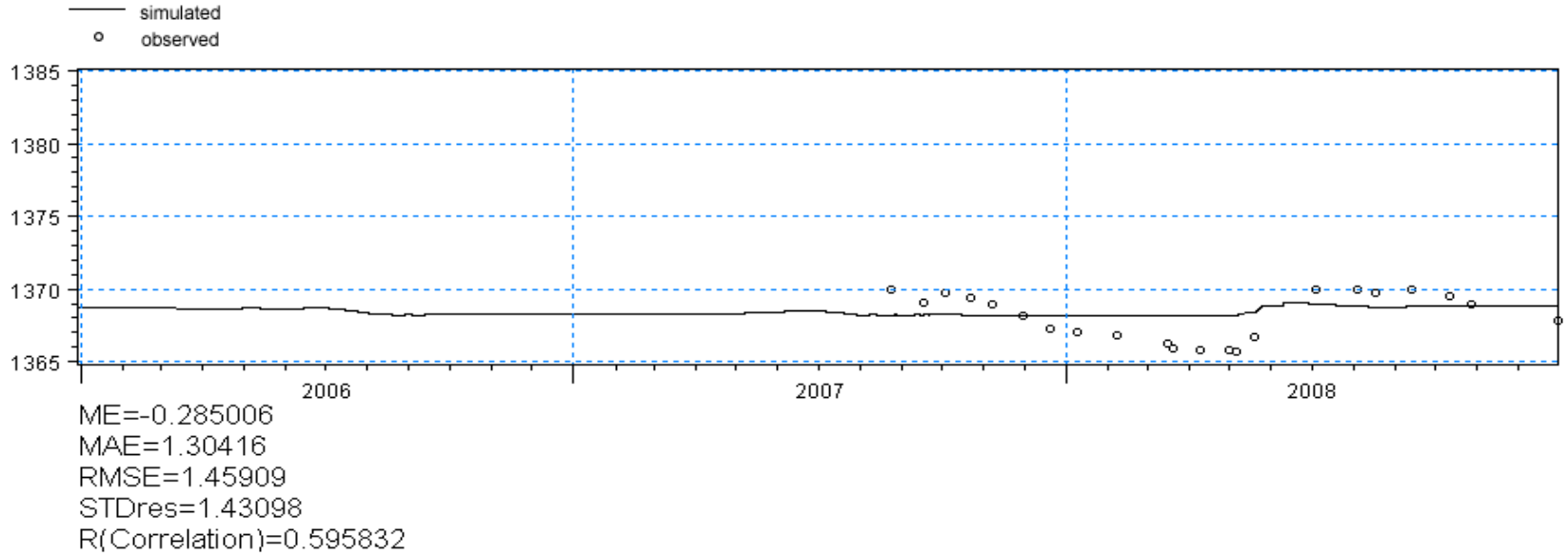

Figure L.4: Results of validation against groundwater levels at Well ID 13 during 2005-2008

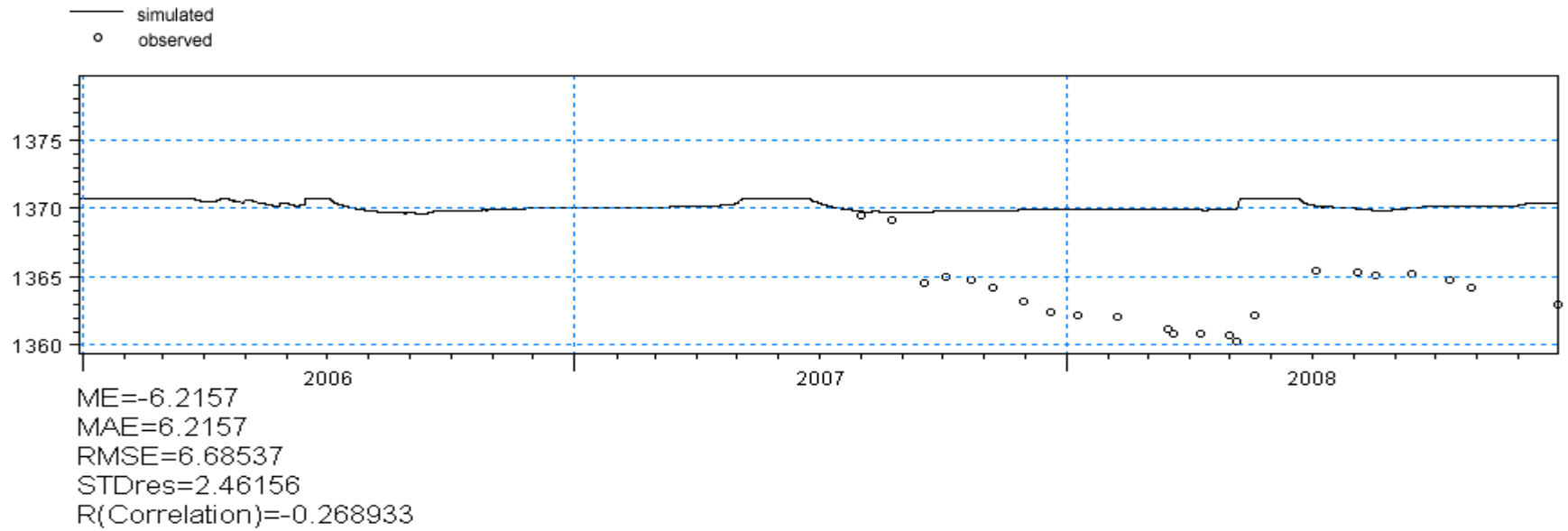

Figure L.5: Results of validation against groundwater levels at Well ID 14 during 2005-2008

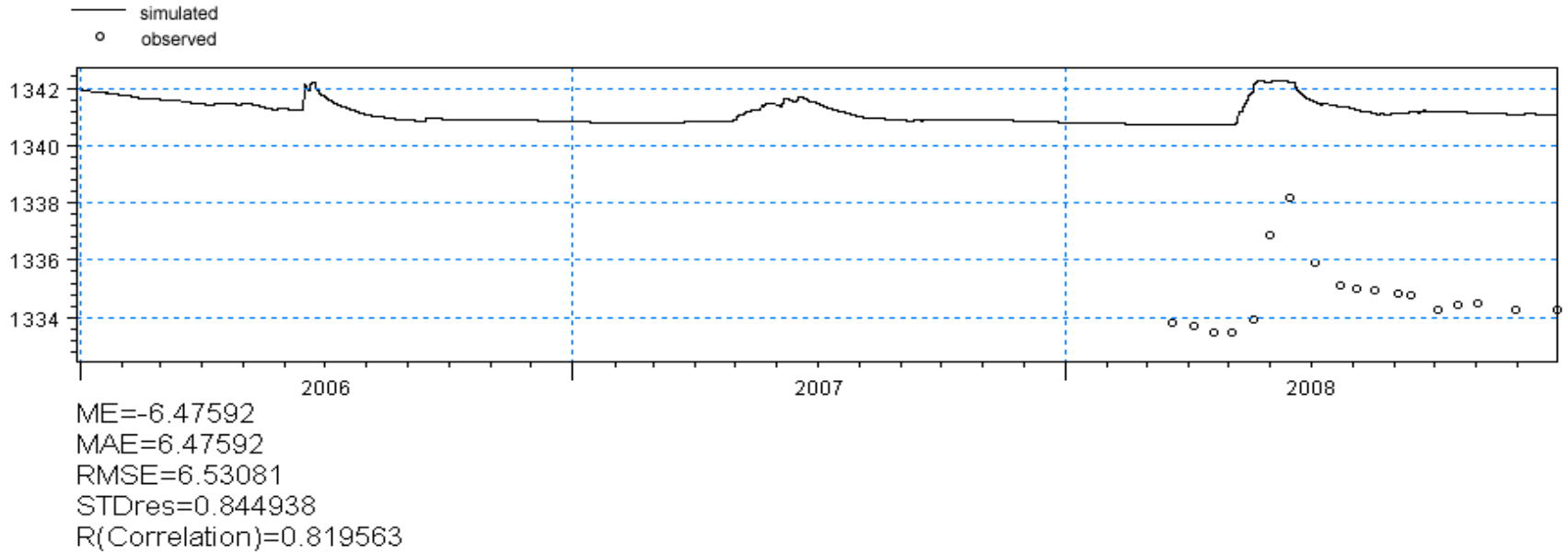

Figure L.6: Results of validation against groundwater levels at Well ID 29 during 2005-2008

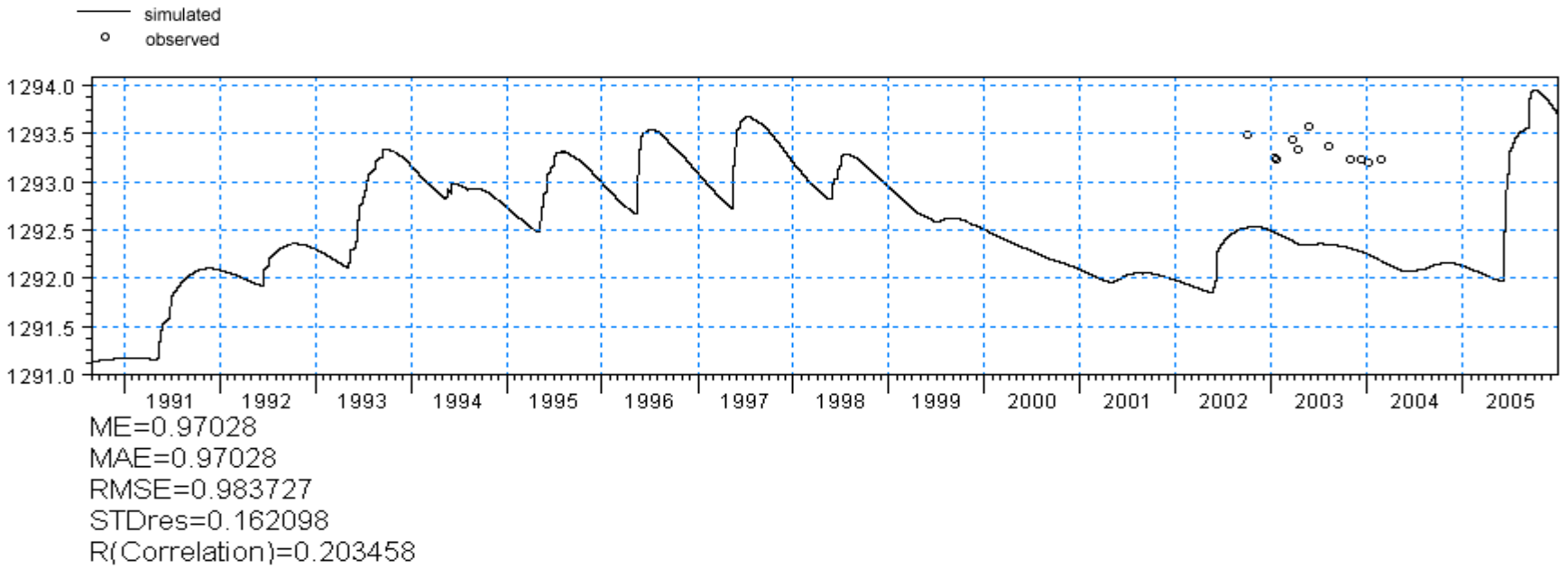

Figure L.7: Results of validation against groundwater levels at Well ID BC-1 during 1990-2005

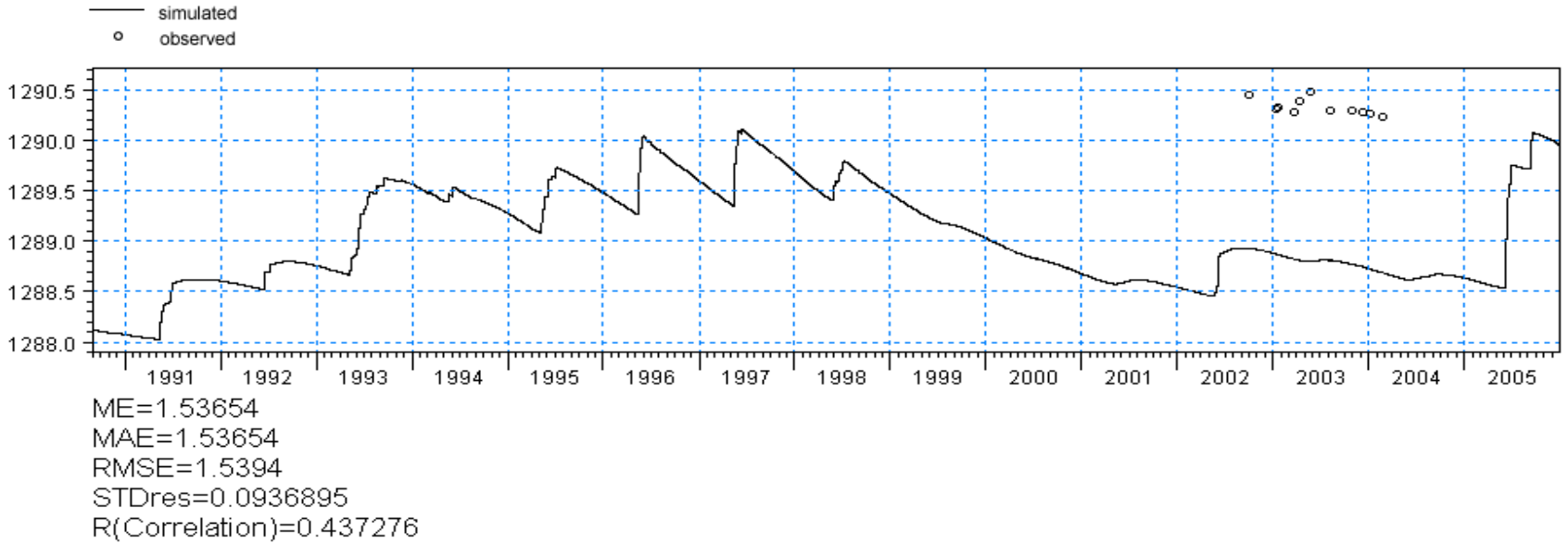

Figure L.8: Results of validation against groundwater levels at Well ID BC-2 during 1990-2005

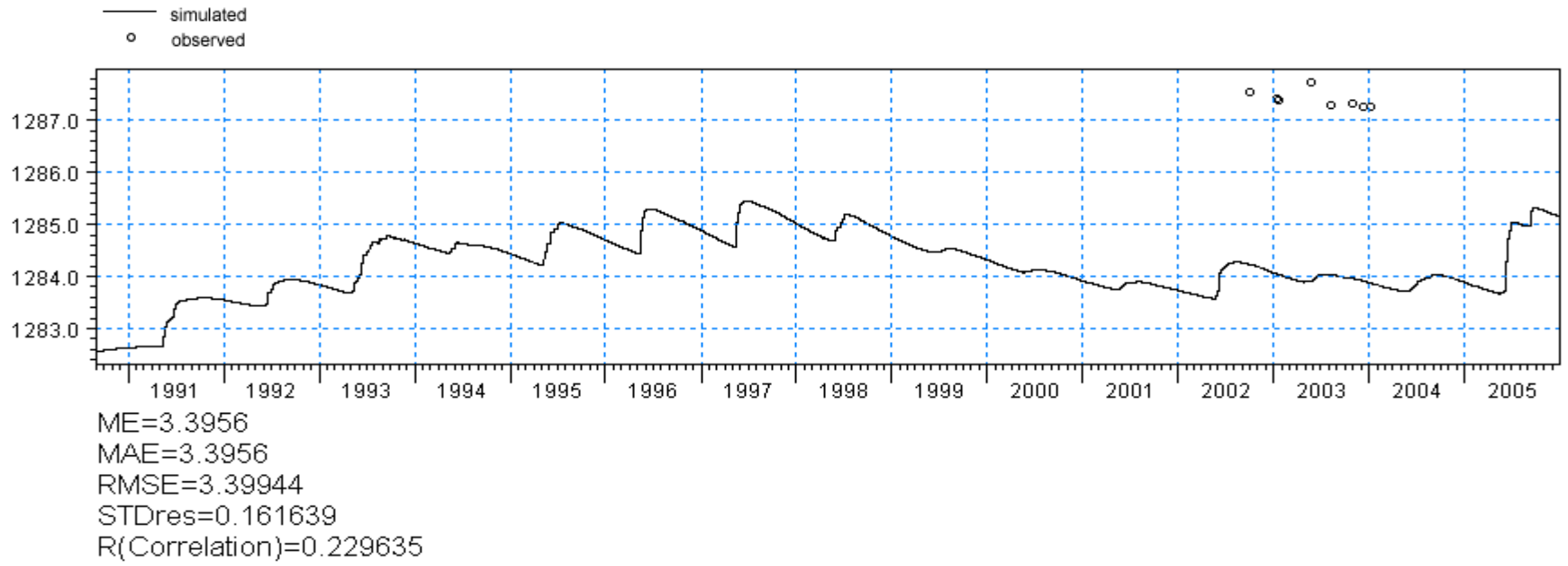

Figure L.9: Results of validation against groundwater levels at Well ID BC-3 during 1990-2005

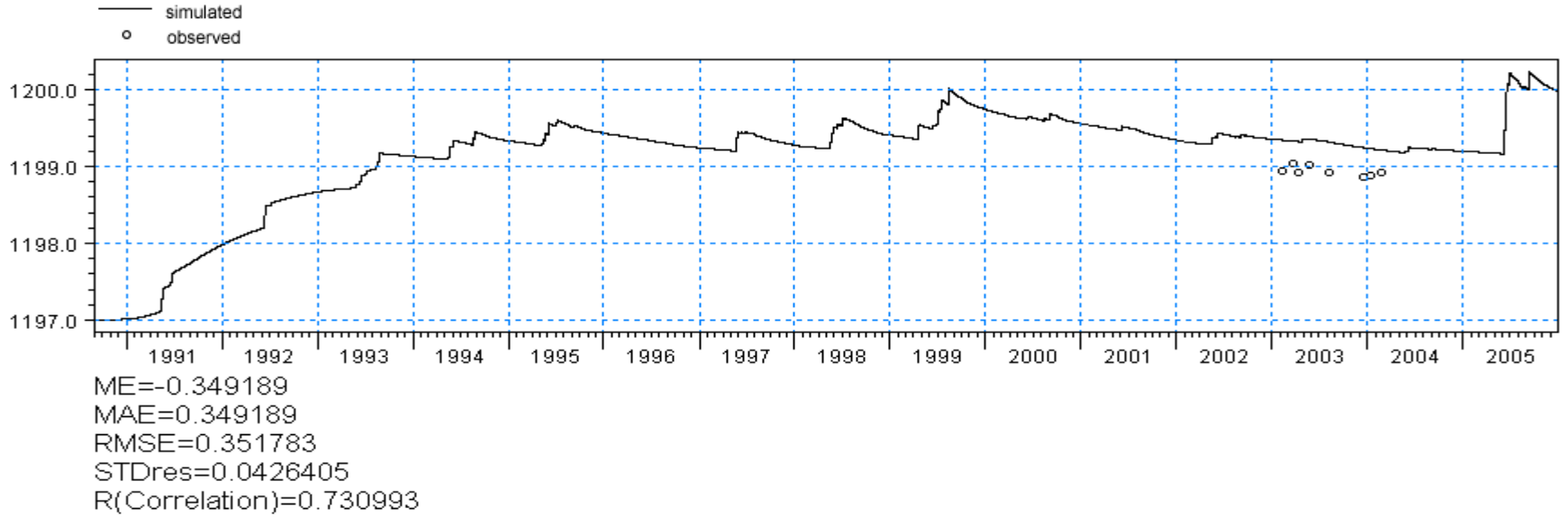

Figure L.10: Results of validation against groundwater levels at Well ID CG-1 during 1990-2005

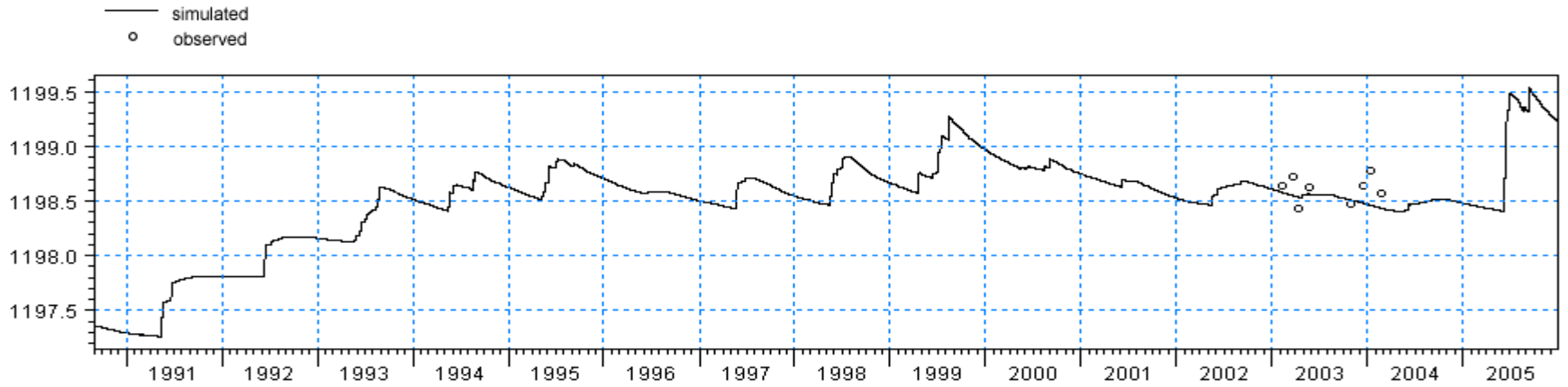

Figure L.11: Results of validation against groundwater levels at Well ID CG-2 during 1990-2005

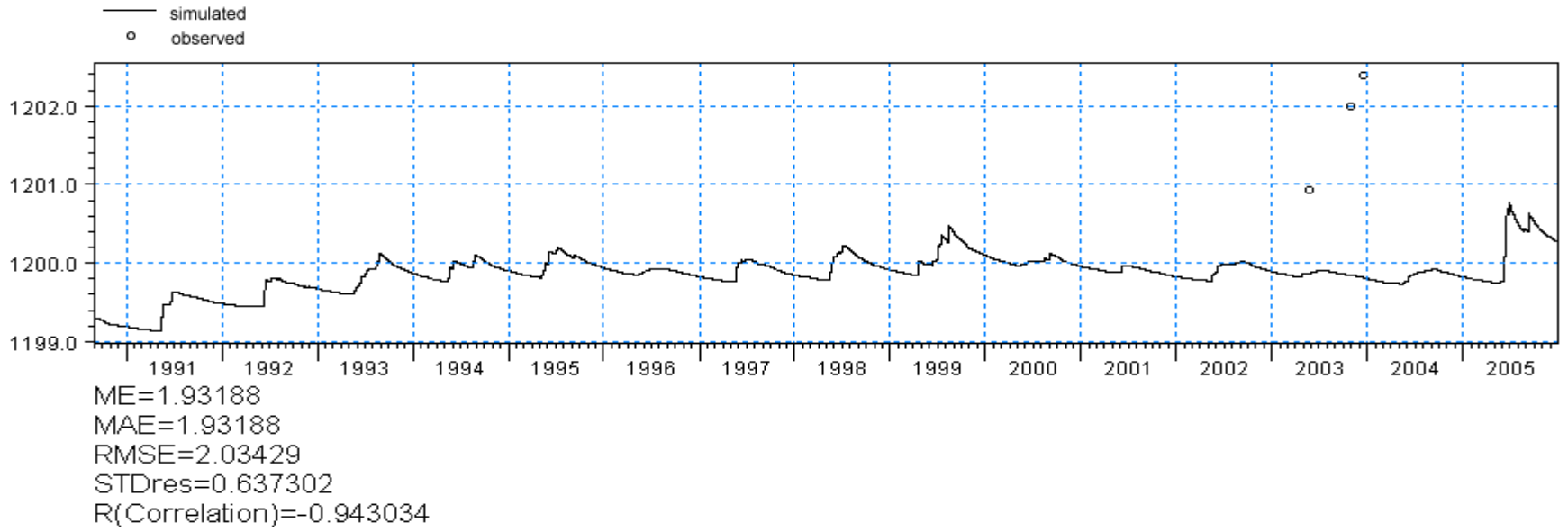

Figure L.12: Results of validation against groundwater levels at Well ID CG-3 during 1990-2005

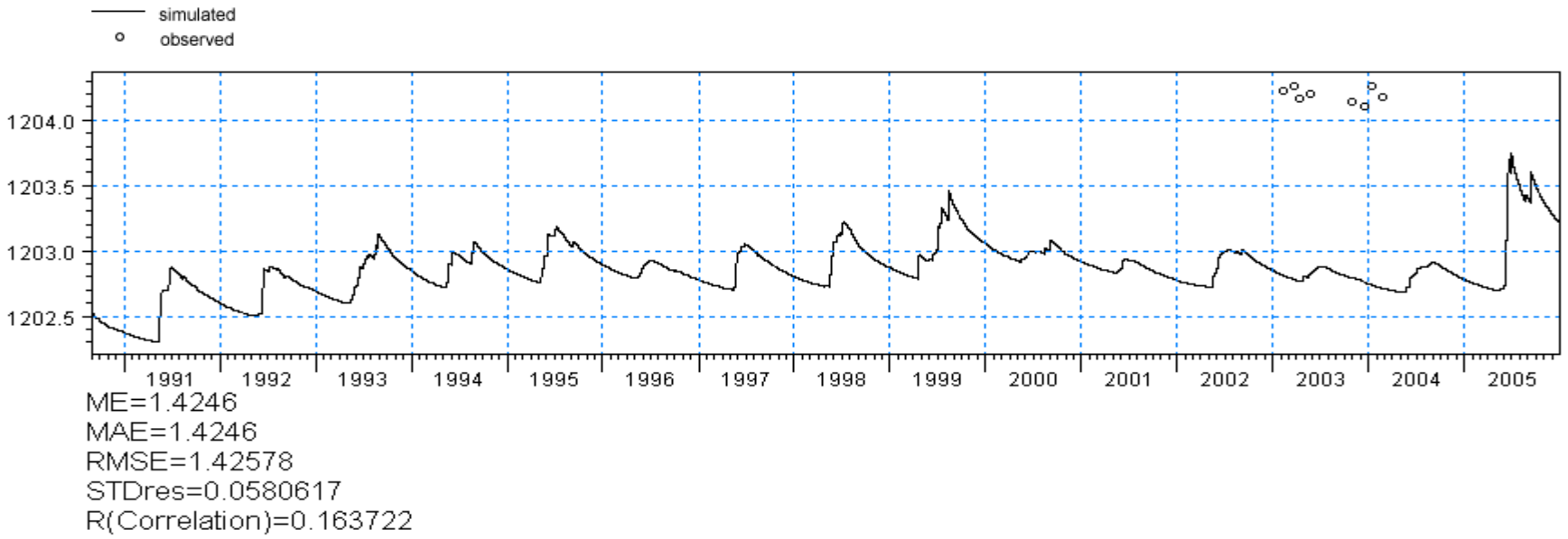

Figure L.13: Results of validation against groundwater levels at Well ID CG-4 during 1990-2005

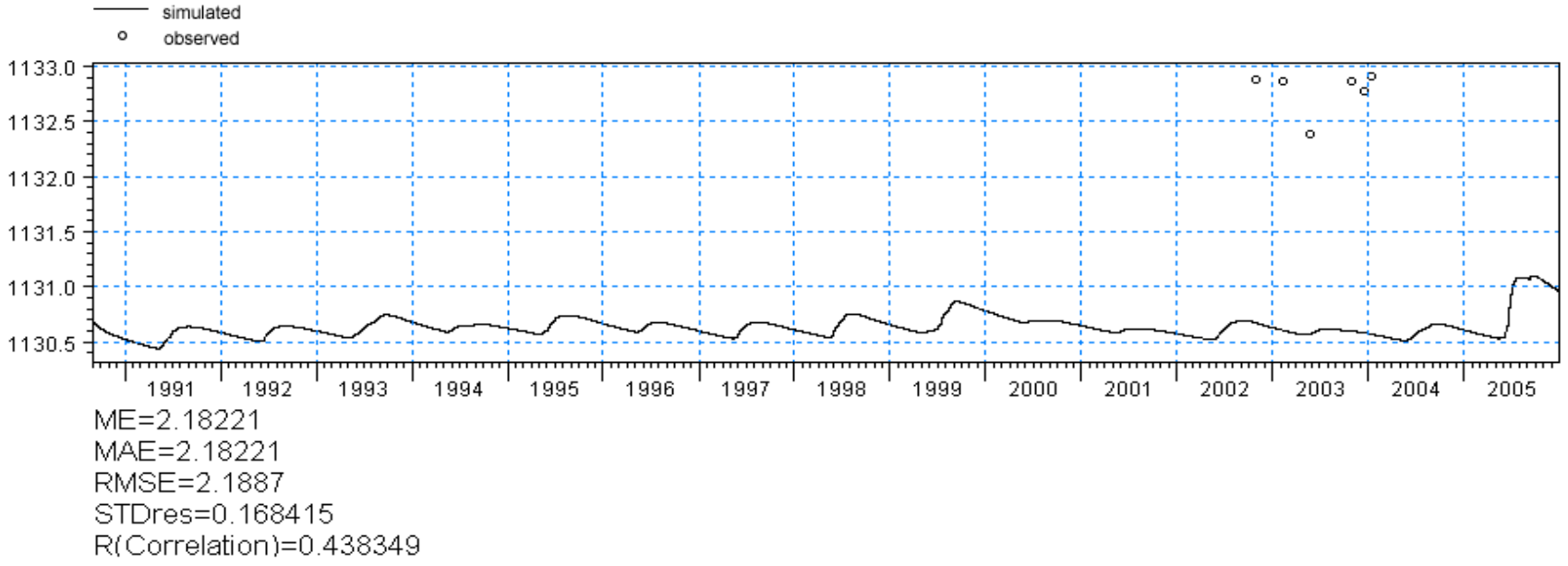

Figure L.14: Results of validation against groundwater levels at Well ID GC-1 during 1990-2005

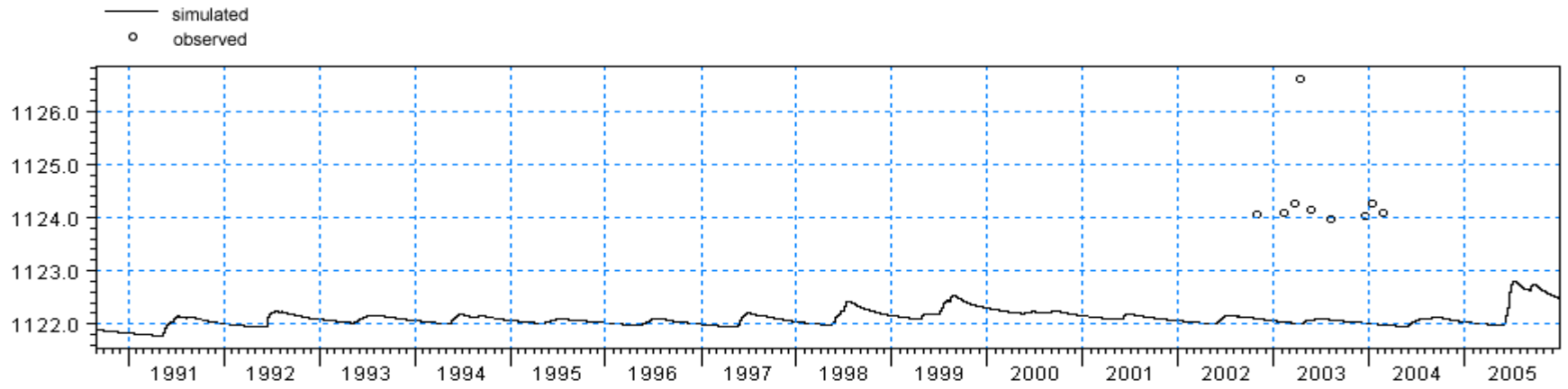

Figure L.15: Results of validation against groundwater levels at Well ID GC-2 during 1990-2005

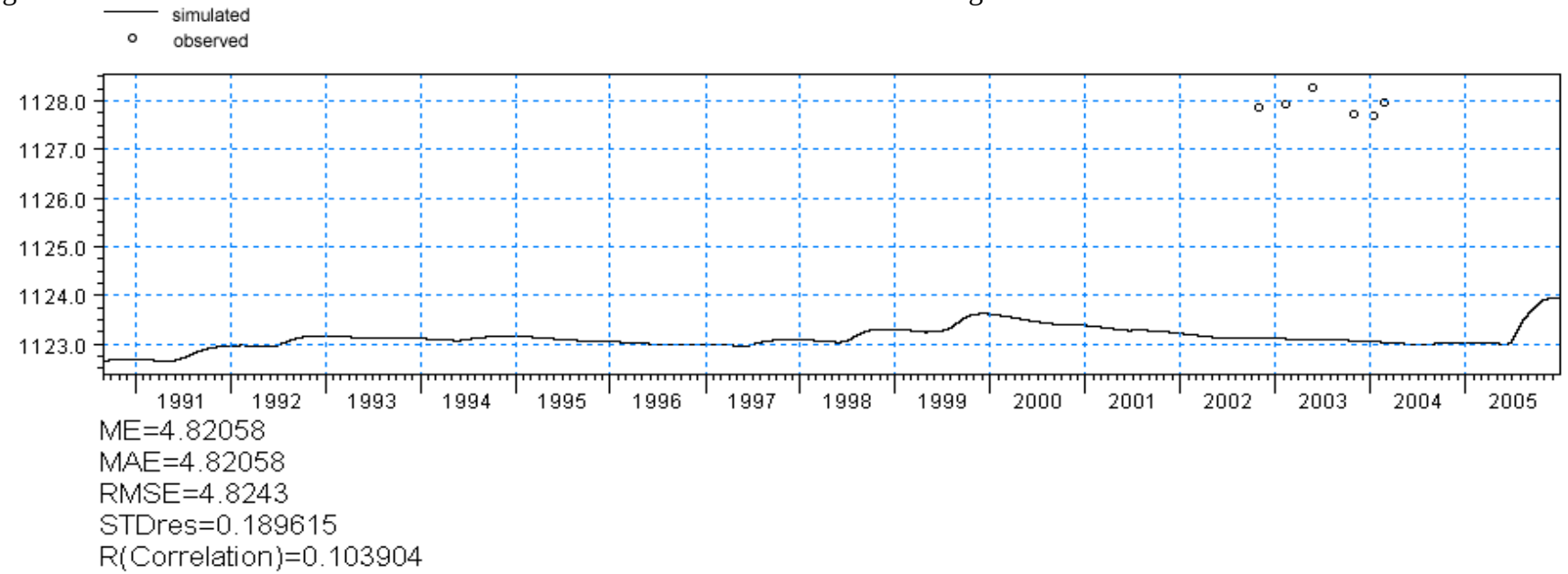

Figure L.16: Results of validation against groundwater levels at Well ID GC-3 during 1990-2005

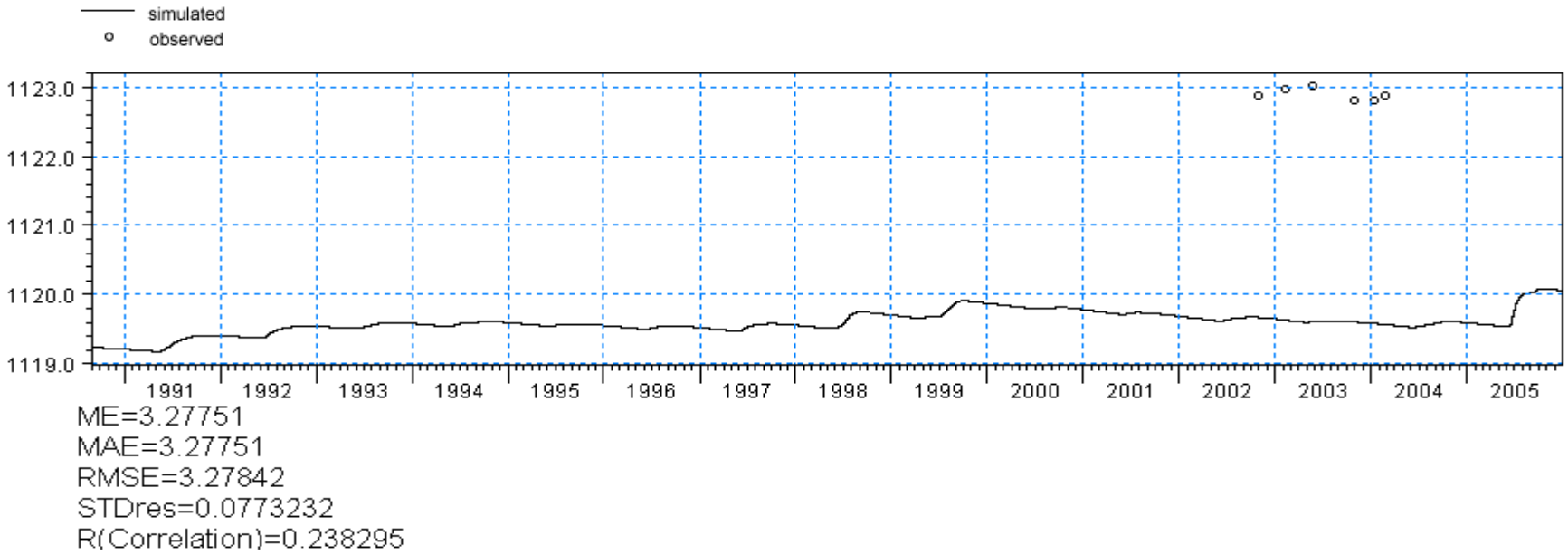

Figure L.17: Results of validation against groundwater levels at Well ID GC-4 during 1990-2005

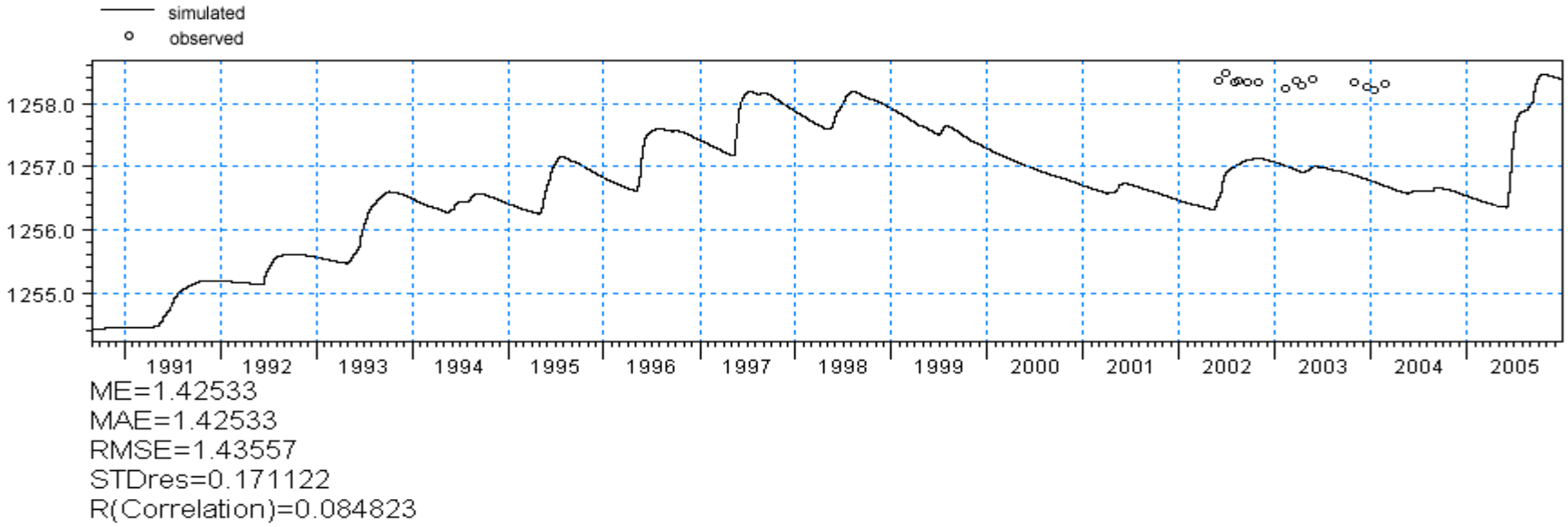

Figure L.18: Results of validation against groundwater levels at Well ID RW-1 during 1990-2005

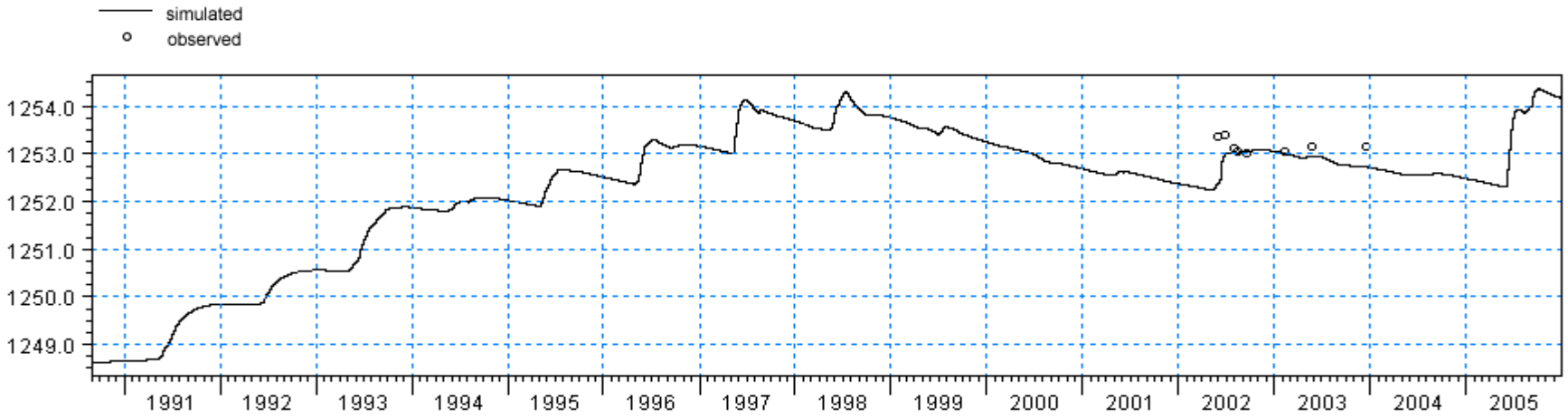

Figure L.19: Results of validation against groundwater levels at Well ID RW-2 during 1990-2005

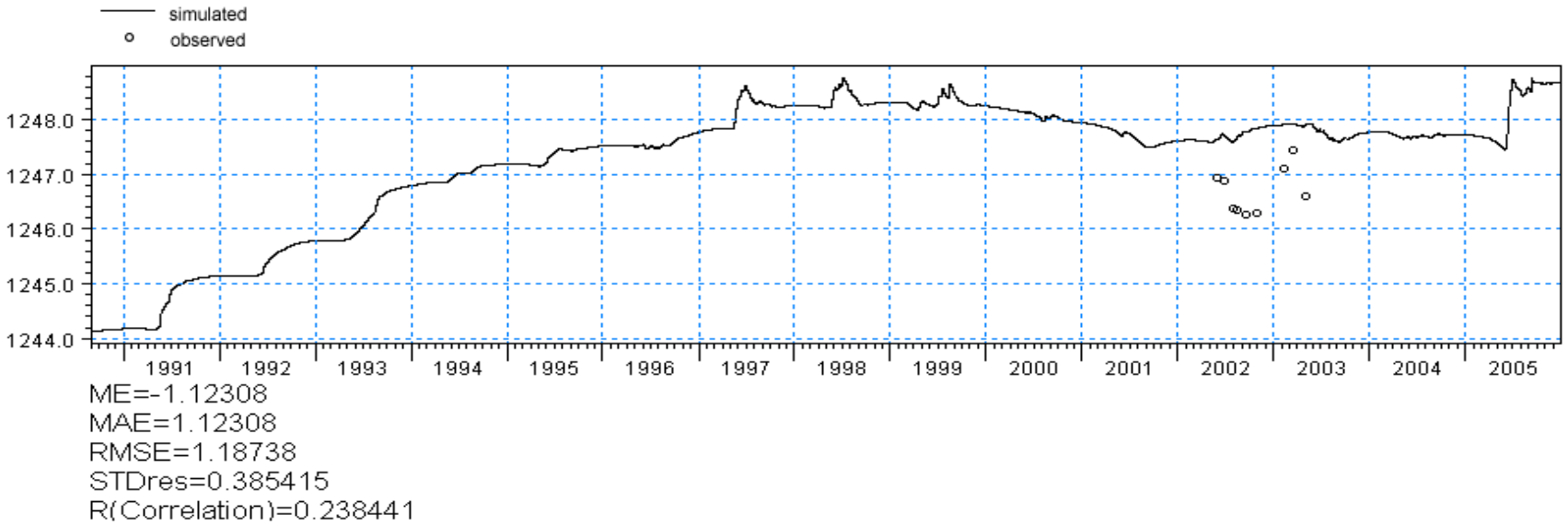

Figure L.20: Results of validation against groundwater levels at Well ID RW-3 during 1990-2005